UNIPA Springer Series

Michele Ciofalo

Thermofluid Dynamics

Unusual Problems with Analytical Solutions

UNIVERSITÀ DEGLI STUDI DI PALERMO

Springer

UNIPA Springer Series

The **UNIPA Springer Series** publishes single and co-authored thematic collected volumes, monographs, handbooks and advanced textbooks on specific issues of particular relevance in six core scientific areas. The issues may be interdisciplinary or within one specific area of interest. Manuscripts are invited for publication in the following fields of study:

1- Clinical Medicine;
2- Biomedical and Life Sciences;
3- Engineering and Physical Sciences;
4- Mathematics, Statistics and Computer Science;
5- Business, Economics and Law;
6- Human, Behavioral and Social Sciences.

Manuscripts submitted to the series are peer reviewed for scientific rigor followed by the usual Springer standards of editing, production, marketing and distribution. The series will allow authors to showcase their research within the context of a dynamic multidisciplinary platform. The series is open to academics from the University of Palermo but also from other universities around the world. Both scientific and teaching contributions are welcome in this series. The editorial products are addressed to researchers and students and will be published in the English language.

The volumes of the series are single-blind peer-reviewed.

Book proposals can be submitted to the *UNIPA Springer Series Technical Secretariat* at unipaspringer@unipa.it
At the following link, you can find some specific information about the submission procedure to the Editorial Board: https://www.unipa.it/strutture/springer/

Michele Ciofalo

Thermofluid Dynamics

Unusual Problems with Analytical Solutions

Springer

Michele Ciofalo
Department of Engineering
University of Palermo
Palermo, Italy

ISSN 2366-7516 ISSN 2366-7524 (electronic)
UNIPA Springer Series
ISBN 978-3-031-30469-9 ISBN 978-3-031-30470-5 (eBook)
https://doi.org/10.1007/978-3-031-30470-5

This Springer imprint is published by the registered company Springer Nature Switzerland AG
The registered company address is: Gewerbestrasse 11, 6330 Cham, Switzerland

Preface

I consider that I understand an equation when I can predict the properties of its solutions, without actually solving it

(Paul Dirac)

This booklet is a collection of thermofluid dynamics problems involving, at some crucial step, the use of analytical solutions. All these problems have been encountered by the author during his research activity; most of the solutions proposed are his own contributions, but a few either are classic literature results or can be reconducted to them.

Chapter 1 ("Introduction") discusses the issue of exact versus approximate solutions to physical problems. The concepts of analytic and numerical solution are rigorously defined, pros and cons of the two approaches are compared, and examples of illustrious solutions obtained long before the computer era are provided. The role of *modelling* in shaping a complex physical problem into a form amenable to exact solutions is also discussed.

Chapter 2 treats the problem of two solid bodies approaching each other in a viscous fluid. Exactly solving the Stokes equations (asymptotic form of the Navier-Stokes equations in the limit of low velocities) leads to the apparent paradox that the bodies will never touch each other, because the frictional forces necessary to squeeze the fluid out of the (vanishing) interposed gap diverge. In the real world, the paradox is avoided by the irregular shape of the facing surfaces and by the loss of validity of the continuum hypothesis itself at sufficiently small length scales.

Chapter 3 regards the velocity and displacement of spherical particles (e.g. droplets) subjected only to drag forces by a surrounding fluid medium (e.g. air). Expressing the drag coefficient as $C_D = (24/\mathrm{Re})(1+0.16\cdot\mathrm{Re}^{0.67})$ ($\mathrm{Re} \leq 10^3$) and assuming that no other force but drag (e.g. gravity) acts on the particles, the exact solution of the relevant equation of motion shows that, for $t \to \infty$, the velocity of a particle tends to zero while its displacement tends to a finite value which depends on the particle's diameter and initial velocity. Thus, for example, in zero gravity identical particles emitted from the same point with the same initial speed but along

different directions will eventually accumulate on a spherical surface surrounding the emission point.

Chapter 4 considers two fluids flowing in parallel- or counter-flow through passages separated by a permeable wall, as occurs in membrane modules used for separation processes such as filtration or hemodialysis. A one-dimensional model of the system is presented and exact solutions for the pressure and flow rate distribution along the module's length are obtained under different assumptions on the wall permeability and on the inlet/outlet pressure—velocity boundary conditions.

Chapter 5 is an extension of Stokes' second problem to the case of oscillatory flow in a plane channel subject to a harmonic forcing $F_x(t) = F_0\cos(\omega t)$. An analytic solution of the relevant Navier-Stokes equations, highly simplified by the assumption of parallel flow, was presented in 1959 by Landau and Lifshitz, and later by other authors, and is discussed here under two alternative physical interpretations.

In Chap. 6, the classic solutions for the Nusselt number in parallel channel flow under conditions of uniform wall temperature and uniform wall heat flux are generalized by imposing third type (Robin) thermal boundary conditions. As a dimensionless parameter R, expressing the ratio of the wall thermal resistance to the channel's conductive resistance, varies between zero and infinity, the two above limiting conditions are recovered, while intermediate values of R yield an intermediate Nusselt number which varies continuously between the two extrema. This problem implies the numerical solution of a non-integrable ordinary differential equation and thus is an example of hybrid analytical-numerical procedure.

Chapter 7 concerns buoyant flow in a heated duct. The one-dimensional momentum equation for the fluid, in conjunction with the classic Boussinesq approximation for thermal expansion and with a suitable friction correlation, form a closed system of equations whose exact steady-state solution is the fluid's flow rate as a function of the imposed inlet/outlet pressures and of the thermal power input. Several special cases can be obtained by letting the boundary conditions, the duct's inclination and other parameters vary. The case of a closed loop with simultaneous heat addition and subtraction can be treated similarly and the solution is the circulating flow rate as a function of the thermal power input/output.

Chapter 8 deals with the stability of two-phase flow in a heated duct. The main purpose of the study is to obtain a curve (internal characteristic) relating the inlet-outlet pressure drop to the mass flow rate for any given geometry, system's pressure and heating power. The intersection of this internal characteristic with the flow rate—prevalence curve characterizing the pump (external characteristic) allows the working point to be determined and its stability to be assessed. The model adopted is based on the one-dimensional continuity, momentum and energy equations for two-phase pipe flow in conjunction with suitable expressions for slip ratio/void fraction and two-phase friction pressure losses, based on the popular Chisholm and Lockhart-Martinelli correlations but modified for consistency and easy computability. In the case of a horizontal pipe, the internal characteristic is obtained in a simple, low-order, polynomial form.

Chapter 9 asks one to derive the wall superheat—wall heat flux relationship in the spray cooling of a flat rectangular target from empirical time-temperature histories

at an internal point. This is a classic transient inverse heat conduction problem and, in the present case, is solved by using exact expressions, due to Stefan [1889], for the wall temperature and the wall heat flux as functions of the midplane temperature and its time derivatives of increasing order. Filtering the raw data is a mandatory step before numerical derivatives can be evaluated.

Chapter 10 regards the apparent Sherwood number in simultaneous diffusive and convective mass transfer from or into a transpiring wall. This is the Sherwood number that would explain the observed overall mass flux from or into the wall if there were no transpiration, i.e. no convective contribution to mass transport. Using only elementary definitions of diffusive and convective mass fluxes, a complete classification of the possible cases is presented and a synthetic map is built representing the apparent Sherwood number as a function of two dimensionless parameters, named "transpiration" and "flux" numbers.

Finally, Chap. 11 considers the magnetohydrodynamics (MHD) flow in a vertically indefinite rectangular channel. Internal heat generation and a nonuniform electric potential may optionally be present. Magnetic field, gravity acceleration and electric potential gradient are assumed to be mutually orthogonal, while the temperature gradient is assumed to be parallel to the electric potential gradient. The governing equations include, besides the fluid's continuity, momentum and energy equations, also an equation for the electric potential and a constitutive relation for the total current density. Exact solutions show that, depending on boundary conditions and source terms, the system can operate in different regimes including direct and reverse EM pump, direct and reverse MHD generator, and a purely dissipative mode. In the presence of buoyancy, the system can also operate as a thermal engine converting thermal power into electrical and/or mechanical power.

The potential readership of this book includes M.Sc./Ph.D. students and scholars in different fields of science and engineering, with special attention to fluid dynamics and heat or mass transfer. To them, hopefully, it may offer food for thought, suggestions for lectures and ideas for further original developments.

Palermo, Italy
March 2023

Michele Ciofalo

Contents

About the Author

Michele Ciofalo (b. 1951) obtained a Master's Degree in Nuclear Engineering from the University of Palermo in 1980, a Ph.D. in Mechanical Engineering from the City University of London in 1993 and the title of *Doctor of Science* from the same University in 1999.

After a period spent at the ENEA-Casaccia Research Centre (1979–1983), he has worked for almost fourty years at the University of Palermo in the field of Nuclear and Thermofluids Engineering, first as an assistant professor (1983–2002), then as an associate professor (2002–2006) and from 2006 as a professor. Between 1986 and 1994 he spent three academic years as a *visiting fellow* at the City University of London. In 2006 he was for shorter periods at the Technical University of Lodz (Poland). Professor Ciofalo has been retired since November 1, 2021, but maintains a scientific collaboration with the Department of Engineering in Palermo.

In the last years he has lectured on *Thermal Hydraulics* (undergraduate course in Energy Engineering), *Computational Thermofluid Dynamics* (postgraduate course in Energy and Nuclear Engineering) and *Models for Thermofluid Dynamics* (postgraduate course in Chemical Engineering).

Since 1980, he has carried out experimental, computational and theoretical research activities in different fields of nuclear, chemical and energy engineering, with special focus on thermofluids phenomena. His most recent research interests have included both fluid dynamics and heat or mass transfer in membrane processes (membrane distillation, electrodialysis and reverse electrodialysis, haemodiafiltration) and the modelling and numerical simulation of turbulence by DNS, LES and RANS methods.

He is the author of more than 100 articles in scientific journals and about as many conference papers, besides several book chapters, monographs and technical reports. His published books include *Termoidraulica del Sodio—Elementi Teorici e Sperimentali* (ENEA, 1982, with V. Mancuso and T. Fanelli, in Italian), *Nanoscale Fluid Dynamics in Physiological Flows—a Review Study* (WIT Press, 1999, with M. W. Collins and T. Hennessy), *Thermofluid Dynamics of Turbulent Flows—Fundamentals and Modelling* (Springer, 2021) and *Lezioni di Termoidraulica* (Esculapio, 2022, in Italian).

Chapter 1
Introduction

There is nothing so practical as a good theory
(*Kurt Lewin*)

Abstract This introductory chapter treats the issue of exact versus approximate solutions to physical problems. The concepts of analytic and numerical solution are rigorously defined, pros and cons of the two approaches are compared, and examples of illustrious solutions obtained long before the computer era are provided. The role of modelling in shaping a complex physical problem into a form amenable to exact solutions is also discussed.

An *analytic* solution to a physical problem is an analytic function that satisfies the set of equations representing the problem in a mathematical form. In a vast class of cases, these will be ordinary or partial differential equations complete with boundary conditions (BC's) and—if appropriate—initial conditions (IC's).

In its turn, an analytic function is any function that can be defined, within a certain convergence region, as the sum of an infinite power series. For mainly historical reasons, some of these power series have been given a name of their own and are usually regarded as "closed form" expressions (e.g. e^x, $\ln(x)$, $\sin(x)$, $J_0(x)$, …) while others have never achieved this status; but no special intrinsic property other than popularity is associated with possessing a name. In the end, $\sin(x)$ is the power series

$$\sin(x) = \sum_{n=0}^{\infty} (-1)^{\mathrm{n}} \frac{x^{2n+1}}{(2n+1)!} \tag{1.1}$$

(or any equivalent form) whether or not we synthetically name it "$\sin(x)$".

Contrariwise, by *numerical* solution to a physical problem one usually means a set of numbers satisfying a (usually very large) system of algebraic equations which, in their turn, are a discrete approximation of the differential equations (plus IC's and BC's) representing the problem.

M. Ciofalo, *Thermofluid Dynamics*, UNIPA Springer Series,
https://doi.org/10.1007/978-3-031-30470-5_1

It is important to recognize that, in most cases, for a physical problem to admit an analytical solution it has to be reduced to a sufficiently simple mathematical description, often at the expense of a complete inclusion of all phenomena. In the field of thermofluid dynamics, typical simplifying assumptions are those of steady state, one-dimensional or two-dimensional flow, constant physical properties, negligible axial conduction and so on. By contrast, a numerical solution does not necessarily rely on such simplifications, and can be obtained for arbitrarily complex mathematical descriptions.

What are, then, the advantages of an analytical solution? Well, first, since it satisfies by definition the equations governing a given problem, an analytical solution is *exact*. Second, at least in principle, it exhibits in an explicit form the *dependence of the solution upon the parameters* specifying the problem, making their influence, and the reasons for this influence, easier to understand. Third, again in principle, an analytical solution is *cheaper to evaluate*, to the point that an electronic computer may not be required.

As an example of the first property (exactness), consider the fully developed flow with heat transfer to or from a constant-property fluid in a straight circular pipe with uniform imposed wall heat flux. It is well known that under these circumstances the Nusselt number is ~4.36… (Ciofalo 2022a). However, perhaps some ignore that " ~ 4.36…" is not a generic truncated real number, but an approximate decimal representation of the fraction 48/11, which is the exact solution of the heat transfer problem under consideration. Of course, no numerical solution will ever achieve the same level of accuracy. Rather, being exact, an analytical solution like this can serve as a *benchmark* against which to test any numerical method for accuracy.

As an example of the second property (explicit dependence of the solution upon the data) consider the thermosyphon loop discussed in Chap. 6 of this book. For a closed circuit of uniform circular cross section and diameter d, consisting of two horizontal branches of length L_h and two vertical branches of length L_v kept at two different temperatures T_B, T_D, under the assumption of fully turbulent flow a one-dimensional model predicts the natural circulation mass flow rate to be

$$G = 2.0114\,\mu d \left(\frac{L_v}{L_v + L_h} \mathrm{Gr} \right)^{5/9} \tag{1.2}$$

in which $\mathrm{Gr} = g\beta\,(T_B - T_D) d^3/(\mu/\rho)^2$ (Grashof number based on d). From the above expression, it is immediate to recognize that, for example, G is proportional to the diameter raised to the power 8/3 or to the thermal dilatation coefficient β raised to the power 5/9 (and so on). A "brute force" solution of the flow and energy equations by computational fluid dynamics (CFD) for the same loop would probably yield more accurate G predictions (thanks to a 2-D or 3-D representation of the problem), but would certainly obscure the solution's dependence upon the data, and a full picture of the system's behavior could only be obtained by simulating a large number of test cases, much as though individual simulations were experimental measurements.

Finally, as an example of the third property (easy computability of the solution) consider the oscillatory flow problem discussed in Chap. 4 of this book. The exact asymptotic (i.e., valid for large times) solution for the streamwise velocity in a plane channel of half-thickness δ subject to a harmonic streamwise driving pressure gradient $F_x(t) = F_0 \cos(\omega t)$ is

$$u(y,t) = \frac{F_0}{\omega\rho\beta_W}\{\,[\sinh\varphi_1(y)\sin\varphi_2(y) + \sinh\varphi_2(y)\sin\varphi_1(y)]\cos(\omega t) + [\beta_W - \cosh\varphi_1(y)\cos\varphi_2(y) - \cosh\varphi_2(y)\cos\varphi_1(y)]\sin(\omega t)\} \quad (1.3)$$

in which $\varphi_1(y) = \frac{\alpha}{\sqrt{2}}\left(1 + \frac{y}{\delta}\right)$, $\varphi_2(y) = \frac{\alpha}{\sqrt{2}}\left(1 - \frac{y}{\delta}\right)$, $\beta_W = \cosh\left(\sqrt{2}\alpha\right) + \cos\left(\sqrt{2}\alpha\right)$ and $\alpha = \delta\sqrt{\omega/\nu}$ is the *Womersley number*.

For any given time t and cross-stream location y, the above formulae allow u to be computed by performing about twenty operations, some of which involve the evaluation of transcendent functions and thus expand in their turn into some 10–20 elementary floating point operations (FLOPS) each, still with a negligible overall consumption of CPU time. Computing the cross-stream velocity profile for a reasonable number of time steps could be done by a hand-held calculator in a matter of minutes. On the other hand, should we use a numerical method to solve the same problem, the prediction of u at any location y and time t would require the calculation of the whole u profile across the computational domain at all previous time steps. The solution would exhibit an accuracy depending crucially on the spatial and temporal discretization and, even if the coarsest acceptable grid and time step were used, could never be practically obtained without an electronic computer and a suitable software.

Of course, this last property of analytic solutions (easy computability) explains why they were so important up to the 1940s–1950s, before electronic computers became available and the science of Computational Fluid Dynamics came into existence. The literature up to ~1940–1950 offers a spectacular repertoire of ingenious analytic solutions to problems that, today, would doubtless be tackled without a second thought by setting up a numerical simulation. Illustrious examples are Stokes'(1850) solution to the so called "Stokes second problem" of oscillatory viscous flow adjacent to a flat plate, partially recalled in Chap. 4 of this book; Stefan's (1889) theory of heat transfer with phase change and melting front propagation, partially recalled in Chap. 8; Boussinesq's (1868) analytic solutions to various problems of viscous fluid flow, including the counter-rotating secondary vortices arising in curved pipes; Blasius' (1908) solutions for the velocity distribution near a flat plate, now the fundament of all boundary layer studies.

Analytic solutions to fluid flow and heat transfer problems have not vanished after the advent of CFD, as is also witnessed by recent books (Emanuel 2015; Brenn 2018); but certainly they regard today only a small fraction of the whole literature on the subject.

The superiority of analytical solutions with respect to numerical ones should not be unduly overemphasized. Quoting Ardourel and Jebeile (2017), "*analytical solutions are sometimes an excessively sophisticated mathematical machinery for the problem*

at stake". The authors cite the example of the simple pendulum problem, which, unless the angular displacement is very small, is described by a nonlinear differential equation. An analytical solution to this does actually exist (Belendez et al. 2007), but involves complicated special functions such as complete and incomplete elliptic integrals of the first kind and Jacobi elliptic functions, all rather cumbersome to calculate; most scientists, if required, will prefer to solve the pendulum's equation of motion numerically, probably with less computational effort and certainly with less *human* (programming) effort. More generally, there is little point in using a very sophisticated computational tool to obtain exact solutions to already very idealized model equations; approximate numerical solutions, possibly to a more complete and realistic mathematical model, can be preferable.

Nevertheless, the intellectual satisfaction gained by finding an analytical solution is priceless. The enterprise may involve the purely mathematical skill necessary to find a viable solution to a formally well-defined problem; and, in this case, it is better left to mathematicians. But it may also rest on the ability to formulate a given general problem in such terms that an analytical solution becomes possible (i.e., the ability to develop *models*); and, in this latter case, also physicists and engineers may have a word on the subject.

Chapter 2
Solid Bodies Approaching Each Other in a Viscous Fluid

How wonderful that we have met with a paradox!
Now we have some hope of making progress
(*Niels Bohr*)

Abstract Consider two solid bodies approaching each other in a viscous fluid. Exactly solving the Stokes equations (asymptotic form of the Navier–Stokes equations in the limit of low velocities) leads to the apparent paradox that the bodies will never touch each other, because the frictional forces necessary to squeeze the fluid out of the (vanishing) interposed gap diverge. In the real world, this paradox is avoided by the irregular shape of the facing surfaces and by the loss of validity of the continuum hypothesis itself at sufficiently low length scales.

Suppose that at $t = 0$ two solid bodies with perfectly flat and parallel surfaces, initially a distance $2\delta_0$ apart, start to move towards each other orthogonally to these surfaces in a fluid of viscosity μ under the influence of an applied force F. As the distance 2δ between the surfaces decreases, the interposed fluid is squeezed out of the interposed region. We want to derive the law of motion $\delta(t)$ for given δ_0, F and μ.

For simplicity, we assume the surfaces to be circular with radius R and cylindrical symmetry to hold, so that the problem can be studied in the cylindrical coordinate system (r, z) as sketched in Fig. 2.1.

The shape of the solid bodies themselves is irrelevant once the approaching surfaces are specified as circular faces of radius R. Also, the results do not significantly change if either of the surfaces is replaced by an indefinite plane.

For symmetry reasons, the fluid-filled computational domain can be limited to the region $0 \le r \le R$, $0 \le y \le \delta$ delimited by the symmetry midplane $y = 0$, the upper plane surface $y = \delta$ and the outlet boundary $r = R$.

Neglecting all inertial terms, the problem is governed by the 2-D continuity and Stokes equations along r and y, written in cylindrical coordinates (r, y):

$$\frac{1}{r}\frac{\partial}{\partial r}(ru) + \frac{\partial v}{\partial y} = 0 \tag{2.1}$$

M. Ciofalo, *Thermofluid Dynamics*, UNIPA Springer Series,
https://doi.org/10.1007/978-3-031-30470-5_2

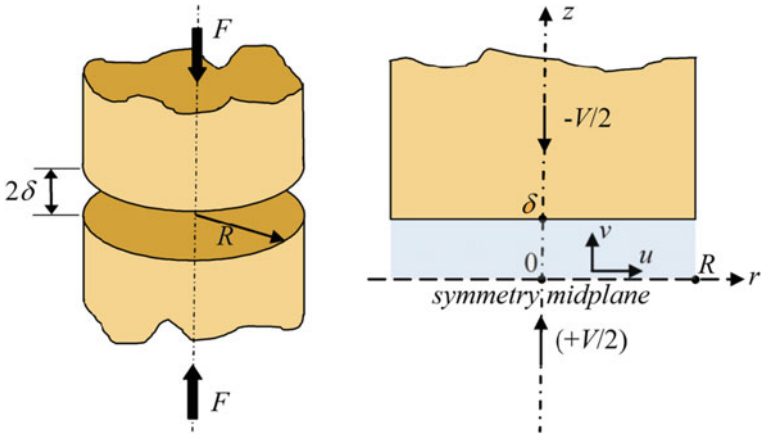

(a) (b)

Fig. 2.1 Approach of plane surfaces in a viscous fluid. **a** Axonometric view; **b** 2-D (r, z) computational domain with symmetry midplane

$$\frac{1}{r}\frac{\partial}{\partial r}(pr) - \mu\frac{\partial^2 u}{\partial y^2} = 0 \tag{2.2}$$

$$\frac{\partial p}{\partial y} + \mu\frac{\partial}{\partial r}\left(r\frac{\partial v}{\partial r}\right) = 0 \tag{2.3}$$

in which u and v are the velocity components along r and y and p is pressure relative to the far fluid.

Boundary conditions appropriate to the problem's formulation are

$$u(0, y) = 0; \quad u(r, \delta) = 0; \quad \frac{\partial u}{\partial y}(r, 0) = 0 \tag{2.4}$$

$$v(r, 0) = 0; \quad v(r, \delta) = -V/2 \tag{2.5}$$

$$p(R, y) = 0 \tag{2.6}$$

in which V is the instantaneous (and so far unknown) relative approach velocity between the two flat surfaces.

We seek solutions of the form $u(r, y) = \varphi(r)\psi(y)$; $v = v(y)$; $p = p(r)$, i.e. solutions in which the pressure p does not depend on the normal coordinate y and the normal velocity v does not depend on the radius r, while the radial velocity u depends on both r and y but can be expressed as the product of a function of r by a function of y.

Substituting $\varphi(r)\psi(y)$ for $u(r, y)$ in the continuity Eq. (2.1) one obtains

$$\frac{1}{r}\frac{\mathrm{d}}{\mathrm{d}r}(r\varphi) = -\frac{1}{\psi}\frac{\mathrm{d}v}{\mathrm{d}y} \tag{2.7}$$

Since the LHS of Eq. (2.7) is a function of r only, while the RHS is a function of y only, for the identity (2.7) to hold for any r and y it is necessary that both sides are equal to a constant which, for physical reasons, must be positive, say B^2:

$$\frac{1}{r}\frac{\mathrm{d}}{\mathrm{d}r}(r\varphi) = B^2 \tag{2.8}$$

$$-\frac{1}{\psi}\frac{\mathrm{d}v}{\mathrm{d}y} = B^2 \tag{2.9}$$

From Eq. (2.8), imposing the first of the boundary conditions (2.4) or just requiring φ to remain finite for $r = 0$, one has

$$\varphi(r) = \frac{B^2 r}{2} \tag{2.10}$$

with B^2 still to be determined.

Similarly, substituting $\varphi(r)\psi(y)$ for $u(r, y)$ in the radial Stokes Eq. (2.2) one obtains

$$\frac{1}{r\varphi}\frac{\mathrm{d}}{\mathrm{d}r}(rp) = \mu\frac{\mathrm{d}^2\psi}{\mathrm{d}y^2} \tag{2.11}$$

Since the LHS of Eq. (2.11) is a function of r only, while the RHS is a function of y only, for the identity (2.11) to hold for any r and y it is necessary that both sides are equal to a constant which in this case, for physical reasons, must be negative, say $-C^2$:

$$\frac{1}{r\varphi}\frac{\mathrm{d}}{\mathrm{d}r}(rp) = -C^2 \tag{2.12}$$

$$\mu\frac{\mathrm{d}^2\psi}{\mathrm{d}y^2} = -C^2 \tag{2.13}$$

The solution to Eq. (2.13) satisfying the boundary conditions $\mathrm{d}\psi/\mathrm{d}y(0) = 0$ and $\psi(\delta) = 0$, which are a consequence of Eq. (2.4), is

$$\psi(y) = \frac{C^2\delta^2}{2\mu}\left(1 - \frac{y^2}{\delta^2}\right) \tag{2.14}$$

By substituting Eq. (2.10) for $\varphi(r)$ and (2.14) for $\psi(y)$ into the expression $u(r, y) = \varphi(r)\psi(y)$, one has

$$u(r, y) = \frac{\alpha^2 \delta^2}{4\mu} r \left(1 - \frac{y^2}{\delta^2}\right) \tag{2.15}$$

in which $\alpha = BC$ is a (single) constant still to be determined.

By substituting Eq. (2.14) for $\psi(y)$ into Eq. (2.9) and imposing to $v(y)$ the first of the two boundary conditions (2.5), i.e. $v(0) = 0$, one has

$$v(y) = -\frac{\alpha^2 \delta^2}{2\mu} y \left(1 - \frac{y^2}{3\delta^2}\right) \tag{2.16}$$

Imposing now to $v(y)$ the second of the two boundary conditions (2.5), i.e. $v(\delta) = -V/2$, one has

$$\alpha^2 = \frac{3\mu V}{2\delta^3} \tag{2.17}$$

which allows $u(r, y)$, Eq. (2.15), and $v(y)$, Eq. (2.16), to be written in closed form:

$$u(r, y) = \frac{3}{8} \frac{V}{\delta} r \left(1 - \frac{y^2}{\delta^2}\right) \tag{2.18}$$

$$v(y) = -\frac{3}{4} \frac{V}{\delta} y \left(1 - \frac{y^2}{3\delta^2}\right) \tag{2.19}$$

Note that from Eq. (2.18) one also has

$$\frac{\partial^2 u}{\partial y^2} = \frac{3}{4} \frac{V}{\delta^3} r \tag{2.20}$$

Now, substituting Eq. (2.18) for u and Eq. (2.20) for $\partial^2 u/\partial y^2$ into the radial Stokes Eq. (2.2), one obtains the following ODE for pressure:

$$\frac{1}{r} \frac{\mathrm{d}}{\mathrm{d}r}(pr) = -\frac{3}{4} \frac{V\mu}{\delta^3} r \tag{2.21}$$

which, integrated with the boundary condition (2.6), yields:

$$p(r) = -\frac{V\mu R^2}{4\delta^3} \left(\frac{R}{r} - \frac{r^2}{R^2}\right) \tag{2.22}$$

Equations (2.18), (2.19) and (2.22) are the complete solution to the problem represented by Eqs. (2.1)–(2.3) with boundary conditions (2.4)–(2.6). Also, due to the linearity of the Stokes equations, the solution found is the only possible one, which means that the assumptions made on the behaviour of u, v and p do not cause any loss of generality.

However, the solution still contains the (unknown) approach velocity V rather than the (known) applied force F. Therefore, as a last step, let us write

$$F = \int_0^R p(r) 2\pi r \mathrm{d}r \tag{2.23}$$

Substituting Eq. (2.22) for p into Eq. (2.23) yields

$$\frac{\mathrm{d}\delta}{\mathrm{d}t} = -\frac{V}{2} = -\frac{4F}{3\pi\mu R^4}\delta^3 \tag{2.24}$$

i.e., an ODE in $\delta(t)$ whose solution, subject to the initial condition $\delta(0) = \delta_0$, is

$$\delta(t) = \left[\frac{1}{\delta_0^2} + \frac{8F}{3\pi\mu R^4}t\right]^{-1/2} \tag{2.25}$$

A noteworthy feature of this solution is that δ remains > 0 for any finite time. Hence, *the two surfaces will never get in contact*, but their distance will only asymptotically tend to zero for any finite value of the applied force.

By deriving $\delta(t)$ with respect to time, one also obtains the behavior of the approaching velocity $V(t)$:

$$V = -2\frac{\mathrm{d}\delta}{\mathrm{d}t} = \frac{8F}{3\pi\mu R^4}\left[\frac{1}{\delta_0^2} + \frac{8F}{3\pi\mu R^4}t\right]^{-3/2} \tag{2.25}$$

As an example, Figs. 2.2 and 2.3 report $\delta(t)$ and $V(t)$ for $R = 0.1$ m, $\delta_0 = 10^{-3}$ m, $F = 1$ N and four values of μ ($1.8 \cdot 10^{-5}$, $0.9 \cdot 10^{-3}$, 0.045 and 2.25 Pa s, roughly representative of air, water, light oil and heavy oil, respectively). Note that the time necessary for δ to decrease from its initial value of 1 mm to molecular size (1 nm) varies between 10^9 and 10^{14} s (30 to 3 million years!) depending on the fluid's viscosity.

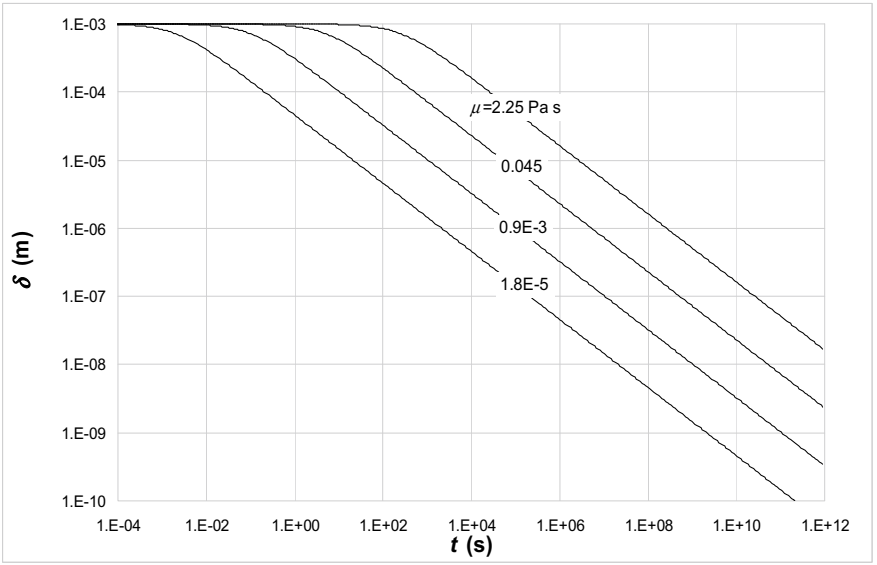

Fig. 2.2 Behaviour of the surface-to-surface half distance δ for $R = 0.1$ m, $\delta_0 = 10^{-3}$ m, $F = 1$ N and four values of μ ($1.8 \cdot 10^{-5}$, $0.9 \cdot 10^{-3}$, 0.045 and 2.25 Pa s)

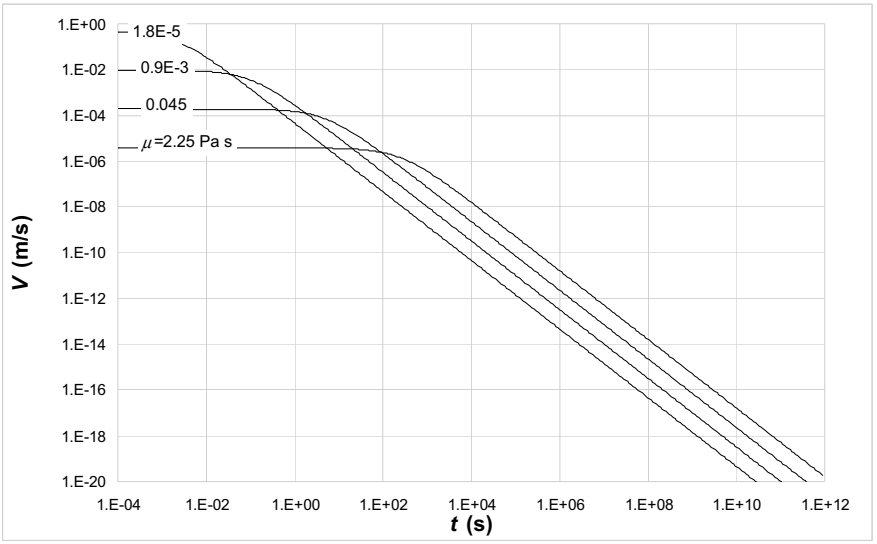

(b)

Fig. 2.3 Behaviour of the approach velocity V for $R = 0.1$ m, $\delta_0 = 10^{-3}$ m, $F = 1$ N and four values of μ ($1.8 \cdot 10^{-5}$, $0.9 \cdot 10^{-3}$, 0.045 and 2.25 Pa s)

Chapter 3
Velocity and Displacement of Spherical Particles Subjected Only to Drag

There are things which seem incredible to those who have not studied Mathematics
(*Archimedes of Syracuse*)

Abstract The problem regards the velocity and displacement of spherical particles (e.g. droplets) subjected only to drag forces by a surrounding fluid medium (e.g. air). Expressing the drag coefficient as $C_D = (24/\mathrm{Re})(1 + 0.16 \cdot \mathrm{Re}^{0.67})$ ($\mathrm{Re} \leq 10^3$) and assuming that no other force but drag (e.g. gravity) acts on the particles, the exact solution of the relevant equation of motion shows that, for $t \to \infty$, the velocity of a particle tends to zero while its displacement tends to a finite value which depends on the particle's diameter and initial velocity. Thus, for example, in zero gravity identical particles emitted from the same point with the same initial speed but along different directions will eventually accumulate on a spherical surface surrounding the emission point.

The drag force F_D on a particle of cross sectional area A that moves with velocity u through a viscous medium of density ρ_m can be expressed as

$$F_D = C_D A \rho_m \frac{u^2}{2} \tag{3.1}$$

in which C_D is the drag coefficient. For spherical particles of diameter d, C_D is a complex function of the Reynolds number $\mathrm{Re} = ud/\nu_\mathrm{m}$, ν_m being the kinematic viscosity of the medium. It is shown as a solid line in Fig. 3.1 (Perry and Green 1984) in the broad range $\mathrm{Re} = 10^{-2}$–10^8.

Clift et al. (1978) report ten simple correlations that approximate CD in as many Reynolds number intervals. However, the single correlation

$$C_D = \frac{a}{\mathrm{Re}}\left(1 + b \cdot \mathrm{Re}^c\right) \tag{3.2}$$

M. Ciofalo, *Thermofluid Dynamics*, UNIPA Springer Series,
https://doi.org/10.1007/978-3-031-30470-5_3

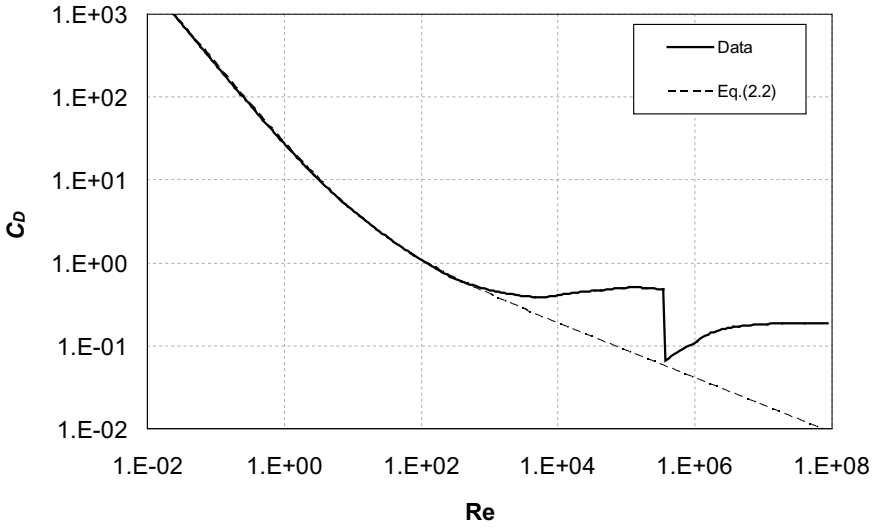

Fig. 3.1 Drag coefficient for spheres as a function of the Reynolds number

with $a = 24$, $b = 0.16$, $c = 0.67$ approximates well the data up to $\mathrm{Re} \approx 10^3$. Equation (3.2) is also reported as a broken line in Fig. 3.1.

If no other force than drag (in particular, gravity) acts on the particle, then, writing the acceleration as $\mathrm{d}u/\mathrm{d}t = -F_D/m$, expressing the mass m as $\rho(4/3)\pi\,(d/2)^3$ and using Eqs. (3.1) and (3.2) for F_D, the following differential equation in u is obtained:

$$\frac{\mathrm{d}u}{\mathrm{d}t} = -\frac{u}{c\tau}\left[1 + \left(\frac{u}{U}\right)^c\right] \tag{3.3}$$

in which τ and U are two constants having physical dimensions of time and velocity, respectively:

$$\tau = \frac{4\rho d^2}{3\rho_m \nu_m a c} \tag{3.4}$$

$$U = \frac{\nu_m}{\mathrm{d}b^{1/c}} \tag{3.5}$$

By introducing the auxiliary variable

$$z = \frac{b\mathrm{Re}^c}{1 + b\mathrm{Re}^c} \tag{3.6}$$

Equation (3.3) simplifies to

$$\frac{\mathrm{d}z}{\mathrm{d}t} = -\frac{z}{\tau} \tag{3.7}$$

whose solution is

$$z = z_0 \exp\left(-\frac{t}{\tau}\right) \tag{3.8}$$

$z_0 = z(0)$ being the value of z for $t = 0$, depending on the initial particle velocity.

The velocity u is then obtained from z by inverting Eq. (3.6), which, taking account of the definition of Re, yields

$$u(t) = U\left(\frac{z}{1-z}\right)^{1/c} \tag{3.9}$$

with z expressed as a function of t by Eq. (3.8). For water droplets in air ($\rho = 10^3$ kg/m^3, $\rho_m = 1.15$ kg/m^3, $\nu_m = 1.5 \cdot 10^{-5}$ m^2/s) the velocity $u(t)$ is reported in Fig. 3.2a for an initial velocity $u_0 = 10$ m/s and different particle diameters d, and in Fig. 3.2b for a particle diameter $d = 1$ mm and different initial velocities u_0.

The displacement x at time t^* is formally given, assuming $x(0) = 0$, by

$$x(t^*) = \int_0^{t^*} u(t)\mathrm{d}t \tag{3.10}$$

Using Eq. (3.9) for $u(t)$, Eq. (3.10) becomes

$$x(t^*) = U\int_0^{t^*} \left(\frac{z}{1-z}\right)^{1/c} \mathrm{d}t \tag{3.11}$$

By observing that from Eq. (3.7) one has $\mathrm{d}t = -\tau\,\mathrm{d}z/z$, Eq. (3.11) becomes

$$x(z^*) = U\tau\int_{z_0}^{z^*} \frac{z^{1/c-1}}{(1-z)^{1/c}}\mathrm{d}z \tag{3.12}$$

where $z^* = z_0\exp(-t^*/\tau)$. The integral in Eq. (3.12) is a particular case of the *incomplete beta function*

$$beta(z^*, \alpha, \beta) = \int_0^{z^*} z^{\alpha-1}(1-z)^{\beta-1}\mathrm{d}z \tag{3.13}$$

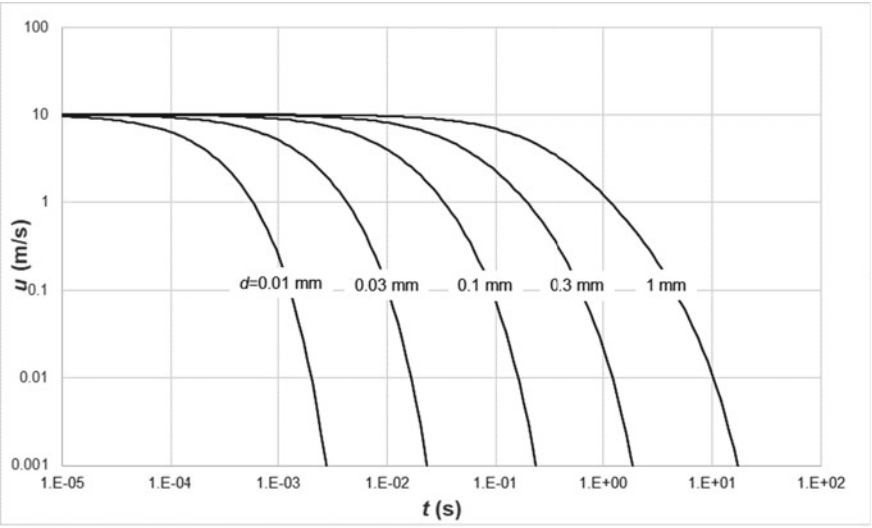

(a)

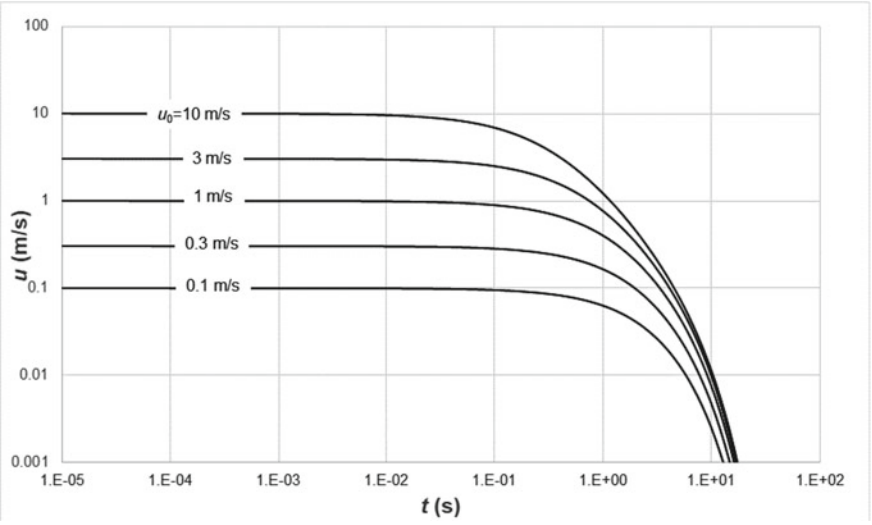

(b)

Fig. 3.2 Spherical particle velocity as a function of time. **a** $u_0 = 10$ m/s, different diameters d; **b** $d = 1$ mm, different initial velocities u_0

(Abramowitz and Stegun 1972) for $\alpha = 1/c$ and $\beta = 1 - 1/c$. More precisely, it can be written as

$$x(z^*) = U\tau\left[beta\left(z_0,\ \frac{1}{c},\ 1-\frac{1}{c}\right) - beta\left(z^*,\ \frac{1}{c},\ 1-\frac{1}{c}\right)\right] \tag{3.14}$$

The incomplete beta function admits the following series expansion

$$beta\left(z^*,\ \alpha,\ \beta\right) = \sum_{k=0}^{\infty} \frac{(1-\beta)_k}{(\alpha+k)k!}\left(z^*\right)^{\alpha+k} \tag{3.15}$$

in which $(1-\beta)_k$ is the *Pochammer symbol*, defined in general as

$$(\Phi)_k = \Phi(\Phi+1)\ldots(\Phi+k-1); \quad (\Phi)_0 = 1 \tag{3.16}$$

Taking account of Eq. (3.15), Eq. (3.14) can be explicitly written as

$$x(z^*) = U\tau\sum_{k=0}^{\infty} \frac{(1/c)_k}{(1/c+k)k!}\left[(z_0)^{1/c+k} - \left(z^*\right)^{1/c+k}\right] \tag{3.17}$$

For water droplets in air ($\rho = 10^3$ kg/m^3, $\rho_m = 1.15$ kg/m^3, $\nu_m = 1.5 \cdot 10^{-5}$ m^2/s) the displacement $x(t)$ is reported in Fig. 3.3a for a given initial velocity $u_0 = 10$ m/s and different particle diameters d, and in Fig. 3.3b for a given particle diameter $d =$ 1 mm and different initial velocities u_0.

A noteworthy feature of the displacement x is that, for $t \to \infty$, *it tends to an asymptotic value* x_∞. For example, for water droplets with $d = 1$ mm travelling in air, x_∞ is ~ 0.243 m for $u_0 = 1$ m/s and ~ 1.36 m for $u_0 = 10$ m/s. In the absence of gravity, droplets issued with random orientations but uniform speed from a point source will form a stationary spherical shell of radius x_∞ surrounding the emission point.

Equations (3.9) for u and (3.17) for x (in which $z = z_0\exp(-t/\tau)$) represent the complete analytical solution to the particle motion problem defined by Eqs. (3.1)–(3.3). Of course, they are applicable only as far as the initial Reynolds number is below 10^3, i.e., the initial velocity is below

$$u_{\lim} = 10^3 \nu_m / d \tag{3.18}$$

For example, for droplets of 1 mm diameter ($d = 10^{-3}$ m) in ambient air ($\nu_m \approx 1.5 \cdot 10^{-5}$ m^2/s), one has $u_{\lim} = 15$ m/s.

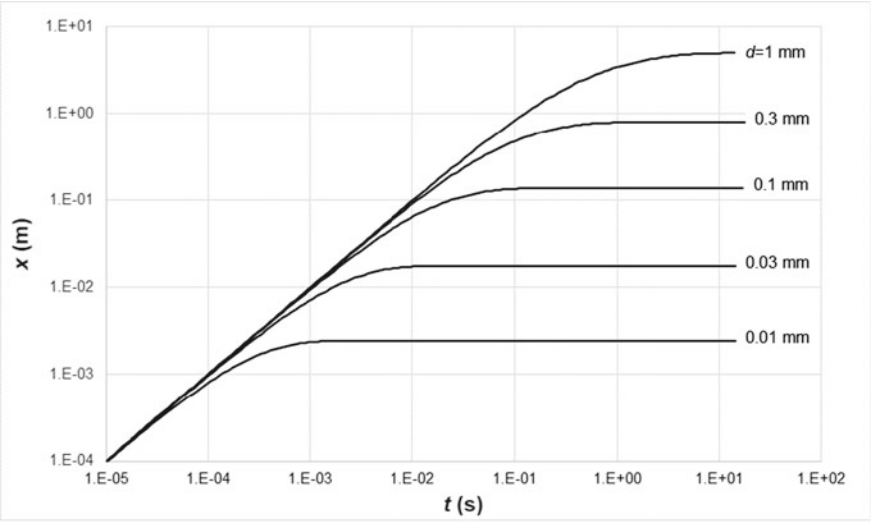

(a)

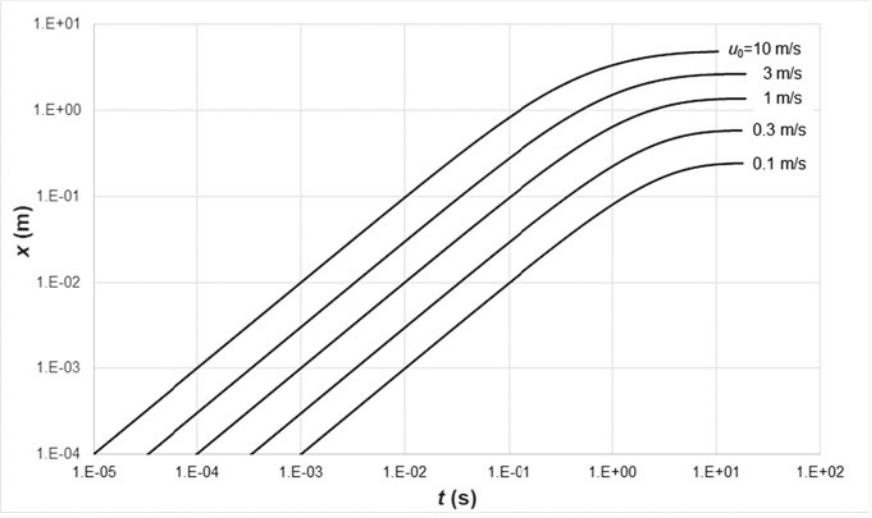

(b)

Fig. 3.3 Spherical particle displacement as a function of time. **a** $u_0 = 10$ m/s, different diameters d; **b** $d = 1$ mm, different initial velocities u_0

Chapter 4
Flow Through Parallel Channels Separated by a Permeable Wall

Prediction is very difficult, especially if it is about the future
(*Niels Bohr*)

Abstract Consider two fluids flowing in parallel- or counter-flow through passages separated by a permeable wall, as occurs in membrane modules used for separation processes such as filtration or hemodialysis. A 1-D model of the system is presented and solutions for the distribution of flow rates and pressures along the module's length are obtained under different assumptions on the inlet/outlet pressure—velocity boundary conditions.

In many applications, one has to consider two fluids flowing in parallel or counter flow through passages separated by a permeable wall. Examples are hollow-fiber membrane modules used for separation processes such as filtration (Nakatsuka et al. 1996), membrane distillation (Yang et al. 2012) or hemodialysis/hemodiafiltration (Kerr and Huang 2010).

Often the fluids are solutions or suspensions sharing the same solvent (e.g. water) but differing in the concentration of one or more solutes or suspended solids on the two sides.

Considering only the hydrodynamic aspects of the problem, the flow of fluid across the dividing permeable wall alters the distribution of both flow rate and pressure in the two compartments. Here a simplified one-dimensional hydrodynamic model of the problem is presented and analytical solutions are derived. Results can be obtained for different configurations by imposing, for each compartment, the appropriate boundary conditions on inlet—outlet flow rates and/or pressures. Figure 4.1 is a conceptual sketch of the computational domain, showing also the basic nomenclature.

- L is the length of the module and Γ is the exchange perimeter, so that $S = L\Gamma$ is the total interfacial area;

M. Ciofalo, *Thermofluid Dynamics*, UNIPA Springer Series,
https://doi.org/10.1007/978-3-031-30470-5_4

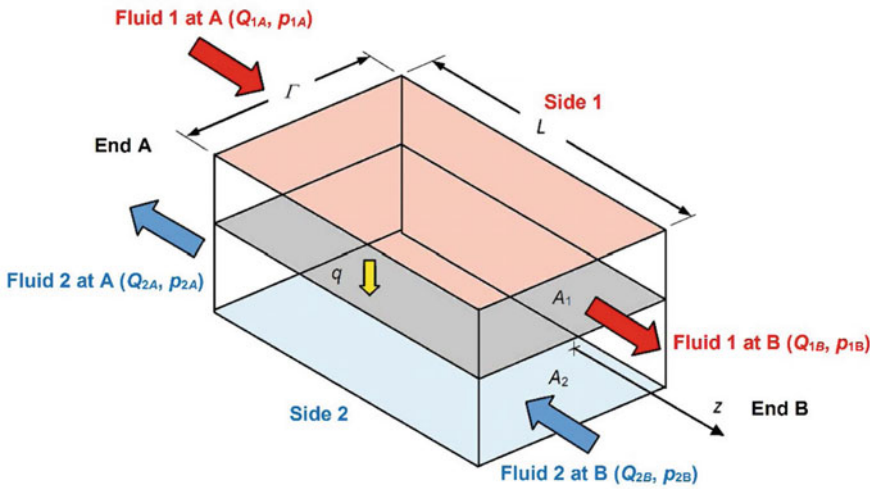

Fig. 4.1 Schematic hydrodynamic model of two fluids flowing in two compartments separated by a permeable wall

- Q_{jA} and Q_{jB} are the flow rates in m^3/s of fluid j ($j = 1$ or 2) at the two ends A and B. The generic flow rate Q_j at any location z in $[0, L]$ and its end values Q_{jA}, Q_{jB} are arbitrarily oriented so that they are positive if directed from A to B, i.e. along the z axis;
- p_{jA} and p_{jB} are the corresponding end pressures in Pa;
- A_1 and A_2 are the cross-sectional areas in m^2 of the two compartments, so that Q_k/A_k is the mean velocity U_k in the k-th compartment in m/s;
- q is the specific volumetric flux in m/s through the permeable membrane (oriented from compartment 1 to compartment 2), so that the net trans-membrane volumetric flow rate $1 \rightarrow 2$ in m^3/s is

$$\int_S q \mathrm{d}S = \Gamma \int_0^L q(z)\mathrm{d}z$$

The following simplifying assumptions are made:

- the trans-membrane flux does not alter the viscosities μ_1, μ_2 of the two fluids (of course, this assumption is trivially true if the two fluids share the same viscosity μ, while, if $\mu_1 \neq \mu_2$, it amounts to assuming that the net trans-membrane flow rate is small with respect to Q_1 and Q_2);
- the membrane is perfectly rigid;
- the flow in both compartments is Darcyan (i.e., the flow rate is proportional to the longitudinal pressure gradient).

Based on these assumptions and on the configuration in Fig. 4.1, the governing equations are the following, independent of the direction of either fluid.

(a) Continuity (volume balance) in compartments 1 and 2:

$$\frac{\mathrm{d}Q_1(z)}{\mathrm{d}z} = -\Gamma q(z) \tag{4.1}$$

$$\frac{\mathrm{d}Q_2(z)}{\mathrm{d}z} = +\Gamma q(z) \tag{4.2}$$

(b) Darcy equations in compartments 1 and 2:

$$Q_1(z) = -\beta_1 \frac{\mathrm{d}p_1(z)}{\mathrm{d}z} \tag{4.3}$$

$$Q_2(z) = -\beta_2 \frac{\mathrm{d}p_2(z)}{\mathrm{d}z} \tag{4.4}$$

in which $\beta_j = K_j A_j/\mu_j$ ($j = 1, 2$) (expressed in $\mathrm{m}^5\mathrm{s/kg}$), being K_j the Darcy permeability of the j-th compartment in m^2;

(c) Constitutive equation relating mass flux to trans-membrane pressure:

$$q(z) = L_p[p_1(z) - p_2(z)] \tag{4.5}$$

in which L_p is the membrane's hydraulic permeability in $\mathrm{m}^3/(\mathrm{m}^2\mathrm{sPa})$.

Taking account of Eq. (4.5), Eqs. (4.1), (4.2) can be re-written as

$$\frac{\mathrm{d}Q_1(z)}{\mathrm{d}z} = -\Gamma L_p\,[p_1(z) - p_2(z)] \tag{4.6}$$

$$\frac{\mathrm{d}Q_2(z)}{\mathrm{d}z} = +\Gamma L_p\,[p_1(z) - p_2(z)] \tag{4.7}$$

Equations (4.3), (4.4), (4.6) and (4.7) form a system of four first-order linear differential equations in the four unknowns Q_1, Q_2, p_1 and p_2.

By expressing Q_1 from Eq. (4.3) and substituting into Eq. (4.6), one has:

$$\frac{\mathrm{d}^2 p_1(z)}{\mathrm{d}z^2} = \frac{\Gamma L_p}{\beta_1}[p_1(z) - p_2(z)] \tag{4.8}$$

Similarly, by expressing Q_2 from Eq. (4.4) and substituting into Eq. (4.7):

$$\frac{\mathrm{d}^2 p_2(z)}{\mathrm{d}z^2} = -\frac{\Gamma L_p}{\beta_2}[p_1(z) - p_2(z)] \tag{4.9}$$

By subtracting Eq. (4.9) from Eq. (4.8) one obtains:

$$\frac{\mathrm{d}^2 \Delta p(z)}{\mathrm{d}z^2} = \alpha^2 \Delta p(z) \tag{4.10}$$

in which $\Delta p = p_1 - p_2$ and $\alpha^2 = \Gamma L_p \left(\frac{1}{\beta_1} + \frac{1}{\beta_2} \right)$

The general solution of the second-order differential Eq. (4.10) is

$$\Delta p(z) = c_1 e^{\alpha z} + c_2 e^{-\alpha z} \tag{4.11}$$

where c_1 and c_2 are two arbitrary integration constants. Substituting Δp from Eq. (4.11) into Eqs. (4.8) and (4.9) and integrating twice yields first

$$\frac{\mathrm{d}p_1(z)}{\mathrm{d}z} = \frac{\Gamma L_p}{\alpha \beta_1} \left(c_1 e^{\alpha z} + c_2 e^{-\alpha z} \right) + c_3 \tag{4.12}$$

$$\frac{\mathrm{d}p_2(z)}{\mathrm{d}z} = -\frac{\Gamma L_p}{\alpha \beta_2} \left(c_1 e^{\alpha z} + c_2 e^{-\alpha z} \right) + c_3 \tag{4.13}$$

and then

$$p_1(z) = \frac{\Gamma L_p}{\alpha^2 \beta_1} \left(c_1 e^{\alpha z} + c_2 e^{-\alpha z} \right) + c_3 z + c_4 \tag{4.14}$$

$$p_2(z) = -\frac{\Gamma L_p}{\alpha^2 \beta_2} \left(c_1 e^{\alpha z} + c_2 e^{-\alpha z} \right) + c_3 z + c_4 \tag{4.15}$$

in which c_3 and c_4 are two further integration constants.

Substituting the pressure derivatives from Eqs. (4.12), (4.13) into Eqs. (4.3), (4.4) yields, for the flow rates:

$$Q_1(z) = -\frac{\Gamma L_p}{\alpha} \left(c_1 e^{\alpha z} - c_2 e^{-\alpha z} \right) - \beta_1 c_3 \tag{4.16}$$

$$Q_2(z) = \frac{\Gamma L_p}{\alpha} \left(c_1 e^{\alpha z} - c_2 e^{-\alpha z} \right) - \beta_2 c_3 \tag{4.17}$$

Solutions depend now on the boundary conditions, specific for each physical configuration considered. Two cases will be treated here, but others are possible.

Case 1): fluids in counter flow with forward- and back-filtration, as commonly encountered in hemodialysis modules.

In this case, assuming that for each fluid the inlet flow rate and the outlet pressure are known, and that the flow rate is positive (A → B) for fluid 1, the appropriate boundary conditions are:

$$Q_1(0) = Q_{1A}(> 0) \tag{4.18}$$

$$Q_2(L) = Q_{1B}(< 0) \tag{4.19}$$

$$p_1(L) = p_{1B} \tag{4.20}$$

$$p_2(0) = p_{2A} \tag{4.21}$$

Taking account of Eqs. (4.14)–(4.17), the above BC's yield a system of four algebraic equations in the four unknowns $c_1 \ldots c_4$:

$$-\frac{\Gamma L_p}{\alpha}(c_1 - c_2) - \beta_1 c_3 = Q_{1A} \tag{4.22}$$

$$\frac{\Gamma L_p}{\alpha}\left(c_1 e^{\alpha L} - c_2 e^{-\alpha L}\right) - \beta_2 c_3 = Q_{2B} \tag{4.23}$$

$$\frac{\Gamma L_p}{\alpha^2 \beta_1}\left(c_1 e^{\alpha L} + c_2 e^{-\alpha L}\right) + c_3 L + c_4 = p_{1B} \tag{4.24}$$

$$-\frac{\Gamma L_p}{\alpha^2 \beta_2}(c_1 + c_2) + c_4 = p_{2A} \tag{4.25}$$

The (somewhat cumbersome) solution of the above system yields

$$c_1 = \frac{a_{22} b_1 - a_{12} b_2}{a_{11} a_{22} - a_{12} a_{21}} \tag{4.26}$$

$$c_2 = \frac{a_{11} b_2 - a_{21} b_1}{a_{11} a_{22} - a_{12} a_{21}} \tag{4.27}$$

$$c_3 = \frac{p_{1B} - p_{2A}}{L} - \frac{\Gamma L_p}{\alpha^2 \beta_2 L}(c_1 + c_2) - \frac{\Gamma L_p}{\alpha^2 \beta_1 L}\left(c_1 e^{\alpha L} + c_2 e^{-\alpha L}\right) \tag{4.28}$$

$$c_4 = p_{2A} + \frac{\Gamma L_p}{\alpha^2 \beta_2}(c_1 + c_2) \tag{4.29}$$

in which the terms a and b are defined as

$$a_{11} = \frac{\Gamma L_p}{\alpha}\left[-1 + \frac{1}{\alpha L}\left(\frac{\beta_1}{\beta_2} + e^{\alpha L}\right)\right] \tag{4.30}$$

$$a_{12} = \frac{\Gamma L_p}{\alpha}\left[1 + \frac{1}{\alpha L}\left(\frac{\beta_1}{\beta_2} + e^{-\alpha L}\right)\right] \tag{4.31}$$

$$a_{21} = \frac{\Gamma L_p}{\alpha} e^{\alpha L}\left[1 + \frac{1}{\alpha L}\left(\frac{\beta_2}{\beta_1} + e^{-\alpha L}\right)\right] \tag{4.32}$$

$$a_{22} = \frac{\Gamma L_p}{\alpha} e^{-\alpha L}\left[-1 + \frac{1}{\alpha L}\left(\frac{\beta_2}{\beta_1} + e^{\alpha L}\right)\right] \tag{4.33}$$

$$b_1 = Q_{1A} + \beta_1 \frac{p_{1B} - p_{2A}}{L} \tag{4.34}$$

$$b_2 = Q_{2B} + \beta_2 \frac{p_{1B} - p_{2A}}{L} \tag{4.35}$$

The complete solution is now given by Eqs. (4.14)–(4.15) for the two pressures and by Eqs. (4.16)–(4.17) for the two flow rates, in which the constants $c_1 \ldots c_4$ are given by Eqs. (4.26)–(4.29) with the positions (4.30)–(4.35).

As an example of the results, Fig. 4.2 compares profiles of pressure (a) and flow rate (b) computed for different values of the wall hydraulic permeability L_p from 10^{-10} m/(sPa) (practically impermeable wall) to 10^{-8} m/(sPa). The remaining data are representative of a hollow-fiber cartridge for hemodiafiltration (Cancilla et al. 2022): $L = 0.244$ m, $\Gamma = 7.21$ m, $A_1 = 3.14 \cdot 10^{-4}$ m^2, $A_2 = 5.38 \cdot 10^{-4}$ m^2, $K_1 = 3.58 \cdot 10^{-10}$ m^2, $K_2 = 8.64 \cdot 10^{-10}$ m^2, $Q_{1A} = 300$ ml/min, $Q_{2B} = -500$ ml/min (oriented flow rates), $p_{1B} = p_{2A} = 0$ (relative outlet pressures) and $\mu_1 = \mu_2 = 0.9 \cdot 10^{-3}$ Pa s (viscosities).

In the presence of a permeable wall, and provided the outlet pressures are such that the pressure profiles exhibit the "butterfly" shape in Fig. 4.2a, in both compartments the flow rate decreases (in absolute value) from the inlet to some intermediate distance and then increases back. The inlet-to-outlet pressure drop decreases significantly in both compartments with respect to the impermeable wall case.

Case 2): dead-end filtration.

In this case, identifying fluid 1 with the feed and fluid 2 with the permeate, the appropriate boundary conditions are:

$$Q_1(0) = Q_{1A} (> 0) \tag{4.36}$$

$$Q_1(L) = 0 \tag{4.37}$$

$$Q_2(0) = 0 \tag{4.38}$$

$$p_2(L) = p_{2B} \tag{4.39}$$

The further condition $Q_2(L) = Q_1(0) = Q_{1A}$ is implicated by the balance Eqs. (4.6)–(4.7) and thus is redundant.

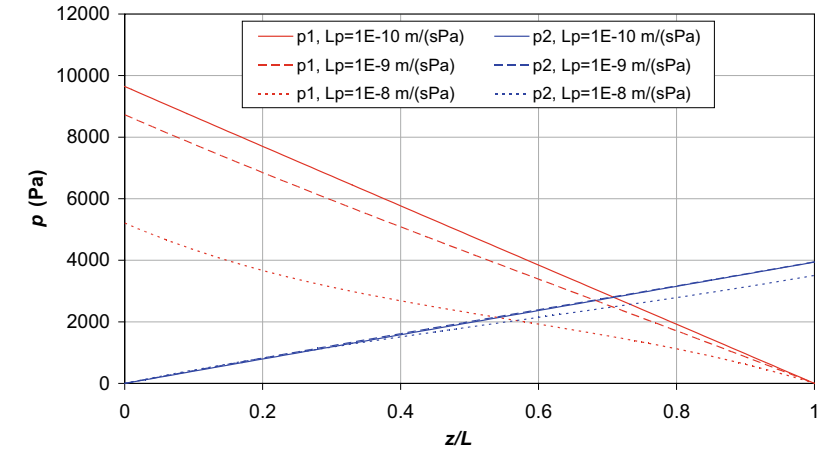

(a)

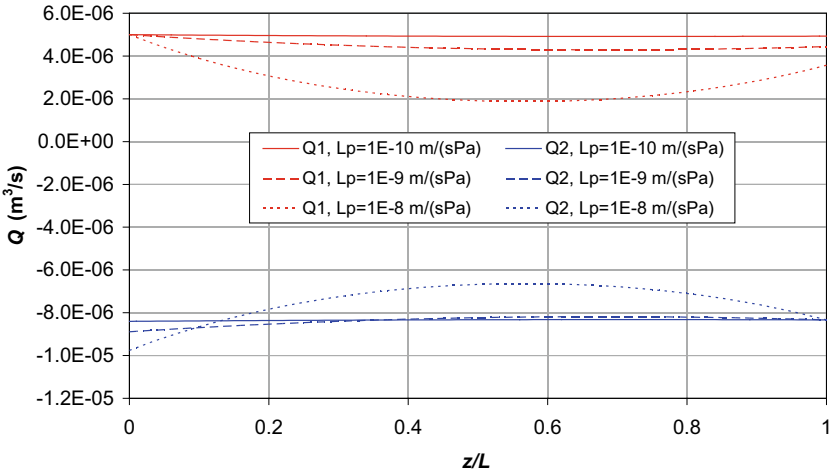

(b)

Fig. 4.2 Profiles of pressures **a** and flow rates **b** computed under conditions representative of a hollow-fiber cartridge for hemodiafiltration and $L_p = 10^{-10}$ to 10^{-8} m^3/(m^{2}sPa)

Taking account of Eqs. (4.14)–(4.17), the above BC's yield the following system of 4 algebraic equations in the four unknowns $c_1 \ldots c_4$:

$$-\frac{\Gamma L_p}{\alpha}(c_1 - c_2) - \beta_1 c_3 = Q_{1A} \tag{4.40}$$

$$-\frac{\Gamma L_p}{\alpha}\left(c_1 e^{\alpha L} - c_2 e^{-\alpha L}\right) - \beta_1 c_3 = 0 \tag{4.41}$$

$$\frac{\Gamma L_p}{\alpha}(c_1 - c_2) - \beta_2 c_3 = 0 \tag{4.42}$$

$$-\frac{\Gamma L_p}{\alpha^2 \beta_2}\left(c_1 e^{\alpha L} + c_2 e^{-\alpha L}\right) + c_3 L + c_4 = p_{2B} \tag{4.43}$$

The solution of the sub-system of Eqs. (4.40)–(4.42) in $c_1 \ldots c_3$ yields

$$c_1 = Q_{1A}\frac{\alpha}{\Gamma L_p}\frac{1 + (\beta_2/\beta_1)e^{-\alpha L}}{(1 + \beta_2/\beta_1)\left(e^{\alpha L} - e^{-\alpha L}\right)} \tag{4.44}$$

$$c_2 = Q_{1A}\frac{\alpha}{\Gamma L_p}\frac{1 + (\beta_2/\beta_1)e^{\alpha L}}{(1 + \beta_2/\beta_1)\left(e^{\alpha L} - e^{-\alpha L}\right)} \tag{4.45}$$

$$c_3 = -\frac{\Gamma L_p}{\alpha \beta_1}\left(c_1 e^{\alpha L} - c_2 e^{-\alpha L}\right) \tag{4.46}$$

while the stand-alone Eq. (4.43) yields

$$c_4 = p_{2B} + \frac{\Gamma L_p}{\alpha^2 \beta_2}\left(c_1 e^{\alpha L} + c_2 e^{-\alpha L}\right) - c_3 L \tag{4.47}$$

The complete solution is now given by Eqs. (4.14)–(4.15) for the two pressures and by Eqs. (4.16)–(4.17) for the two flow rates, in which the constants c_1–c_4 are given by Eqs. (4.44)–(4.47).

As an example of the results, Fig. 4.3 compares profiles of pressure (a) and flow rate (b) computed for different values of the wall hydraulic permeability L_p from 10^{-10} (practically impermeable wall) to 10^{-8} m^3/(m^{2}s Pa). The remaining data are representative of a hollow-fiber filter cartridge for the production of ultra-pure water: $L = 0.15$ m, $\Gamma = 5$ m, viscosities, areas and Darcy permeabilities as in case 1 ($\mu_1 = \mu_2 = 0.9 \cdot 10^{-3}$ Pa s, $A_1 = 3.14 \cdot 10^{-4}$ m^2, $A_2 = 5.38 \cdot 10^{-4}$ m^2, $K_1 = 3.58 \cdot 10^{-10}$ m^2, $K_2 = 8.64 \cdot 10^{-10}$ m^2), $Q_{1A} = 100$ mL/min (feed flow rate) and $p_{2B} = 0$ (relative outlet pressures).

Note that a logarithmic scale was used for pressures. For any value of L_p, the pressure in the permeate compartment (2) remains low while that in the feed compartment (1) increases approximately as $1/L_p$. Profiles of flow rate along the filter length are roughly linear in all cases.

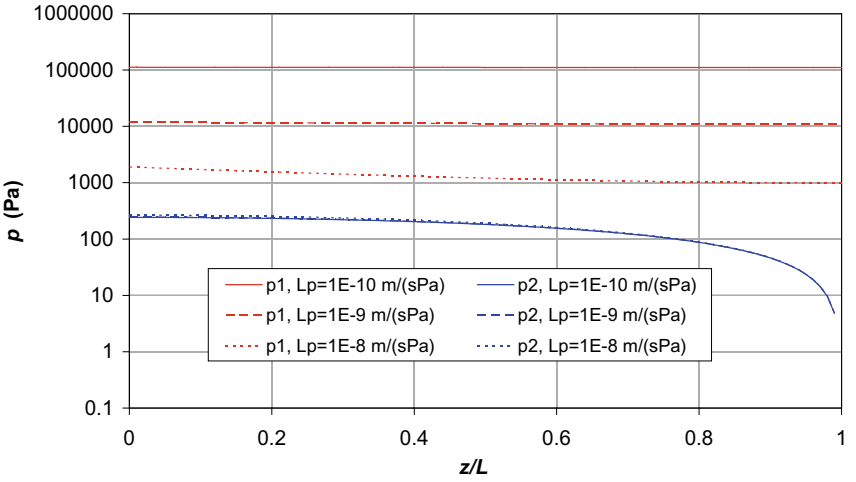

(a)

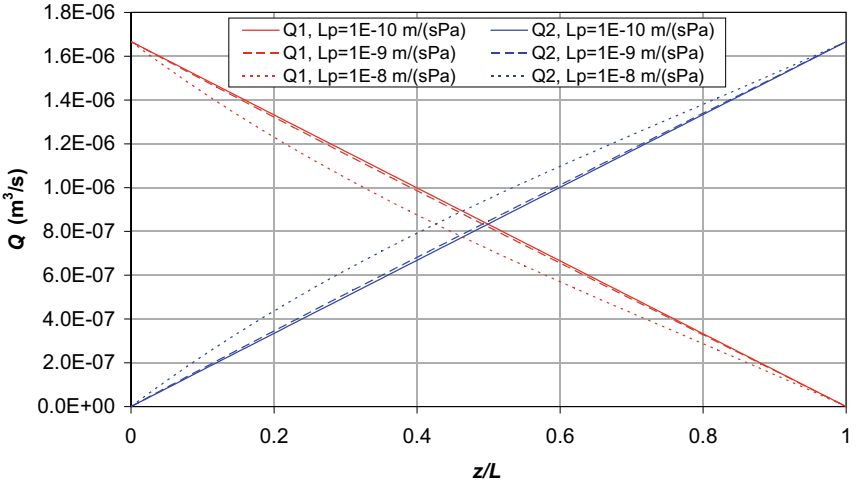

(b)

Fig. 4.3 Profiles of pressures **a** and flow rates **b** computed under conditions representative of a hollow-fiber cartridge for dead-end filtration and $L_p = 10^{-10}$ to 10^{-8} m^3/(m^{2}s Pa)

Chapter 5
Laminar Oscillatory Flow in a Plane Channel

A theory with mathematical beauty is more likely to be correct than an ugly one that fits some experimental data
(*Paul Dirac*)

Abstract This problem regards the oscillatory flow in a plane channel subject to a harmonic forcing $F_x(t) = F_0\cos(\omega t)$. An analytic solution to the relevant Navier–Stokes equations, highly simplified by the assumption of parallel flow, was presented for example by Landau and Lifshitz (1959) and later by other authors and is discussed here under two possible physical interpretations.

The simplest oscillatory flow is that studied in the so called *Stokes' second problem* (Stokes 1850): the motion of a viscous fluid adjacent to an indefinite plane wall which oscillates harmonically along x with velocity

$$u_w(t) = u_0 \sin(wt) \tag{5.1}$$

The analytical solution found by Stokes for the fluid's velocity is:

$$u(y, t) = u_0 \exp(-y/l_S) \sin(wt - y/l_S) \tag{5.2}$$

where y is the normal distance from the wall and $l_S = (2\nu/\omega)^{1/2}$. Today l_S is called *Stokes length*, and the near-wall region of thickness l_S is called *Stokes layer*. Equation (5.2) shows that the perturbation caused by the wall's motion decreases exponentially with y and penetrates a few Stokes lengths into the fluid.

Only slightly more complex is the oscillatory flow in a channel. The problem has been investigated for its relevance in physiology (Womersely 1955) but finds applications also in the field of industrial engineering (Mackley and Stonestreet 1995). Often the flow is classified as *pulsatile* when the flow rate oscillates about a non-zero mean value, *reciprocating* when this value is nil.

In the following, we will consider an indefinite plane channel of half height δ, with the origin of the coordinate y in the channel's midplane (Fig. 5.1).

M. Ciofalo, *Thermofluid Dynamics*, UNIPA Springer Series,
https://doi.org/10.1007/978-3-031-30470-5_5

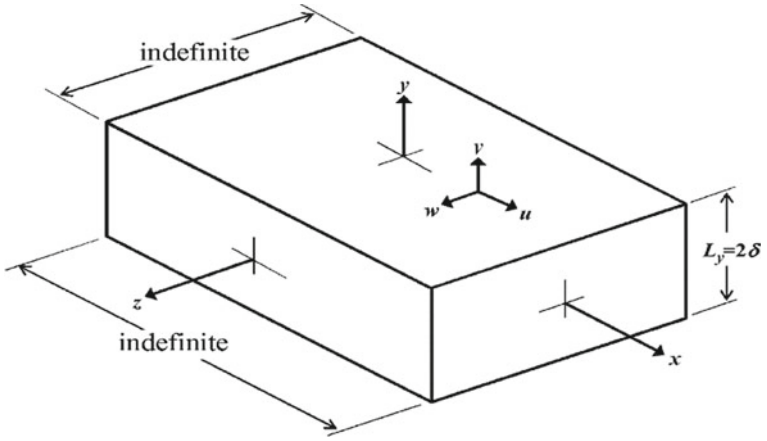

Fig. 5.1 A streamwise and spanwise indefinite plane channel

We will first consider the case of *reciprocating* flow. In the laminar regime, the flow is purely parallel, $\mathbf{u} = (u, 0, 0)$, and is a function of only y and time. The only relevant Navier–Stokes equation is that along x and reduces to

$$\frac{\partial u}{\partial t} = \nu \frac{\partial^2 u}{\partial y^2} + \frac{1}{\rho} F_x(t) \tag{5.3}$$

in which F_x is a forcing term (dimensionally, a force per unit volume) which can be interpreted either as a pressure gradient or as a body force, as will be discussed below. In any case, F_x is assumed to vary harmonically in time as

$$F_x(t) = F_0 \cos(wt) \tag{5.4}$$

The hydrodynamic problem consists of determining $u(y, t)$ for any choice of δ, F_0, ω and fluid's physical properties (density ρ, viscosity $\mu = \rho\nu$). The main parameter controlling the solution is the ratio between the momentum diffusion time scale (viscous scale), δ^2/ν, and the period of the forced oscillation, $T = 2\pi/\omega$. It is customary to use the *Womersley number* α, proportional to the square root of the above ratio:

$$\alpha = \delta\sqrt{\omega/\nu} \tag{5.5}$$

If $T \gg \delta^2/\nu$ (slow oscillations, small α) the Stokes layer has time to grow along the channel's walls as the harmonic forcing term increases, and the u profile follows closely a sequence of stationary Poiseuille profiles $u(y, t) = F_x/(2\mu) \times (\delta^2 - y^2)$. Contrarywise, if $T \ll \delta^2/\nu$ (rapid oscillations, large α), instantaneous u profiles are affected by inertial terms and differ largely from the parabolic, steady-state shape; they may exhibit local maxima out of the midplane and also change sign along y.

Maxima of u are smaller than the steady-state value $F_x\delta^2/(2\mu)$ and are out of phase with respect to the forcing term; amplitude damping and phase lag increase with α.

The analytical solution for $u(y, t)$ was given, in a rather concise form, by Landau and Lifschitz (1959); a more explicit formulation was presented by Loudon and Tordesillas (1998):

$$u(y,t) = \frac{F_0}{\omega\rho\beta_W}\{[\sinh\varphi_1(y)\sin\varphi_2(y) + \sinh\varphi_2(y)\sin\varphi_1(y)]\cos(\omega t) + [\beta_W - \cosh\varphi_1(y)\cos\varphi_2(y) - \cosh\varphi_2(y)\cos\varphi_1(y)]\sin(\omega t)\} \quad (5.6)$$

in which

$$\varphi_1(y) = \frac{\alpha}{\sqrt{2}}\left(1 + \frac{y}{\delta}\right) \quad (5.7)$$

$$\varphi_2(y) = \frac{\alpha}{\sqrt{2}}\left(1 - \frac{y}{\delta}\right) \quad (5.8)$$

$$\beta_W = \cosh\left(\sqrt{2}\alpha\right) + \cos\left(\sqrt{2}\alpha\right) \quad (5.9)$$

The problem admits two distinct physical interpretations.

On one hand, F_x can be regarded as a pressure gradient, $F_x = -\mathrm{d}p/\mathrm{d}x$, applied to a fluid confined between fixed walls; in this case, u is the absolute velocity in the laboratory reference frame.

As an alternative, more consistent with Stokes' second problem, the channel's walls can be assumed to move along x according to the harmonic law

$$x_w = x_0\cos(wt) \quad (5.10)$$

which implies velocity and acceleration

$$\dot{x}_w = -\omega x_0\sin(\omega t) \quad (5.11)$$

$$\ddot{x}_w = -\omega^2 x_0\cos(\omega t) \quad (5.12)$$

In this second interpretation, the channel can be assumed to be open at both ends to a uniform-pressure environment, so that no pressure gradient exists and the *true* force F_x is nil. However, if the resulting flow is described with respect to an accelerated (*non-inertial*) reference frame integral with the walls, then a fictitious acceleration, opposite to that of the walls, must be added to the RHS of the momentum equation. This is obtained by setting $F_0 = \rho\omega^2 x_0$ in Eq. (5.4). In this case, u must be interpreted as the velocity of the fluid relative to the walls, while its absolute velocity (in the laboratory reference frame) will be

$$u_{abs}(y,t) = u(y,t) + \dot{x}_W(t) = u(y,t) - wx_0\sin(wt) \quad (5.13)$$

Note that the amplitude u_0 of the walls' velocity $\dot{x}_w$ is $\omega x_0 = F_0/(\rho\omega)$.

As an example of the results obtained for different values of the Womersley number, Figs. 5.2 and 5.3 report the cross-stream profiles of u (a) and u_{abs} (b) at different phase angles ωt for $\alpha = 1$ and $\alpha = 5$, respectively. In both cases, velocities are normalized with respect to u_0 and their profiles are reported only for $y \leq 0$ since they are symmetric with respect to the midplane.

For low α, Fig. 5.2, the velocity perturbation caused by the oscillating walls (or pressure gradient) has time to diffuse to the bulk of the fluid during a semi-period, and the flow field can be described as a sequence of steady parabolic (Poiseuille) profiles in instantaneous equilibrium with the applied forcing. Velocity maxima are attained for $\omega t \approx 0$, in phase with the forcing term.

Results are different for higher α, Fig. 5.3. A noteworthy feature of the solution is evidenced by the absolute velocity profiles in Fig. 5.3b: the central region of the fluid moves very little with respect to the laboratory reference frame through the whole period of the oscillations, while only the fluid layers adjacent to the walls follow the harmonic oscillations of these latter. Therefore, with respect to the walls, Fig. 5.3a, the bulk of the fluid oscillates with a velocity amplitude close to that of the walls themselves, $u_0 = F_0/(\rho\omega)$. The maximum relative velocity is attained for $\omega t \approx 90°$, in quadrature with the forcing term $F(t)$.

Velocity damping can be better appreciated by comparing the peak value of the midplane velocity, u_{peak}, with the value that would be attained if F_0 were applied statically, which is the Poiseuille value $(u_{peak})_0 = F_0\delta^2/(2\mu)$.

Figure 5.4 reports Bode plots of the amplitude damping $u_{peak}/(u_{peak})_0$ (a) and of the associated phase lag (b) as functions of the Womersley number α. Note that, as shown in Fig. 5.2a, for large α peak velocities may be attained at locations away from the midplane. Figure 5.3 shows that, for $\alpha > 2$–3, the amplitude of the peak midplane velocity decreases as α^{-2}. The phase lag increases as α^2 up to $\alpha \approx 1$ and attains its limiting value of 90° for $\alpha \approx 3$.

If a laminar, parallel channel flow is *pulsatile* rather than reciprocating, i.e., if the mean value of the flow rate is *not* nil, then the linear nature of the governing Eq. (5.3) allows the overall instantaneous flow to be obtained as the simple superposition of its constant component and its oscillatory component, the former being the Poiseuille solution and the latter being identical to the above solution for reciprocating flow (principle of superposition of effects). Therefore, the case of pulsatile flow does *not* present any real novelty with respect to reciprocating flow.

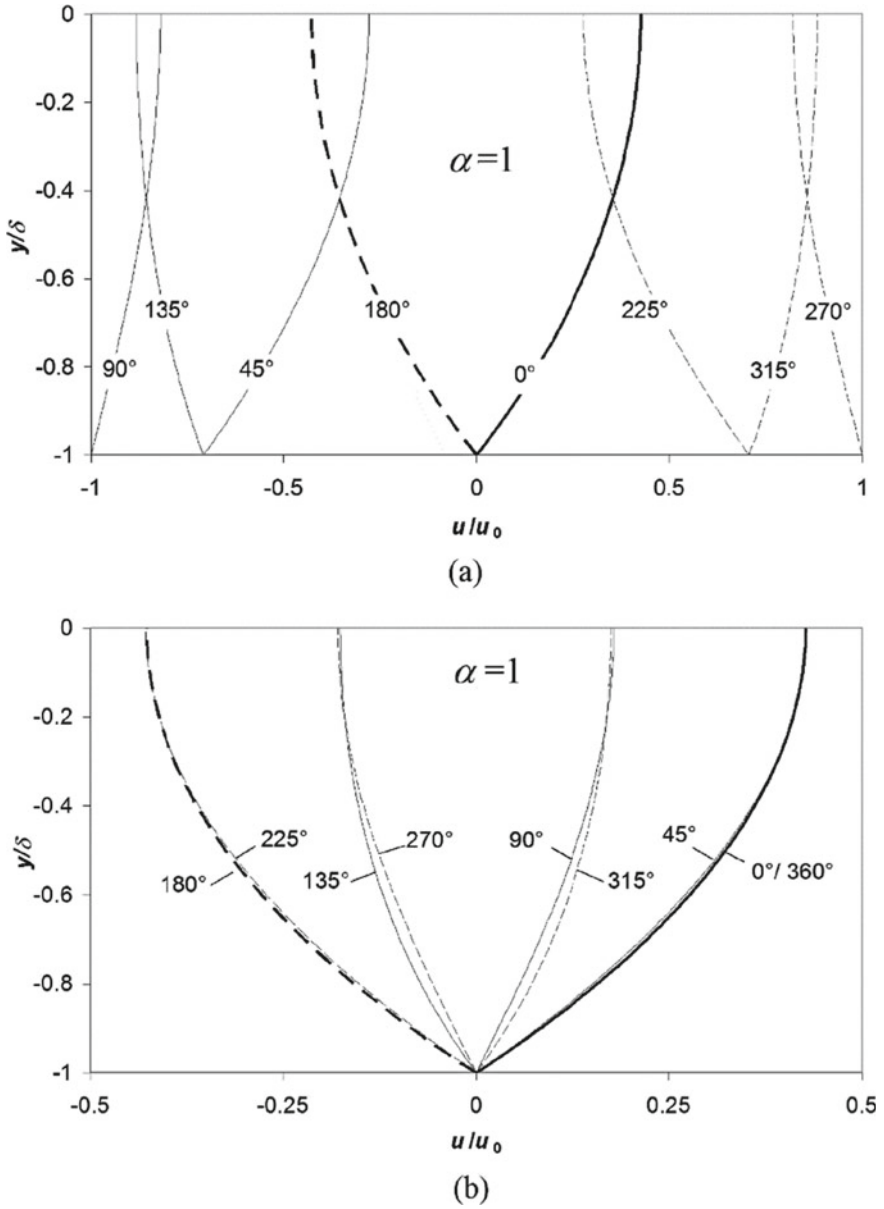

Fig. 5.2 Case $\alpha = 1$: cross stream velocity profiles, normalized by $u_0 = F_0/(\rho\omega)$, at different phase angles ωt. **a** Velocity relative to oscillating walls, equal to the velocity in a still channel under the effect of an oscillating pressure gradient; **b** absolute velocity between oscillating walls

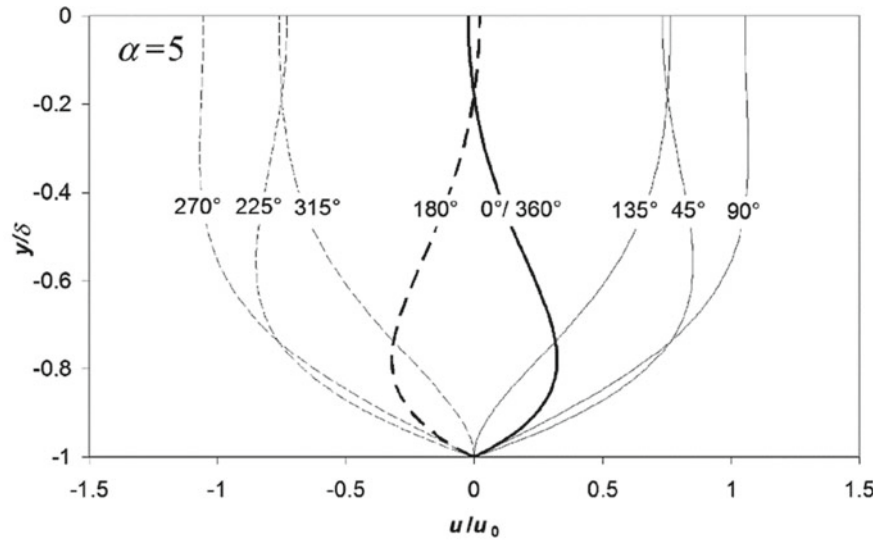

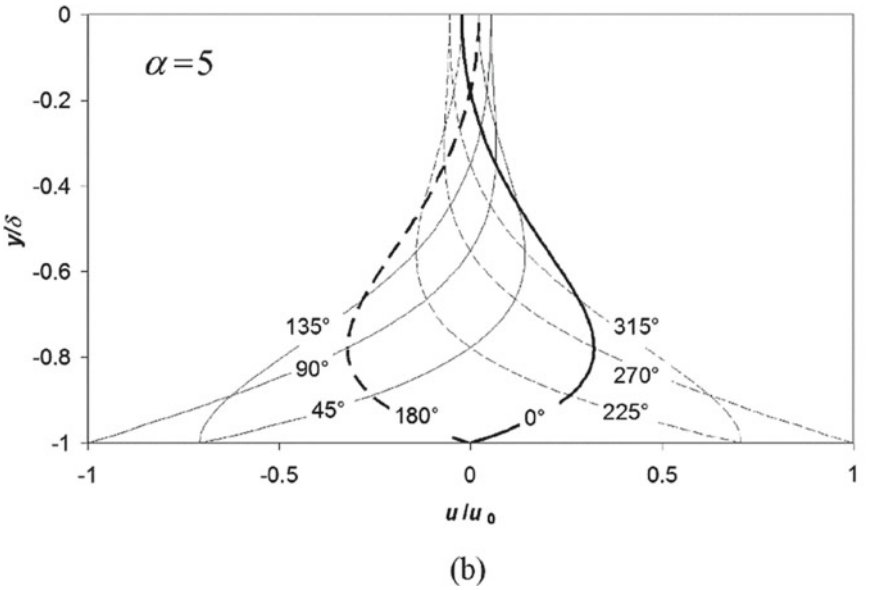

Fig. 5.3 Case $\alpha = 5$: cross stream velocity profiles, normalized by $u_0 = F_0/(\rho\omega)$, at different phase angles ωt. **a** Velocity relative to oscillating walls, equal to the velocity in a still channel under the effect of an oscillating pressure gradient; **b** absolute velocity between oscillating walls

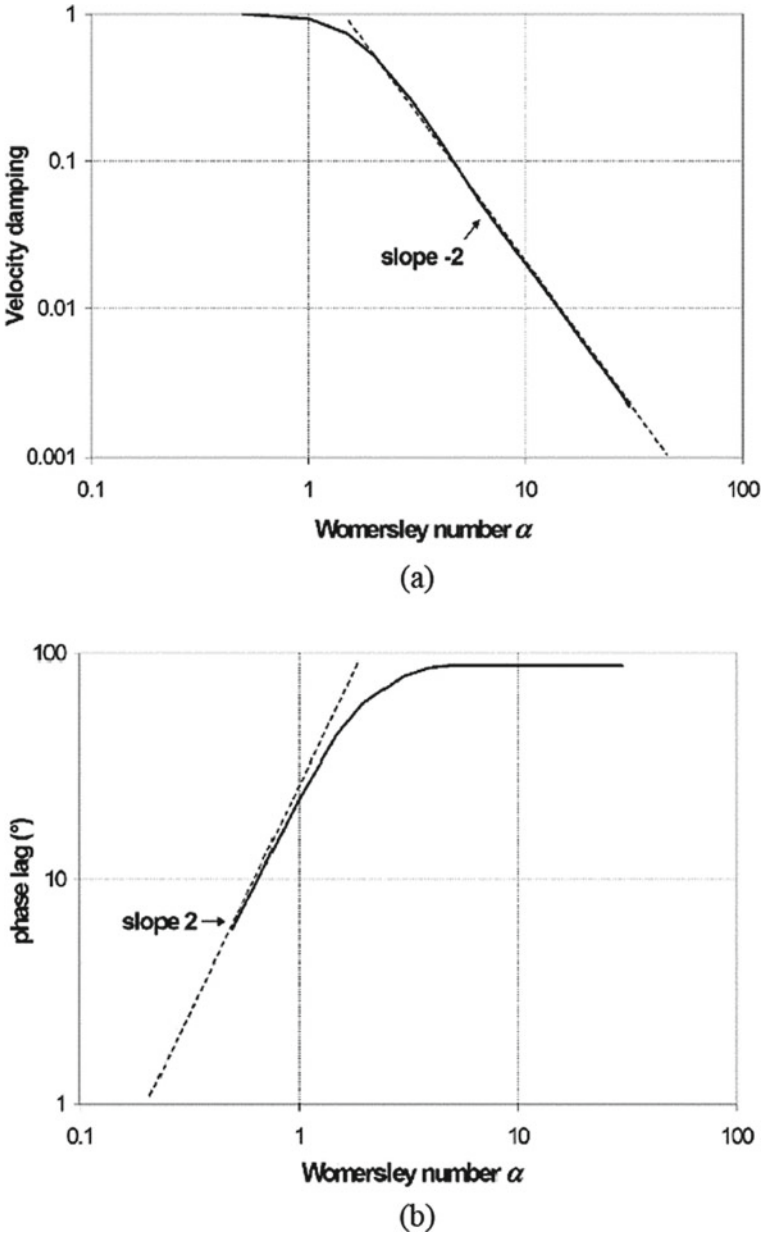

Fig. 5.4 Bode plots of the amplitude damping **a** and of the phase lag **b** of the velocity at the midplane as functions of the Womersley number α for laminar reciprocating flow in a plane channel

Chapter 6
Nusselt Number in Channel Flow with General Thermal Boundary Conditions

Before I came here I was confused about this subject. Having listened to your lecture I am still confused. But on a higher level (*Enrico Fermi*)

Abstract The classic solutions for the Nusselt number in parallel channel flow under conditions of uniform wall temperature and uniform wall heat flux are generalized by imposing third type (Robin) thermal boundary conditions. As a dimensionless parameter R, expressing the ratio of the wall thermal resistance to the channel's conductive resistance, varies between 0 and infinity, the two above limiting conditions are recovered, while intermediate values of R yield an intermediate Nusselt number that varies continuously between the two extrema.

Consider the steady, hydrodynamically and thermally fully developed, flow of a constant-property fluid in a streamwise and spanwise indefinite plane channel of half-thickness δ (as in Fig. 5.1). Let x and y be the streamwise and cross stream directions, with $y = 0$ at the midplane, and let $u(y)$ be the velocity along x, U its average, $T(x, y)$ the temperature and $\alpha = \lambda/(\rho c_p)$ the thermal diffusivity.

Let us first deal with the case of symmetric two-side cooling, which can be characterized by a symmetry condition at the midplane and a general (3rd type, or Robin) boundary conditions at one wall:

$$\left[\frac{\partial T}{\partial y}\right]_0 = 0; \quad -\lambda\left[\frac{\partial T}{\partial y}\right]_\delta = \frac{1}{r}[T(x,\delta) - T_\infty] \tag{6.1}$$

T_∞ being a uniform external temperature and r an interposed thermal resistance. Let $\vartheta = T - T_\infty$ and

$$\vartheta_b = \frac{1}{2\delta\rho U}\int_{-\delta}^{\delta} \vartheta\, u\, \mathrm{d}y \tag{6.2}$$

M. Ciofalo, *Thermofluid Dynamics*, UNIPA Springer Series,
https://doi.org/10.1007/978-3-031-30470-5_6

its bulk (i.e., mass flow averaged) value. By introducing the following dimensionless variables:

$$\eta \equiv \frac{y}{\delta}; \xi \equiv \frac{x}{\delta}; \tilde{u} \equiv \frac{u}{U}; \mathrm{Pe}_\delta \equiv \frac{U\delta}{\alpha} \tag{6.3}$$

the Poiseuille velocity distribution and the energy balance equation can be written

$$\tilde{u} = \frac{3}{2}\left(1 - \eta^2\right) \tag{6.4}$$

$$\frac{\partial^2 \vartheta}{\partial \eta^2} = Pe_\delta \, \tilde{u} \frac{\partial \vartheta}{\partial \xi} \tag{6.5}$$

The assumption of thermally fully developed flow implies

$$\vartheta = \vartheta_b(x)\varphi(y) \tag{6.6}$$

so that Eq. (6.5) can be written

$$\frac{1}{\varphi \tilde{u}} \frac{d^2\varphi}{d\eta^2} = Pe_\delta \frac{d\vartheta_b}{d\xi} \tag{6.7}$$

Following the method of separation of variables, Eq. (6.7) splits into the two distinct equations

$$\frac{1}{\varphi \tilde{u}} \frac{d^2\varphi}{d\eta^2} = -B^2 \tag{6.8}$$

$$\mathrm{Pe}_\delta \frac{1}{\vartheta_b} \frac{\mathrm{d}\vartheta_b}{\mathrm{d}\xi} = -B^2 \tag{6.9}$$

in which the constant $-B^2$ must be negative for physical reasons (for example, $\vartheta_b > 0$ implies $\mathrm{d}\vartheta_b/\mathrm{d}\xi < 0$, i.e. cooled fluid).

By substituting the velocity profile of Eq. (6.4) into Eq. (6.8) one obtains

$$\frac{\mathrm{d}^2\varphi}{\mathrm{d}\eta^2} + \frac{3}{2}B^2\left(1 - \eta^2\right)\varphi = 0 \tag{6.10}$$

This is a non-integrable ODE with non-constant coefficients which must be solved numerically. The boundary conditions for φ are derived from Eqs. (6.1) and (6.6):

$$\left[\frac{d\varphi}{d\eta}\right]_0 = 0; \quad \varphi(1) = B^2 R \tag{6.11}$$

in which $R = r\lambda/\delta$ (dimensionless thermal resistance). The following condition must also be satisfied:

$$\left[\frac{d\varphi}{d\eta}\right]_1 = -B^2 \tag{6.12}$$

which is derived from the enthalpy balance:

$$-\lambda\left[\frac{\partial\vartheta}{\partial y}\right]_\delta = -\delta\rho c_p U\frac{\mathrm{d}\vartheta_b}{\mathrm{d}x} \tag{6.13}$$

Conceptually, Eq. (6.10) for $\varphi(\eta)$, with B.C.'s (6.11), must be solved numerically for any generic value of B^2, which must be made to vary so as to satisfy Eq. (6.12). A simple iterative procedure was implemented in Fortran to perform this calculation. After convergence, the heat transfer coefficient is

$$h = \frac{q''_w}{\vartheta_b} = -\frac{\lambda}{\delta\vartheta_b}\left[\frac{\partial\vartheta}{\partial\eta}\right]_\delta \tag{6.14}$$

which can be made dimensionless as a Nusselt number $\mathrm{Nu} = h(4\delta/\lambda)$ (based on the channel hydraulic diameter 4δ). From the above equations and definitions it follows that

$$\mathrm{Nu} = \frac{4}{R}\frac{\varphi(1)}{1-\varphi(1)} \tag{6.15}$$

Note that a different value of Nu and a different profile $\varphi(\eta)$ are computed for each choice of the dimensionless thermal resistance R. Note also that the Dirichlet and Neumann conditions are obtained as limiting cases for $R = 0$ and $R \to \infty$, respectively. The function $\mathrm{Nu}(R)$ is represented in Fig. 6.1 by the "Two-side" line.

Consider then the case of one-side cooling, i.e. cooling from one wall with the opposite wall adiabatic. The thermal boundary conditions (6.1) are replaced by

$$\left[\frac{\partial T}{\partial y}\right]_{-\delta} = 0; \quad -\lambda\left[\frac{\partial T}{\partial y}\right]_\delta = \frac{1}{r}[T(x,\delta) - T_\infty] \tag{6.16}$$

and their dimensionless counterparts (6.11) are replaced by

$$\left[\frac{\partial\varphi}{\partial\eta}\right]_{-1} = 0; \quad \varphi(1) = 2B^2R \tag{6.17}$$

while all other equations and definitions remain unchanged. The solution for Nu is reported in Fig. 6.1 as the "One-side" line. Note the lower levels of Nu with respect to the "Two-side" case.

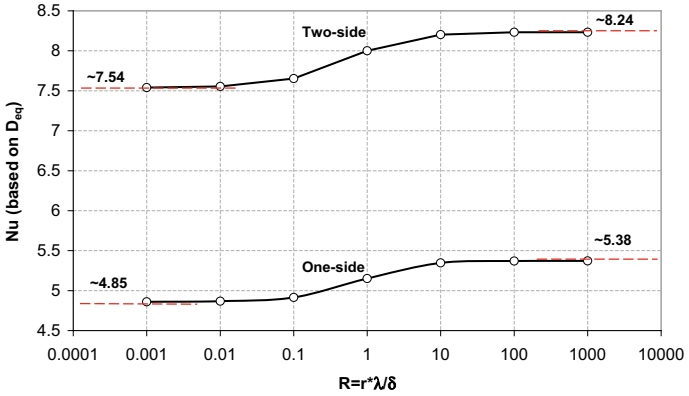

Fig. 6.1 Nusselt number in a plane channel as a function of the dimensionless thermal resistance R

The above results can easily be extended to the case of parallel flow in a cylindrical duct. Also, by substituting mass transfer resistances for thermal resistances and a Schmidt number for the Prandtl number, the results can be interpreted as predicting the Sherwood number (dimensionless mass transfer coefficient) *in lieu* of the Nusselt number.

Chapter 7
Buoyant Flow in a Duct or a Loop

The light dove, cleaving the air in her free flight, and feeling its resistance, might imagine that its flight would be still easier in empty space
(*Immanuel Kant*)

Abstract Buoyant flow in a heated duct is considered. The one-dimensional momentum equation for the fluid, in conjunction with the classic Boussinesq approximation for thermal expansion and with a suitable friction correlation, form a closed system of equations whose exact steady-state solution is the fluid's flow rate as a function of the imposed inlet/outlet pressures and of the thermal power input. Several special cases can be obtained by letting the boundary conditions, the duct's inclination and other parameters vary. The case of a closed loop with simultaneous heat addition and subtraction can be treated similarly and the solution is the circulating flow rate as a function of the thermal power input/output.

(a) *Duct*. Consider first the steady-state flow of a thermally dilatable fluid in a heated (or cooled) duct of uniform cross section A, between Sections 1 and 2 in the presence of a gravitational field (Fig. 7.1).

Let G be the fluid's mass flow rate, g the acceleration of gravity and q' a uniform linear thermal power density (positive or negative) entering the fluid.

We want to express the relation linking the pressure difference $p_1 - p_2$ between Sections 1 and 2 to the mass flow rate G in the presence of thermal buoyancy.

The live forces theorem, written for an infinitesimal tract $\mathrm{d}z$ of duct, gives:

$$\alpha U dU = -g\mathrm{d}z - v\mathrm{d}p - \delta r \tag{7.1}$$

The left hand side of this equation is the infinitesimal increase of the fluid's kinetic energy per unit mass; U is the mean (i.e., cross section-averaged) velocity and α is a shape coefficient which depends on the velocity distribution and is very close to unity in the case of turbulent flow (flat velocity distribution).

M. Ciofalo, *Thermofluid Dynamics*, UNIPA Springer Series,
https://doi.org/10.1007/978-3-031-30470-5_7

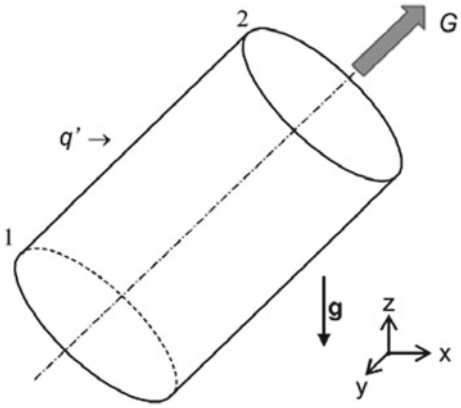

Fig. 7.1 Flow of a thermally dilatable fluid in a duct

The right hand side of the equation includes the infinitesimal work (per unit mass) of gravitational forces, $-g\mathrm{d}z$; the infinitesimal work of pressure, $-v\mathrm{d}p$ ($v = 1/\rho$ being the fluid's specific volume); and the infinitesimal work of friction.

Let's adopt Boussinesq's (1897) approximation for buoyancy, which consists of treating the density ρ as constant (and equal to some reference value ρ_0) in all terms except the gravitational one, where it is expressed as a function of the temperature T as:

$$\rho(T) = \rho_0[1 - \beta(T - T_0)] \tag{7.2}$$

in which $\beta = -(1/\rho_0)\mathrm{d}\rho/\mathrm{d}T$ is the cubic dilatation coefficient of the fluid and T_0 is the reference temperature for which $\rho = \rho_0$.

Consistently, the LHS of Eq. (7.1) vanishes; multiplying the remaining terms in Eq. (7.1) by ρ_0, except the gravitational term $-g\mathrm{d}z$ which is multiplied by $\rho(T)$ as provided by Eq. (7.2), one has:

$$0 = -g\rho_0[1 - \beta(T - T_0)]\mathrm{d}z - \mathrm{d}p - \rho_0\delta r \tag{7.3}$$

(in which the assumption $v \approx 1/\rho_0$ was made). Integrating Eq. (7.3) between Sections 1 and 2 and observing that $z_2 - z_1 = L\cos(\varphi)$, where φ is the angle formed by the duct's axis with the vertical direction, yields:

$$p_1 - p_2 = g\rho_0 L\cos(\varphi)\left[1 - \beta\left(\overline{T} - T_0\right)\right] + |\Delta p|_{FR} \tag{7.4}$$

in which $\overline{T}$ is the mean bulk temperature in the duct and $|\Delta p|_{FR}$ is the work done by the fluid against the frictional forces per unit volume, represented as a frictional pressure drop (dimensions = energy/volume). Consistent with the Boussinesq approximation, it can be expressed as:

$$|\Delta p|_{FR} = f\frac{L}{d_{eq}}\rho_0\frac{U^2}{2} \tag{7.5}$$

in which d_{eq} is the hydraulic diameter and f is the Darcy friction coefficient. Expressing f, for example, by the McAdams (1933) correlation, valid for $5000 < \mathrm{Re} < 2 \cdot 10^5$:

$$f = 0.184\mathrm{Re}^{-0.2} \tag{7.6}$$

and writing $\mathrm{Re} = Ud_{eq}\rho_0/\mu$, $U = G/(\rho_0 A)$, Eq. (7.5) becomes

$$|\Delta p|_{FR} = \frac{0.092\mu_0^{0.2}}{\rho_0 A^{1.8} d_{eq}^{1.2}} G^{1.8} L \tag{7.7}$$

where also μ was evaluated at the reference temperature T_0.

Evaluating also the fluid's specific heat c_p at T_0, the fluid's bulk temperature varies along the duct as

$$T(z) = T_1 + \frac{q'}{Gc_{p0}} l \tag{7.8}$$

in which l is a coordinate along the duct's axis. Therefore, the mean bulk temperature in the duct is

$$\overline{T} = T_1 + \frac{q'L}{2Gc_{p0}} \tag{7.9}$$

Substituting Eq. (7.9) for $\overline{T}$ in the expansion term of Eq. (7.4) yields

$$1 - \beta\left(\overline{T} - T_0\right) = 1 - \beta\left[(T_1 - T_0) + \frac{q'L}{2Gc_{p0}}\right] \tag{7.10}$$

Finally, taking account of Eq. (7.10) for the gravitational term and of Eq. (7.7) for the frictional term, Eq. (7.4) becomes:

$$p_1 - p_2 = g\rho_0 L\cos(\varphi)\left\{[1 - \beta(T_1 - T_0)] - \frac{\beta q' L}{2Gc_{p0}}\right\} + \frac{0.092\mu_0^{0.2}}{\rho_0 A^{1.8} d_{eq}^{1.2}} G^{1.8} L \tag{7.11}$$

This can be synthetically written:

$$p_1 - p_2 = C - \frac{E}{G} + FG^{1.8} \tag{7.12}$$

in which

$$C = g\rho_0 L\cos(\varphi)[1-\beta(T_1-T_0)] \tag{7.13a}$$

$$E = g\rho_0\cos(\varphi)\frac{\beta q' L^2}{2c_{p0}} \tag{7.13b}$$

$$F = \frac{0.092\mu_0^{0.2}L}{\rho_0 A^{1.8} d_{eq}^{1.2}} \tag{7.13c}$$

Note that the condition $T_2 = T_1 + (q'L)/(Gc_p) < T_{sat}$ must be met for any G; this sets for any q' a minimum value of G, below which saturated boiling would occur in the pipe and, of course, the present treatment would lose validity:

$$|G| > \frac{L}{c_p(T_{sat}-T_1)}q' \tag{7.14}$$

(the reason for using the absolute value of G is discussed immediately below).

The equations derived so far are based on the assumption that the flow is directed upward ($G > 0$). If the fluid flows downward ($G < 0$), but *Sections 1 and 2 remain as they are defined in* Fig. 7.1 (i.e., with $z_1 < z_2$), a moment's reflection shows that.

- the (hydrostatic) term C remains unchanged as it is independent of G;
- the buoyancy term E remains unchanged despite G changing sign;
- the friction term changes sign.

This behaviour can be described by re-formulating Eq. (7.12) as:

$$p_1 - p_2 = C - \frac{E}{|G|} + FG|G|^{0.8} \tag{7.15}$$

In addition, in downward flow it is consistent to adopt the temperature in 2 (which is now the inlet section) as the boundary condition, which amounts to re-formulating Eqs. (7.13a–c) with the subscript "i" (either "1" or "2") instead of "1":

$$C = g\rho_0 L\cos(\varphi)[1-\beta(T_i-T_0)] \tag{7.16a}$$

$$E = g\rho_0\cos(\varphi)\frac{\beta q' L^2}{2c_{p0}} \tag{7.16b}$$

$$F = \frac{0.092\mu_0^{0.2}L}{\rho_0 A^{1.8} d_{eq}^{1.2}} \tag{7.16c}$$

Equations (7.15) and (7.16) generalize Eqs. (7.12) and (7.13) to the case of either upward or downward flow. As an example, Fig. 7.2 reports the three components of $p_1 - p_2$, as provided by Eqs. (7.15) and (7.16), and their sum as functions of the mass flow rate G for water entering at 300 K ($\rho_i = 1000$ kg/m^3, $\mu_i = 0.9 \cdot 10^{-3}$ Pa

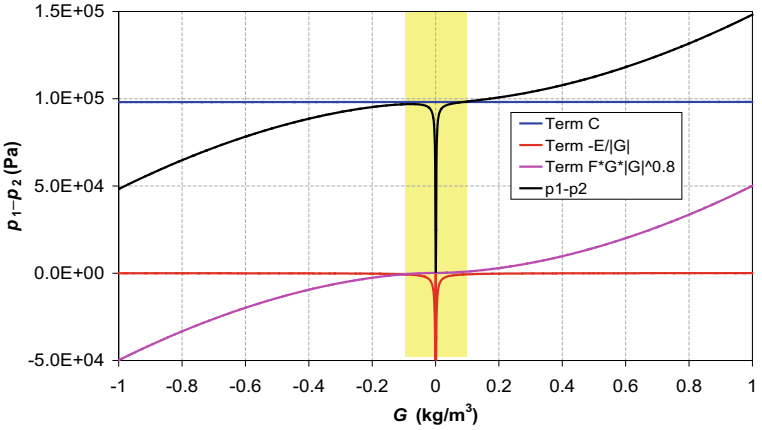

Fig. 7.2 Separate contributions to $p_1 - p_2$ and corresponding sum as functions of the mass flow rate G in a water-filled channel for $q' = 3000$ W/m

s, $c_p = 4186$ J/(kg K), $\beta = 2.1 \cdot 10^{-4}$ K^{-1}) a vertical circular pipe 2 cm in diameter and 10 m in length ($A = \pi \cdot 10^{-4}$ m^2, $d_{eq} = 2 \cdot 10^{-2}$ m), heated by a power density $q' = 3000$ W/m.

For $T_{sat} = 373.15$ K (atmospheric pressure), Eq. (7.14) gives the condition $|G| > 0.098$ kg/s; the "forbidden" G range has been highlighted to stress that corresponding results are purely virtual but could never be realized in a single-phase fluid. The reference temperature T_0 was assumed equal to the inlet temperature $T_i = T_1$ (300 K). In the admissible G range, the contribution of buoyancy (term $-E/|G|$) is negligible and pressure drop mainly consists of the sum of the frictional and mean hydrostatic components.

Figure 7.3 reports the overall pressure difference $p_1 - p_2$ as a function of G for the same water-filled channel of the above example and q' varying between 100 and 3000 W/m. "Forbidden" values have been represented by broken lines. Note that, as q' increases, the "forbidden" G range broadens and the importance of buoyancy, which tends to reduce $p_1 - p_2$, increases.

Similarly, Fig. 7.4 reports the overall pressure difference $p_1 - p_2$ as a function of G for $q' = 1000$ W/m but the pipe diameter D varying between 1.5 and 3 cm. As in the previous Fig., "forbidden" values have been represented by broken lines. Note that, as D decreases, $p_1 - p_2$ increases strongly, mainly because of the contribution of friction.

Figure 7.5 is for the flow of air ($\rho_i = 1.25$ kg/m^3, $\mu_i = 1.8 \cdot 10^{-5}$ Pa s, $c_p = 1005$ J/(kg K), $\beta = 1/T = 1/300$ K^{-1}) entering at 300 K a vertical, circular pipe 2 cm in diameter and 10 m in length ($A = \pi\ 10^{-4}$ m^2, $d_{eq} = 2 \cdot 10^{-2}$ m) heated by a linear power density q' varying between 30 and 1000 W/m. In this case there is no phase change issue and thus all flow rates are admissible (except, of course, $G = 0$ which is incompatible with the condition of steady-state heating).

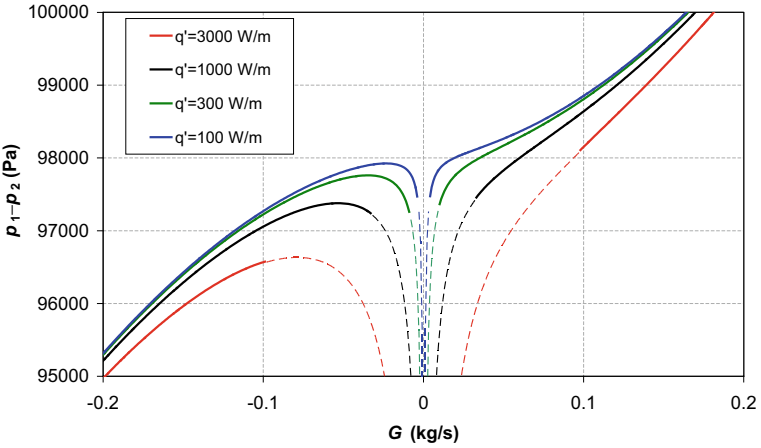

Fig. 7.3 Pressure drop $p_1 - p_2$ as a function of the mass flow rate G in a water-filled pipe for $D =$ 2 cm and $q' =$ varying between 100 and 3000 W/m

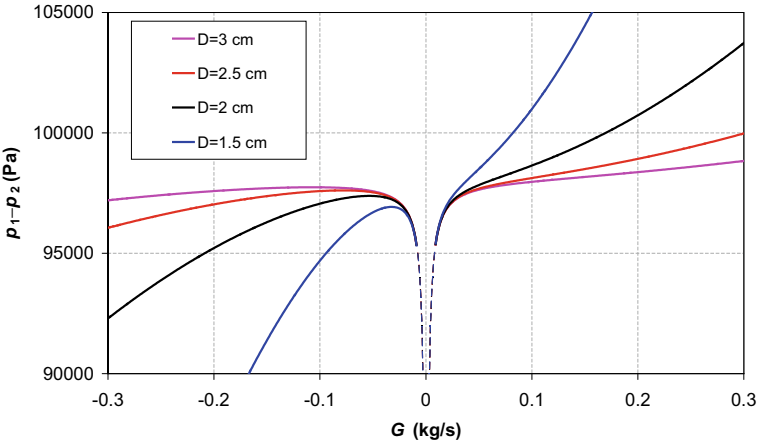

Fig. 7.4 Pressure drop $p_1 - p_2$ as a function of the mass flow rate G in a water-filled pipe for $q' =$ 1000 W/m and D varying between 1.5 and 3 cm

Note that it is possible to have $G > 0$ with $p_1 - p_2 = 0$ (pure natural convection); this would be the case of a duct with both ends open to the (uniform pressure) environment, in which the driving force for the flow is only the thermal buoyancy caused by heating. In the example of Fig. 7.5, this flow rate increases from 0 to ~ 0.3 $\cdot 10^{-3}$ kg/s as q' increases from 0 to 1000 W/m.

The purely buoyant flow rate G can be computed by imposing $p_1 - p_2 = 0$ in Eq. (7.15), restricting the attention to positive values of G (upward flow) and taking account of Eqs. (7.16a–c). The following relation is thus obtained between

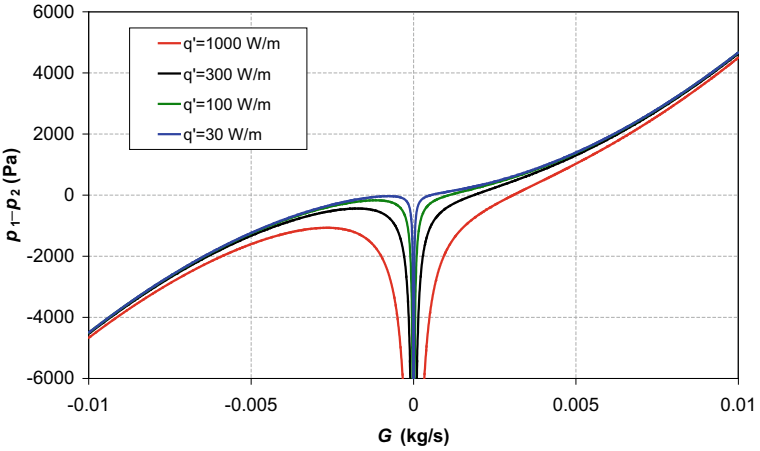

Fig. 7.5 Pressure drop $p_1 - p_2$ as a function of the mass flow rate G for air flowing through a pipe for q' varying between 30 and 1000 W/m

the controlling parameters and G:

$$G^{2.8} + MG = N \tag{7.17}$$

$$M = g\cos(\varphi)\frac{\rho_0^2 A^{1.8} d_{eq}^{1.2}}{0.092\mu_0^{0.2}}[1 - \beta(T_i - T_0)] \tag{7.18a}$$

$$N = g\cos(\varphi)\frac{\beta q' L}{2c_{p0}}\frac{\rho_0^2 A^{1.8} d_{eq}^{1.2}}{0.092\mu_0^{0.2}} \tag{7.18b}$$

For example, one may let q' vary while all other quantities are kept fixed, re-compute for each q' the parameter N and solve Eq. (7.17) by any suitable numerical method to obtain the corresponding value of G.

(b) *Thermosyphon loop.* The results obtained above for a single duct can be used to compute the buoyancy-induced flow rate in a closed thermosyphon loop. Consider, for example, that schematically shown in Fig. 7.6.

It consists of two adiabatic vertical pipes of length L_v and two horizontal pipes of length L_h, respectively heated and cooled by a uniform linear power density q'_0. For simplicity, let the duct cross section be the same through the whole loop, so that the hydraulic diameter d_{eq} and the area A are the same in all branches.

The general form of $p_1 - p_2$, from Eqs. (7.15) and (7.16), is:

$$p_1 - p_2 = g\rho_0 L\cos(\varphi)[1 - \beta(T_i - T_0)] - g\rho_0\cos(\varphi)\frac{\beta q' L^2}{2c_{p0}}\frac{1}{|G|} + \frac{0.092\mu_0^{0.2} L}{\rho_0 A^{1.8} d_{eq}^{1.2}} G|G|^{0.8} \tag{7.19}$$

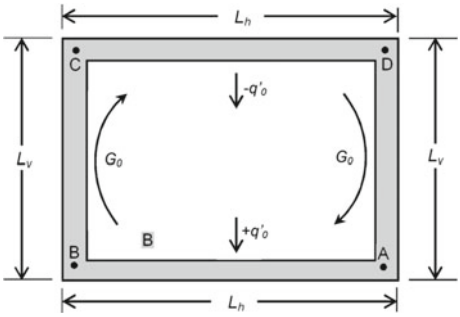

Fig. 7.6 Schematic of a thermosyphon loop

This can be written for each of the four branches AB, BC, CD and DA in Fig. 7.6. In the horizontal branches AB and CD one has $C = E = 0$ since $\cos(\varphi) = 0$, so that, calling G_0 the mass flow rate in the clockwise direction:

$$p_A - p_B = \frac{0.092\mu_0^{0.2} L_h}{\rho_0 A^{1.8} d_{eq}^{1.2}} G_0^{1.8} \tag{7.20}$$

$$p_C - p_D = \frac{0.092\mu_0^{0.2} L_h}{\rho_0 A^{1.8} d_{eq}^{1.2}} G_0^{0.8} \tag{7.21}$$

In the vertical branch BC with upward flow ($i = 1 = \mathrm{B}$, $2 = \mathrm{C}$, $L = L_v$, $\cos(\varphi) = 1$, $G = +G_0$, $q' = 0$):

$$p_B - p_C = g\rho_0 L_v[1 - \beta(T_B - T_0)] + \frac{0.092\mu_0^{0.2} L_v}{\rho_0 A^{1.8} d_{eq}^{1.2}} G_0^{1.8} \tag{7.22}$$

In the vertical branch DA with downward flow ($1 = \mathrm{A}$, $i = 2 = \mathrm{D}$, $L = L_v$, $\cos(\varphi) = 1$, $G = -G_0$, $q' = 0$):

$$p_D - p_A = -g\rho_0 L_v[1 - \beta(T_D - T_0)] + \frac{0.092\mu_0^{0.2} L_v}{\rho_0 A^{1.8} d_{eq}^{1.2}} G_0^{1.8} \tag{7.23}$$

Note that the heat flux q' does not appear in any of the individual pressure drops. By summing Eqs. (7.20)–(7.23) one has

$$\frac{0.184\mu_0^{0.2}(L_h + L_v)}{\rho_0 A^{1.8} d_{eq}^{1.2}} G_0^{1.8} - g\rho_0 L_v \beta(T_B - T_D) = 0 \tag{7.24}$$

Substituting, from a heat balance:

$$T_B - T_D = \frac{q_0' L_h}{G_0 c_{p0}} \tag{7.25}$$

and solving for G_0 one has

$$G_0 = \left[g\beta q_0' \frac{\rho_0^2 A^{1.8} d_{eq}^{1.2}}{0.184 \mu_0^{0.2} c_{p0}} \cdot \frac{L_h L_v}{L_h + L_v} \right]^{5/14} \tag{7.26}$$

For example, in a water loop with circular cross section, $D = 0.05$ m, $L_h = L_v = 10$ m, $q'_0 = 10^4$ W/m, using the same conventional properties as in the previous examples, one has $G_0 = 3.341$ kg/s, corresponding to a mean velocity $U = 1.702$ m/s and to a Reynolds number Re = 94,556. The maximum temperature difference in the system, Eq. (7.25), is $T_B - T_D = 7.15$ K.

If it is the temperature difference between the two vertical branches, $T_B - T_D$, that is imposed instead of the linear heat flux q'_0, Eq. (7.24) can be directly solved yielding

$$G_0 = \left[g\beta (T_B - T_D) \frac{\rho_0^2 A^{1.8} d_{eq}^{1.2}}{0.184 \mu_0^{0.2}} \frac{L_v}{L_h + L_v} \right]^{5/9} \tag{7.27}$$

After some manipulations, this solution can be put in the synthetic form

$$\mathrm{Re} = 2.561 \left(\frac{\mathrm{Gr}}{1 + h} \right)^{5/9} \tag{7.28}$$

in which

Re $= \frac{U d_{eq}}{\nu_0}$ (Reynolds number, with $U = G_0/(\rho_0 A)$ and $\nu_0 = \mu_0/\rho_0$);

Gr $= \frac{g\beta (T_B - T_D) d_{eq}^3}{\nu_0^2}$ (Grashof number based on the hydraulic diameter);

$h = \frac{L_h}{L_v}$ (aspect ratio of the loop).

This treatment must be appropriately modified if the flow is laminar, in which case Eq. (7.6) has to be replaced by $f = 64/\mathrm{Re}$ or similar (according to the shape of the ducts' cross section), or if it is a low-Re turbulent flow, in which case Eq. (7.6) can be replaced, for example, by Blasius' correlation $f = 0.316\ \mathrm{Re}^{-0.25}$.

Chapter 8
Stability of Two-Phase Flow in a Heated Duct

Lectures which really teach will never be popular; lectures which are popular will never really teach
(*Michael Faraday*)

Abstract The stability of two-phase flow in a heated duct is considered. The main purpose of the study is to obtain a curve (internal characteristic) relating the mass flow rate with the inlet–outlet pressure drop for any given geometry, system's pressure and heating power. The intersection of this internal characteristic with the flow rate—prevalence curve characterizing the pump (external characteristic) allows the working point to be determined and its stability to be assessed. The model adopted is based on the 1-D continuity, momentum and energy equations for two-phase pipe flow together with suitable expressions for slip ratio/void fraction and two-phase friction pressure losses, based on the Chisholm and Lockhart-Martinelli correlations but modified for consistency and easy computability. In the case of a horizontal pipe, the internal characteristic is obtained in a simple, low-order, polynomial form.

Consider a straight duct of length L, hydraulic diameter D and cross sectional area A in which a subcooled fluid enters with mass flow rate G and inlet specific enthalpy J_i. Let also a throttling valve of hydraulic resistance K be present at the foot of the duct (Fig. 8.1).

Let the fluid receive a uniform thermal power per unit length $q' = q/L$ along its whole length L, so that its bulk enthalpy increases linearly from J_i at $z = 0$ to $J_o = J_i + q'z/G$ at a generic z, up to $J_o = J_i + q'L/G$ at $z = L$.

By using the generalized definition of quality x:

$$x = \frac{J - J_f}{J_{fg}} \tag{8.1}$$

(in which J_f and J_g are the enthalpies of saturated liquid and saturated vapour, respectively, and $J_{fg} = J_g - J_f$ is the latent heat of vaporization), one can write, along the whole pipe length:

M. Ciofalo, *Thermofluid Dynamics*, UNIPA Springer Series,
https://doi.org/10.1007/978-3-031-30470-5_8

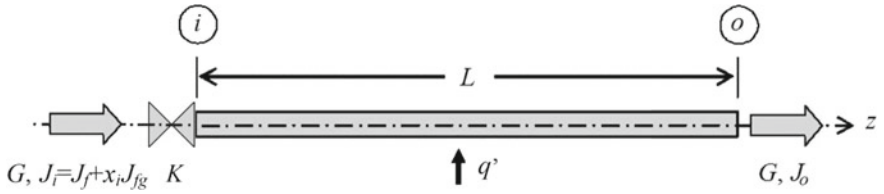

Fig. 8.1 Generic fluid flowing through a heated duct

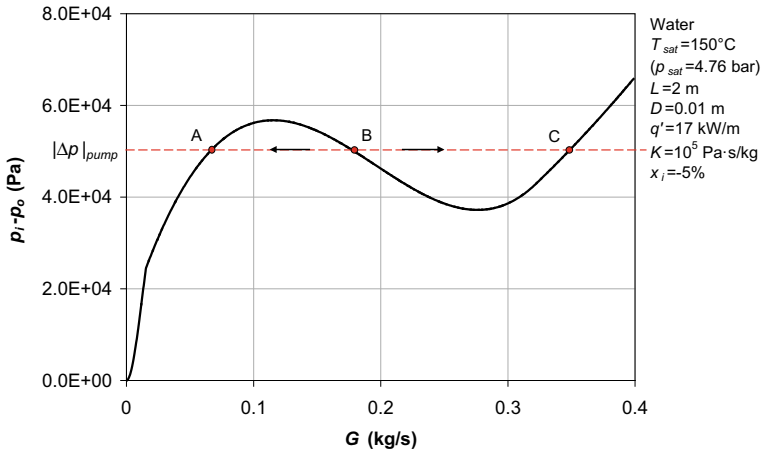

Fig. 8.2 Characteristic S-curve of a boiling duct, exhibiting stable and unstable working points

$$x = x_i + \frac{q'z}{GJ_{fg}} \tag{8.2}$$

Since $x_i < 0$ (subcooled fluid at inlet), for any q' and L two special flow rates can be identified, $G_0 = q'L/[(1 - x_i)J_{fg}]$ and $G_1 = -q'L/[x_iJ_{fg}]$ ($G_0 < G_1$) such that:

(a) For $G \geq G_1$, one has $x_o \leq 0$ (single-phase subcooled liquid flow throughout L);
(b) For $G_0 < G < G_1$, one has $0 < x_o < 1$ (single-phase subcooled liquid flow up to, say, z_f and two-phase flow at increasing quality from z_f to L);
(c) For $G \leq G_0$, one has $x_o \geq 1$ (single-phase subcooled liquid flow up to a location z_f, two-phase flow at increasing quality from z_f to, say, z_g and superheated vapour flow in the remaining end region $L - z_g$).

It is well known (Butterworth and Hewitt 1977) that in such a system (boiling duct) the curve representing the overall pressure drop $p_i - p_o$ as a function of the mass flow rate G (*internal characteristic*) may exhibit, under appropriate circumstances, a non-monotonic behaviour (S-shape), with a relative maximum at low values of G and a relative minimum at higher values. Figure 8.2 illustrates this behaviour for water at $T_{sat} = 150$ °C ($p = 4.76$ bar).

Here and in the following, the properties of water are taken from the *UK Steam Tables in SI Units* (United Kingdom Committee on the Properties of Steam 1970).

If the duct is fed by an *ideal* pump providing a prevalence $|\Delta p|_{pump}$ included in a suitable interval, three hypothetical working points A, B, C are obtained. It is easily shown that points A and B are stable, while point B is unstable: any infinitesimal perturbation will push a system starting from B towards either A or C, according to the sign of the initial disturbance. The criterion for stability is, in this case, $\partial(p_i - p_o)/\partial G > 0$, and is clearly met by points A and C but not B.

The analysis is easily extended to a *real* pump, providing a prevalence $|\Delta p|_{pump} = |\Delta p|_0 - K_p G^2$, by including the internal resistance K_p in the constant K.

Investigating the system's behaviour as a function of the controlling parameters (system's pressure p, length L, hydraulic diameter D, inlet subcooling x_i, power rate q', local resistance K) is of paramount importance, e.g. in the stability analysis of a boiling water nuclear reactor (Lahey and Moody 1996). Yet, when two-phase flow is implied, the pressure drop is usually obtained by the application of different empirical correlation providing slip ratio, void fraction and two-phase friction multipliers, so that the dependence of the system's behaviour from the controlling parameters is obscured by the heavy formalism and by the necessarily numerical approach.

Therefore, it would be desirable to express the dependence of $p_i - p_o$ upon G in a closed, possibly polynomial, form, so that the methods of stability analysis can be easily applied.

In the following, such a polynomial form will be derived under two main simplifying assumptions:

- the physical properties of both phases are constant and equal to those evaluated on the saturation line at the mean system pressure;
- the friction coefficient for turbulent single-phase flow is not a function of G and can be evaluated at a suitable intermediate flow rate G_{REF}.

We will also assume the duct to be *horizontal*, so that gravitational contributions to pressure drop can be omitted. Further approximations will be discussed as they will be introduced.

The pressure drop $p_i - p_o$ consists of two components:

i. distributed frictional pressure loss $(p_i - p_o)_{FR}$;
ii. expansion term $(p_i - p_o)_{EXP}$.

To these terms one has to add the singular pressure loss in the valve V, which can be always be written for simplicity as KG^2.

Let's discuss the three flow rate ranges (a)–(c) separately.

Case (a) ($G \geq G_1, x_o \leq 0$)

In this case, one has single-phase subcooled liquid flow in the whole duct.

(1) *Distributed frictional pressure loss*

The distributed frictional term, assuming fully turbulent flow, can be computed as usual by the Weisbach formula

$$(p_i - p_o)_{FR} = f\frac{L}{D}\rho\frac{u^2}{2} \tag{8.3}$$

using for the Darcy friction coefficient f the MacAdams correlation $f = 0.184 \cdot \mathrm{Re}^{-0.2}$. Since we look for simple (polynomial) expressions of $(p_i - p_o)$ as a function of the flow rate G, f can be evaluated not at the actual flow rate G but at some fixed flow rate G_{REF} representative of the whole range considered, e.g. $G_{REF} = (G_0 + G_1)/2$. Thus, writing $\mathrm{Re} = u_f D\rho_f/\mu_f$ (i.e., identifying the physical properties of the subcooled liquid with the saturation ones) and $u_f = G/(\rho_f A)$ (mean fluid velocity), one has

$$f = 0.184\left(\frac{G_{REF}D}{A\mu_f}\right)^{-0.2} \tag{8.4}$$

$$|\Delta p|_{FR} = \frac{fL}{2D\rho_f A^2}G^2 = FLG^2 \tag{8.5}$$

in which $F = f/(2D\rho_f A^2)$.

(2) *Expansion term*

Since there is only liquid in the whole duct, the expansion term can be neglected:

$$|\Delta p|_{EXP} = 0 \tag{8.6}$$

(3) *Summary pressure loss for case a*

Using Eqs. (8.5) and (8.6), and taking into account also the pressure drop in the foot valve, simply parameterized as KG^2, in case (a) ($G \geq G_1$) one has:

$$(p_i - p_0)_{\text{case a}} = (K + FL)G^2 \tag{8.7}$$

Case (b) ($G_0 < G < G_1$, $0 < x_o < 1$).

In this case one has single-phase subcooled liquid flow up to a location z_f identified by the condition

$$x_i + \frac{q'z_f}{GJ_{fg}} = 0 \quad \rightarrow \quad z_f = -\frac{J_{fg}x_i}{q'}G \tag{8.8}$$

in force of Eq. (8.2), and two-phase flow at increasing quality in the remaining tract from $z = z_f$ to $z = L$. Note that, by hypothesis, $x_i < 0$ and thus $z_f > 0$.

(1) *Pressure drop in the single-phase tract*

In the single-phase tract $z = 0$ to z_f, the pressure drop can be computed as in case (a), with the obvious substitution of z_f for L; in particular, the expansion term can be neglected. Thus, apart from the localized loss in the valve, one has:

$$|\Delta p|_{SP} = F z_f G^2 \tag{8.9}$$

(where "*SP*" stays for "single phase region"). Taking account of the expression of z_f in Eq. (8.8), Eq. (8.9) becomes

$$|\Delta p|_{SP} = -\frac{F J_{fg} x_i}{q'} G^3 \tag{8.10}$$

In the two-phase tract $z = z_f$ to L, the computation of both pressure drop components (i-ii) requires a more careful treatment.

(2) *Distributed frictional pressure loss in the two-phase tract*

The frictional term, following the classic procedure introduced by Lockhart and Martinelli (1949) and other authors, can be expressed for a generic elementary length dz as the product of two factors:

$$|\mathrm{d}p|_{FR} = |\mathrm{d}p|_{FR,LO} \Phi_{LO}^2 \tag{8.11}$$

in which $|\mathrm{d}p|_{FR,LO}$ is the frictional loss that would be experienced if the whole fluid, with its total flow rate G, was liquid, while ${\Phi_{LO}}^2$ is a two-phase friction multiplier.

The first factor, in analogy with Eq. (8.5), can be expressed as

$$|\mathrm{d}p|_{FR,LO} = F \mathrm{d}z G^2 \tag{8.12}$$

The second factor, i.e. the two-phase multiplier, following Chisholm (1983) and several other authors, can be approximated, for the case of turbulent flow in both phases, by

$$\Phi_{LO}^2 = (1-x)^2 \left(1 + \frac{21}{X_{LM}} + \frac{1}{X_{LM}^2}\right) \tag{8.13}$$

in which X_{LM} is the dimensionless Lockhart-Martinelli parameter, defined as

$$X_{LM} = \left(\frac{1-x}{x}\right)^{0.9} \left(\frac{\rho_g}{\rho_f}\right)^{0.5} \left(\frac{\mu_f}{\mu_g}\right)^{0.1} \tag{8.14}$$

${X_{LM}}^2$ is the ratio between the frictional pressure drops that would occur if only the liquid fraction $(1-x)G$ and only the vapour fraction xG, respectively, flowed through the duct.

Substituting Eqs. (8.12) and (8.13) into Eq. (8.11) yields

$$|\mathrm{d}p|_{FR} = F \mathrm{d}z G^2 (1-x)^2 \left(1 + \frac{21}{X_{LM}} + \frac{1}{X_{LM}^2}\right) \tag{8.15}$$

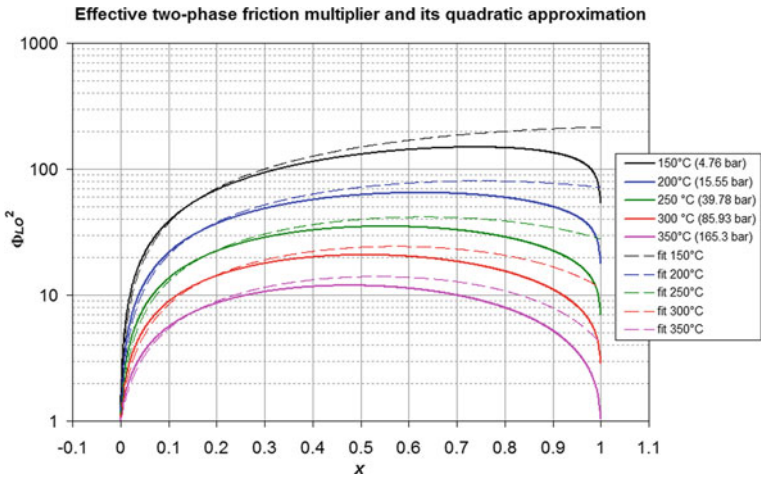

Fig. 8.3 Two-phase "liquid only" friction multiplier $\Phi_{LO}{}^2$ as a function of the quality x for water: empirical correlation (8.13) (solid lines) versus quadratic approximation (8.16) (broken lines) at different saturation pressures and temperatures

For physical consistency reasons, $\Phi_{LO}{}^2$ must attain (I) the value 1 for $x = 0$ ("liquid only" condition), and (II) the value $\varphi = (\rho_f/\rho_g)(\mu_g/\mu_f)^{0.2}$ for $x = 1$ ("gas only" condition). Moreover, (III) at intermediate values of the quality x, $\Phi_{LO}{}^2$ is known to exhibit a maximum M, the more marked as lower the pressure. Equation (8.13) satisfies conditions (I) and (III) but not (II), despite its widespread adoption in the literature. A simple quadratic expression that satisfies all three conditions (I)–(III) is

$$\Phi_{LO}^2 = \frac{(x - x_1)(x - x_2)}{x_1 x_2} \tag{8.16}$$

Equation (8.16) implicitly satisfies condition (I) for any x_1, x_2; the values of $x_1 < 0$ and $x_2 > 1$ are computed (for each given system pressure) by imposing condition (II) and by imposing the best agreement with correlation (8.13) for $\Phi_{LO}{}^2$ in the range in which it is applicable (say, $x < 30\%$).

For example, Fig. 8.3 compares (in a logarithmic plot) the two-phase "liquid only" friction multiplier $\Phi_{LO}{}^2$ as computed by Eq. (8.13) and by its quadratic approximation (8.16) for water at different values of the system's pressure (and corresponding saturation temperature).

Note that Eq. (8.16) is an acceptable approximation of the well-established Eq. (8.13) at relatively low qualities, where this latter is consistently applicable, and exhibits the correct asymptotic behaviour for $x \to 1$, where Eq. (8.13) fails.

Once Eq. (8.16) is used for $\Phi_{LO}{}^2$, Eq. (8.11) becomes

$$|\mathrm{d}p|_{FR} = F\mathrm{d}z\frac{(x - x_1)(x - x_2)}{x_1 x_2}G^2 \tag{8.17}$$

Substituting $x_i + (q'z)/(GJ_{fg})$ for x in force of Eqs. (8.2, 8.17) becomes, after a few passages:

$$|\mathrm{d}p|_{FR} = \frac{F}{x_1 x_2}\left[(x_i - x_1)(x_i - x_2)G^2 + (2x_i - x_1 - x_2)\frac{q'z}{J_{fg}}G + \frac{q'^2 z^2}{J_{fg}^2}\right]\mathrm{d}z \tag{8.18}$$

By integrating between $z = z_f$ (beginning of the two-phase region) and $z = L$, one has

$$\begin{aligned}|\Delta p|_{FR} &= \frac{F}{x_1 x_2}\times \\ &\left[(x_i - x_1)(x_i - x_2)\left(L - z_f\right)G^2 + (2x_i - x_1 - x_2)\frac{q'}{2J_{fg}}\left(L^2 - z_f^2\right)G\right. \\ &\left.+\frac{q'^2}{3J_{fg}^2}\left(L^3 - z_f^3\right)\right]\end{aligned} \tag{8.19}$$

Finally, by substituting Eq. (8.8) for z_f, Eq. (8.19) becomes after a few passages:

$$\begin{aligned}|\Delta p|_{FR} &= \frac{F}{x_1 x_2}\times \\ &\left\{\begin{array}{l}\dfrac{J_{fg}}{q'}\left[(x_i - x_1)(x_i - x_2)x_i - x_i^2\left(x_i - \dfrac{x_1 + x_2}{2}\right) + \dfrac{x_i^3}{3}\right]G^3 \\ +(x_i - x_1)(x_i - x_2)LG^2 + \left(x_i - \dfrac{x_1 + x_2}{2}\right)\dfrac{q'}{J_{fg}}L^2 G + \dfrac{q'^2}{3J_{fg}^2}L^3\end{array}\right\}\end{aligned} \tag{8.20}$$

This can be more synthetically written as

$$|\Delta p|_{FR} = \frac{F}{x_1 x_2}\left(a_3 G^3 + a_2 L G^2 + a_1 L_2 G + a_0 L^3\right) \tag{8.21}$$

provided

$$a_3 = \frac{J_{fg}}{q'}\left[(x_i - x_1)(x_i - x_2)x_i - x_i^2\left(x_i - \frac{x_1 + x_2}{2}\right) + \frac{x_i^3}{3}\right] \tag{8.22}$$

$$a_2 = (x_i - x_1)(x_i - x_2) \tag{8.23}$$

$$a_1 = \left(x_i - \frac{x_1 + x_2}{2}\right)\frac{q'}{J_{fg}} \tag{8.24}$$

$$a_0 = \frac{q'^2}{3J_{fg}^2} \tag{8.25}$$

(3) *Expansion term in the two-phase tract*

The expansion term in the two-phase region from z_f to L can be written as

$$|\Delta p|_{EXP} = \left[\rho_f u_f^2(1-\alpha) + \rho_g u_g^2 \alpha\right]_o - \left[\rho_f u_f^2\right]_{z_f} \tag{8.26}$$

because $\alpha = 0$ at $z = z_f$ (beginning of the two-phase region). At z_f one has

$$\left[\rho_f u_f^2\right]_{z_f} = \frac{G^2}{\rho_f A^2} \tag{8.27}$$

whereas at the outlet, being $u_f = [G(1-x)]/[\rho_f(1-\alpha)A]$ and $u_g = [Gx]/[\rho_g \alpha A]$, one has

$$\left[\rho_f u_f^2(1-\alpha) + \rho_g u_g^2 \alpha\right]_o = \frac{G^2}{\rho_f A^2}\left[\frac{(1-x)^2}{1-\alpha} + \frac{\rho_f}{\rho_g}\frac{x^2}{\alpha}\right]_o = \frac{G^2}{\rho_f A^2}\Psi_o \tag{8.28}$$

in which the term Ψ in square brackets is a function of x, α and of the densities (i.e., of the system's pressure). Therefore, the expansion term in Eq. (8.26) can be written

$$|\Delta p|_{EXP} = \frac{G^2}{\rho_f A^2}[\Psi_o - 1] \tag{8.29}$$

The void fraction can be expressed as a function of x and of the densities by using the fundamental relation between x, a and S (slip ratio u_g/u_f):

$$\alpha = \frac{1}{1 + S\frac{\rho_g}{\rho_f}\frac{1-x}{x}} \tag{8.30}$$

and computing S by Chisholm's (1983) correlation:

$$S = \sqrt{1 + x\left(\frac{\rho_f}{\rho_g} - 1\right)} \tag{8.31}$$

In this way, Ψ becomes a function of x and densities (i.e., pressure) only. The solid lines in Fig. 8.4 illustrate its behaviour for water at different pressures. Broken lines show the simple quadratic approximation

$$\Psi = 1 + \frac{\rho_f - \rho_g}{\rho_g}x^2 \tag{8.32}$$

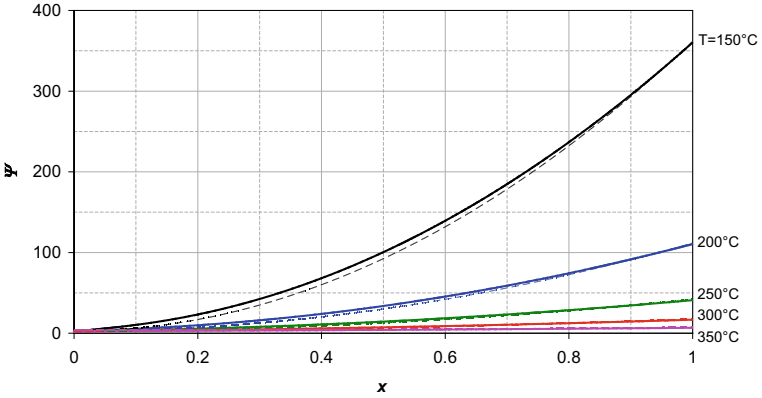

Fig. 8.4 Function Ψ, Eq. (8.28), for water as a function of the quality x: values computed from Chisholm's slip correlation (solid lines) versus quadratic approximation (8.32) (broken lines) at different saturation temperatures

which has the correct behaviour at $x = 0$ and $x = 1$ and approximates fairly well the computed profile of Ψ provided the system's pressure p is sufficiently high (say, $p \geq 40$ bar as for the quadratic approximation of the frictional term).

By using the approximation (8.32) for Ψ, the expansion term (8.29) can be written as

$$|\Delta p|_{EXP} = \frac{\rho_f - \rho_g}{\rho_f \rho_g} \frac{x_o^2}{A^2} G^2 = \frac{v_{fg} x_o^2}{A^2} G^2 \tag{8.33}$$

in which $v_{fg} = 1/\rho_g - 1/\rho_f = v_g - v_f$ is the difference between the specific volumes of the gas and liquid phases.

By substituting $x_i + q'L/(GJ_{fg})$ for x_o in force of Eq. (8.2), Eq. (8.33) becomes:

$$|\Delta p|_{EXP} = \frac{v_{fg}}{A^2} \left(x_i^2 G^2 + 2 x_i \frac{q'L}{J_{fg}} G + \frac{q'^2 L^2}{J_{fg}^2} \right) \tag{8.34}$$

(4) *Summary pressure loss for case b*

By assembling Eqs. (8.21) for the frictional two-phase pressure drop and (8.34) for the expansion term, the overall pressure drop in the two-phase region from $z = z_f$ to $z = L$ in case (b) ($G_0 < G < G_1$, $0 < x_o < 1$) can be written as

$$\begin{aligned} |\Delta p|_{TP} = {} & \frac{F}{x_1 x_2} \left(a_3 G^3 + a_2 L G^2 + a_1 L^2 G + a_0 L^3 \right) \\ & + \frac{v_{fg}}{A^2} \left(x_i^2 G^2 + 2 x_i \frac{q'L}{J_{fg}} G + \frac{q'^2 L^2}{J_{fg}^2} \right) \end{aligned} \tag{8.35}$$

Finally, by adding the pressure drop KG^2 in the foot valve and the pressure drop in the single-phase (subcooled liquid) region from $z = 0$ to $z = z_f$, given by Eq. (8.10), one has

$$p_i - p_o = KG^2 - \frac{FJ_{fg}x_i}{q'}G^3 + \frac{F}{x_1x_2}\left(a_3G^3 + a_2LG^2 + a_1L^2G + a_0L^3\right) + \frac{v_{fg}}{A^2}\left(x_i^2G^2 + 2x_i\frac{q'L}{J_{fg}}G + \frac{q'^2L^2}{J_{fg}^2}\right) \tag{8.36}$$

The terms in Eq. (8.36) can be ordered by decreasing powers of G yielding

$$(p_i - p_o)_{\text{case b}} = F\left(\frac{a_3}{x_1x_2} - \frac{J_{fg}x_i}{q'}\right)G^3 + \left[K + \left(\frac{Fa_2L}{x_1x_2} + \frac{v_{fg}x_i^2}{A^2}\right)\right]G^2 + \left(\frac{Fa_1L}{x_1x_2} + \frac{2v_{fg}x_i}{A^2}\frac{q'}{J_{fg}}\right)LG + \left(\frac{Fa_0L}{x_1x_2} + \frac{v_{fg}}{A^2}\frac{q'^2}{J_{fg}^2}\right)L^2 \tag{8.37}$$

with the terms $a_0 \ldots a_3$ given by Eqs. (8.22)–(8.25).

Case (c) ($G \le G_0, x_o \ge 1$)

This case exhibits single-phase subcooled liquid flow up to a location z_f, two-phase flow at increasing quality from z_f to, say, z_g and superheated vapour flow in the remaining end region $L - z_g$.

The location z_g is provided by Eq. (8.2) written for $x = 1$:

$$x_i + \frac{q'z_g}{GJ_{fg}} = 1 \quad \rightarrow \quad z_g = \frac{GJ_{fg}(1 - x_i)}{q'} \tag{8.38}$$

(1) *Pressure loss in the single-phase tract*

The pressure drop in the single-phase tract $z = 0$ to z_f, can be computed as in case (b), Eq. (8.10), which therefore does not need to be repeated here.

(2) *Pressure loss in the two-phase tract*

The distributed frictional pressure loss between $z = z_f$ (beginning of the two-phase region) and $z = z_g$ (end of the two-phase region) can be obtained as that for case (b), Eq. (8.20), with the substitution of z_g for L:

$$|\Delta p|_{FR} = \frac{F}{x_1x_2} \times \left(a_3G^3 + a_2z_gG^2 + a_1z_g^2G + a_0z_g^3\right) \tag{8.39}$$

where the terms $a_0 \ldots a_3$ are given by Eqs. (8.22)–(8.25). By substituting $GJ_{fg}(1 - x_i)/q'$ for z_g in force of Eqs. (8.38, 8.39) and simplifying, becomes:

$$|\Delta p|_{FR} = \frac{F J_{fg}}{q'}\left[1 - \frac{x_1 + x_2}{2x_1 x_2} + \frac{1}{3x_1 x_2}\right]G^3 \tag{8.40}$$

The expansion loss in the two-phase region between $z = z_f$ (where $x = 0, \alpha = 0$) and $z = z_g$ (where $x = 1, \alpha = 1$) can be written as

$$|\Delta p|_{EXP} = \rho_g u_g^2 - \rho_f u_f^2 = \frac{v_{fg}}{A^2} G^2 \tag{8.41}$$

(3) *Pressure loss in the superheated vapour tract*

The pressure drop between $z = z_g$ (end of the two-phase region) and $z = L$ (channel outlet) consists only of single-phase (superheated vapour) frictional pressure losses, while expansion losses can be neglected. Therefore, in analogy with Eq. (8.7), one has:

$$p_g - p_0 = \frac{f(L - z_g)}{2D\rho_g A^2} G^2 = F\frac{\rho_f}{\rho_g}(L - z_g)G^2 \tag{8.42}$$

By substituting $GJ_{fg}(1 - x_i)/q'$ for z_g in force of Eqs. (8.41, 8.42) becomes:

$$p_g - p_0 = -\left[F\frac{\rho_f}{\rho_g}\frac{J_{fg}(1 - x_i)}{q'}\right]G^3 + \left[F\frac{\rho_f}{\rho_g}L\right]G^2 \tag{8.43}$$

(4) *Summary pressure loss for case c*

By summing the various terms (8.10), (8.40), (8.41) and (8.43), adding the local loss KG^2, simplifying and ordering, as usual, by decreasing powers of G, an expression containing only the second and third powers of G is obtained:

$$(p_i - p_o)_{\text{case c}} = \frac{F J_{fg}}{q'}\left[-\frac{x_1 + x_2}{2x_1 x_2} + \frac{1}{3x_1 x_2} - \frac{\rho_f - \rho_g}{\rho_g}(1 - x_i)\right]G^3 + \left[K + \frac{v_{fg}}{A^2} + F\frac{\rho_f}{\rho_g}L\right]G^2 \tag{8.44}$$

Complete solution

Equations (8.7), (8.37) and (8.44) are the complete solution for pressure drop, respectively in the three ranges of flow rate: (a) $G \geq G_1$ ($x_o \leq 0$, single-phase subcooled liquid flow throughout L); (b) $G_0 < G < G1$ ($0 < x_o < 1$, single-phase subcooled liquid flow up to z_f and two-phase flow in the remaining tract $L - z_f$); and (c) $G \leq G0$ ($x_o \geq 1$, single-phase subcooled liquid flow up to z_f, two-phase flow from z_f to z_g and superheated vapour flow in the remaining region $L - z_g$).

Figure 8.5 reports the results obtained for water at $T_{sat} = 200\,°\text{C}$ ($p_{sat} = 15.55$ bar) flowing in a pipe with $L = 4$ m, $D = 1$ cm, $q' = 20$ kW/m, $x_i = -0.05$ (subcooled inlet

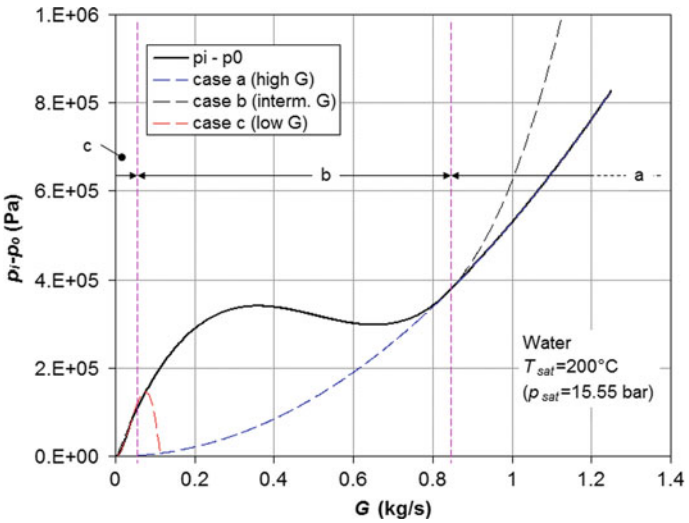

Fig. 8.5 Pressure drop in a heated horizontal channel for water at $T_{sat} = 200$ °C. Broken lines: partial solutions (8.7), (8.37) and (8.44) in the high, intermediate and low flow rate ranges. Solid line: complete curve

at $T \approx 188$ °C), $K = 10^4$ Pa s/kg. Under these conditions one has $G_0 \approx 0.04$ kg/s, $G_1 \approx 0.833$ kg/s. Note that, in the intermediate flow rate range (e.g. $G = 0.3$ kg/s), pressure drops as high as ~ 3.5 bar can be obtained. Since this value is *not* much smaller than the mean system pressure (15.55 bar), it is clear that the assumptions made of constant fluid properties are barely tenable.

The simple polynomial expression of $(p_i - p_o)$ proposed here allows a rapid evaluation of the influence of the parameters affecting the pressure drop (length L, diameter D and linear power rate q' of the channel, mean system pressure p, degree of subcooling x_i, value of the foot hydraulic resistance K).

For example, Fig. 8.6 shows the influence of the inlet subcooling (expressed as negative quality x_i) with all other parameters fixed at the values indicated. As the subcooling decreases (i.e., as x_i increases) the overall pressure drop increases while its maximum is attained at larger values of the flow rate G and tends to become more shallow, until it disappears for $x_i \geq -0.025$.

Figure 8.7 shows the surface $G = G(p_i - p_o, K)$ for the conditions indicated in the caption. It can be clearly seen that a *cusp catastrophe* exists (Arnold 1992), the function G being triple-valued for low K (whence the existence of the instability region delimited by the broken grey lines) and becoming single-valued only in the range $K \geq \sim 8 \cdot 10^5$ Pa s/kg, where the fold vanishes and the instability region disappears.

As a further step towards the *a priori* assessment of stability conditions, note that unstable conditions, if any, can only occur in the intermediate range of flow rates $G_0 < G < G_1$, where single-phase and two-phase flow regions coexist in the channel ($0 <$

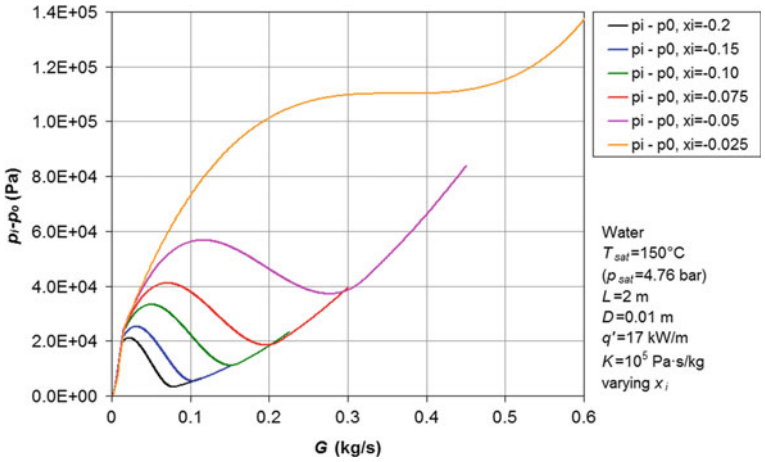

Fig. 8.6 Pressure drop in a heated horizontal channel for water at $T_{sat} = 150$ °C and different values of inlet subcooling (expressed as a negative quality x_i)

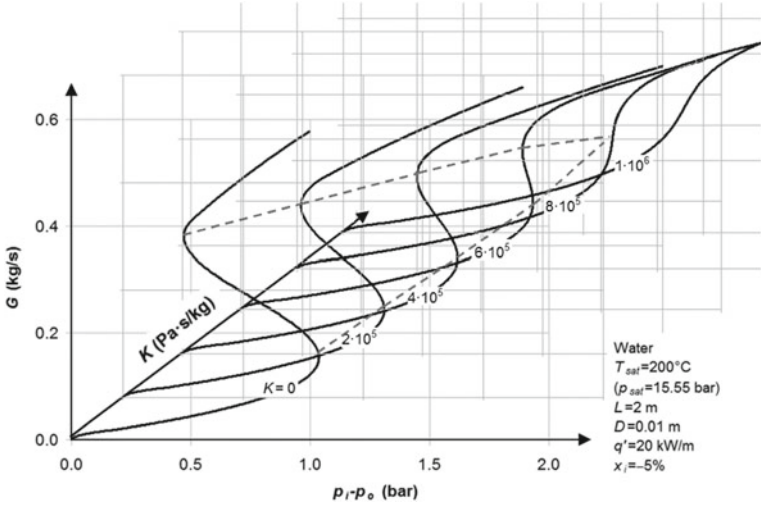

Fig. 8.7 Pressure drop in a heated horizontal channel for water at $T_{sat} = 150$ °C and different values of the inlet hydraulic resistance K (in Pa s/kg)

$x_o < 1$). In this range, the pressure drop is given by Eq. (8.37), which can be written as

$$p_i - p_o = aG^3 + bG^2 + cG + d \tag{8.45}$$

with

$$a = F\left(\frac{a_3}{x_1 x_2} - \frac{J_{fg} x_i}{q'}\right) \tag{8.46}$$

$$b = K + \left(\frac{F a_2 L}{x_1 x_2} + \frac{v_{fg} x_i^2}{A^2}\right) \tag{8.47}$$

$$c = L\left(\frac{F a_1 L}{x_1 x_2} + \frac{2 v_{fg} x_i}{A^2}\frac{q'}{J_{fg}}\right) \tag{8.48}$$

$$d = L^2\left(\frac{F a_0 L}{x_1 x_2} + \frac{v_{fg}}{A^2}\frac{q'^2}{J_{fg}^2}\right) \tag{8.49}$$

and the terms $a_0 \ldots a_3$ given by Eqs. (8.22)–(8.25).

Unstable flow may exist only if the polynomial function $(p_i - p_o) = f(G)$ in Eq. (8.45) exhibits a relative maximum and a relative minimum, i.e. if the equation $\mathrm{d}(p_i - p_o)/\mathrm{d}G = 0$ has at least one real root. By deriving Eq. (8.45) with respect to G this condition can be written as

$$\frac{\mathrm{d}}{\mathrm{d}G}(p_i - p_o) = 3aG^2 + 2bG + c = 0 \tag{8.50}$$

which possesses real roots if

$$\Delta = b^2 - 3ac \geq 0 \tag{8.51}$$

By using Eqs. (8.46)–(8.48), in addition to Eqs. (8.22)–(8.24), to obtain a, b and c, Δ can be computed for any combination of the operating parameters of the boiling channel and the existence of instability conditions can be checked. Equations providing *a priori* the limiting values of parameters such as K, L, q' and so on for instabilities to occur might also be derived from Eq. (8.51).

Chapter 9
Heat Transfer in Spray Cooling as an Inverse Problem

In any particular natural science, one encounters genuine scientific substance only to the extent that mathematics is present (*Immanuel Kant*)

Abstract The wall superheat—wall heat flux relationship in the spray cooling of a flat rectangular target is derived here from empirical time–temperature histories at an internal point. This is a classic transient inverse heat conduction problem and, in the present case, is solved by using exact expressions, due to Stefan (1889), for the wall temperature and the wall heat flux as functions of the midplane temperature and its time derivatives of increasing order.

Suppose that we want to investigate heat transfer in spray cooling by measuring the transient response of the midplane temperature $T_{mp}(t)$ in a cooled slab (target) and reconstructing from this the time histories of both the surface temperature $T_w(t)$ and the surface heat flux $q''_w(t)$, so that a "boiling curve" representing q''_w as a function of T_w (or $T_w - T_{sat}$) can be drawn.

Figure 9.1 shows the experimental arrangement used by Ciofalo et al. (2007). The target is first pre-heated up to 450–500 °C by an induction heater and then rapidly placed between twin spray jets issuing from identical nozzles under pressures ranging from 2 to 20 bar.

Figure 9.2 shows a detail of the target, made up of two aluminum slabs sandwiching three thin-foil thermocouples of negligible thermal inertia.

As it has been formulated above, the problem is a typical *transient inverse heat conduction* problem (Carslaw and Jaeger 1959). It can be reconducted to a Volterra equation of the first kind:

$$\mathbf{T}(t) = \int_a^t \mathbf{K}(t, \vartheta) \cdot \mathbf{q}(\vartheta) \mathrm{d}\vartheta \tag{9.1}$$

M. Ciofalo, *Thermofluid Dynamics*, UNIPA Springer Series,
https://doi.org/10.1007/978-3-031-30470-5_9

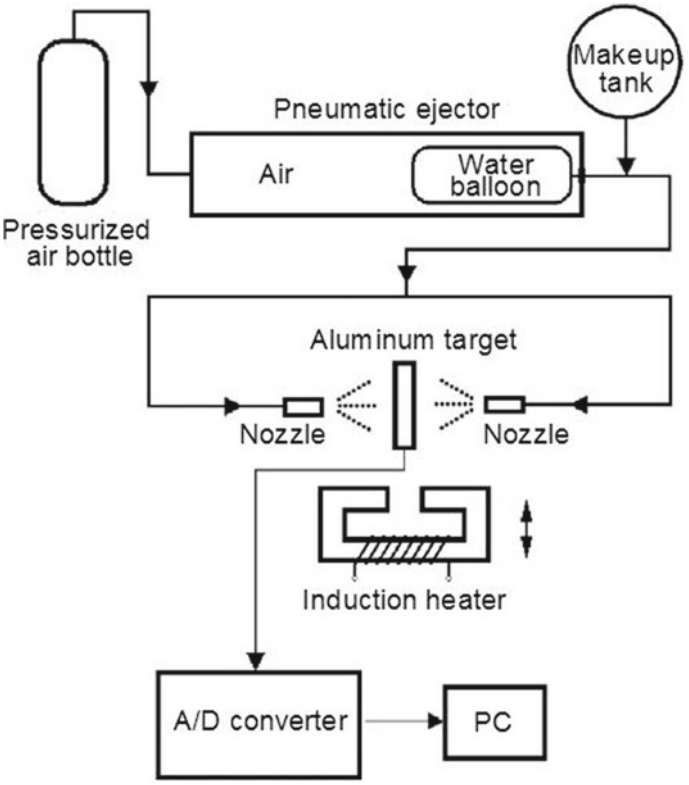

Fig. 9.1 Sketch of the test apparatus to investigate spray cooling

in which $\mathbf{T}(t)$ is an array containing n_T (≥ 1) *known* time histories (typically, measured internal temperatures as functions of time), $\mathbf{K}(t, \vartheta)$ is a given continuous kernel function and $\mathbf{q}(\vartheta)$ is an array of n_q time-dependent *unknown* parameters to be determined (typically describing surface heat flux, surface temperature or surface heat transfer coefficient). In the present application, $\mathbf{T}(t)$ is a single temperature–time history (average of the three mid-plane TC readings) while $\mathbf{q}(\vartheta)$ includes the time histories of both the surface heat flux q''_w and the surface temperature T_w, both assumed uniform over the target's surface.

In most inverse heat conduction problems an explicit expression for the kernel function $\mathbf{K}(t, \vartheta)$ and/or an explicit solution of Eq. (9.1) cannot be determined, and the problem is formulated as a best estimate one (Beck 1970): minimise the error function (in the least square sense)

$$E(\mathbf{q}) = \|\mathbf{T}_{EXP} - \mathbf{T}_{DIR}\|_2^2 \tag{9.2}$$

with respect to the array $\mathbf{q}$ of parameters describing the time history of the quantities to be determined (in the present case, the surface heat flux and the surface temperature).

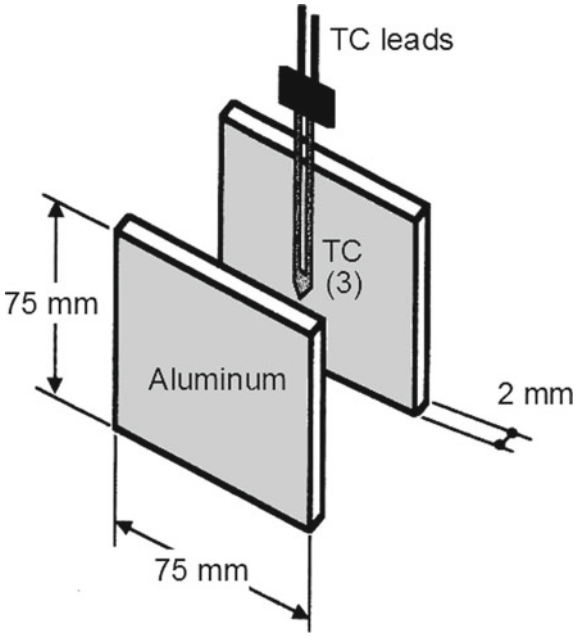

Fig. 9.2 Detail of the aluminum target

The right hand side of Eq. (9.2) is the square of the 2-norm of the array of differences between $\mathbf{T}_{EXP}$ (the experimental history of $\mathbf{T}$) and $\mathbf{T}_{DIR}$ (the history of $\mathbf{T}$ obtained by solving the corresponding direct problem in which $\mathbf{q}$ is imposed as a boundary condition). The error function can be defined in different modified ways to include a regularization parameter (Tikhonov and Arsenin 1977).

The present case, however, is one of the rare cases in which an exact (analytic) solution of the inverse conduction problem exists. It was given by Stefan as early in 1889, in the context of a paper dedicated to ice formation, and can be written

$$T_w(t) = T_{mp}(t) + \frac{1}{2}\tau\frac{\mathrm{d}T_{mp}}{\mathrm{d}t} + \frac{1}{24}\tau^2\frac{\mathrm{d}^2T_{mp}}{\mathrm{d}t^2} + \ldots \tag{9.3}$$

$$q''_w(t) = -\frac{\lambda}{\delta}\left[\tau\frac{\mathrm{d}T_{mp}}{\mathrm{d}t} + \frac{1}{6}\tau^2\frac{\mathrm{d}^2T_{mp}}{\mathrm{d}t^2} + \ldots\right] \tag{9.4}$$

in which $\tau = \alpha\delta^2/\alpha$ is the conductive time constant of the target (whose half-thickness is δ, see Fig. 9.2) and $\alpha = \lambda/(\rho c_p)$ is its thermal diffusivity. Further terms in the series give a negligible contribution to T_w and q''_w and can be omitted; their evaluation would require the computation of third- and higher-order time derivatives, very difficult from uncertainty-affected experimental data. Stefan's solution is valid for a uniform initial temperature, an assumption well satisfied in the experiments, and for a symmetry condition in the target's midplane; this is why experiments were conducted with (supposedly symmetric) two-side cooling.

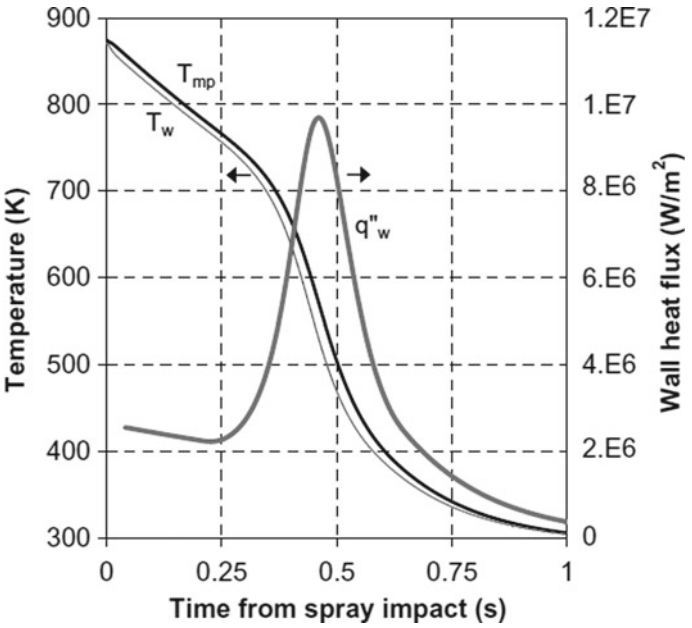

Fig. 9.3 Qualitative relation between mid-plane time–temperature histories and reconstructed wall temperature and wall heat flux (arbitrary data)

The relation between the time history of the mid-plane temperature and the corresponding histories of wall temperature and wall heat flux, as predicted by Eqs. (9.3) and (9.4), is schematically elucidated in Fig. 9.3. Note that the heat flux peak corresponds to the steepest tract of the mid-plane temperature descent and that, for the present data, the wall temperature remains close to the mid-plane one throughout the transient.

Even truncated to the second term, the series in Eqs. (9.3) and (9.4) are obviously highly sensitive to noise. Unfortunately, temperature–time histories exhibit significant noise, with special regard to interference from the 50-Hz grid. Therefore, some amount of data filtering is mandatory before applying Eqs. (9.3) and (9.4). Preliminary tests showed that the best results are obtained by using a Gauss filter, i.e. by substituting for the original signal $T_{mp}(t)$ its smoothed counterpart

$$\langle T_{mp} \rangle (t) = \frac{1}{\sqrt{2\pi}\sigma} \int_{-\infty}^{+\infty} T_{mp}(\vartheta) \exp\left[-\frac{(t-\vartheta)^2}{2\sigma^2} \right] \mathrm{d}\vartheta \tag{9.5}$$

in which σ is the filter half-width. σ must be large enough to eliminate most of the noise but small enough to preserve the overall behavior of the signal. In practice, the integral in Eq. (9.5) can be restricted to the interval $[t - n\sigma, t + n\sigma]$ with $n = 2 -$

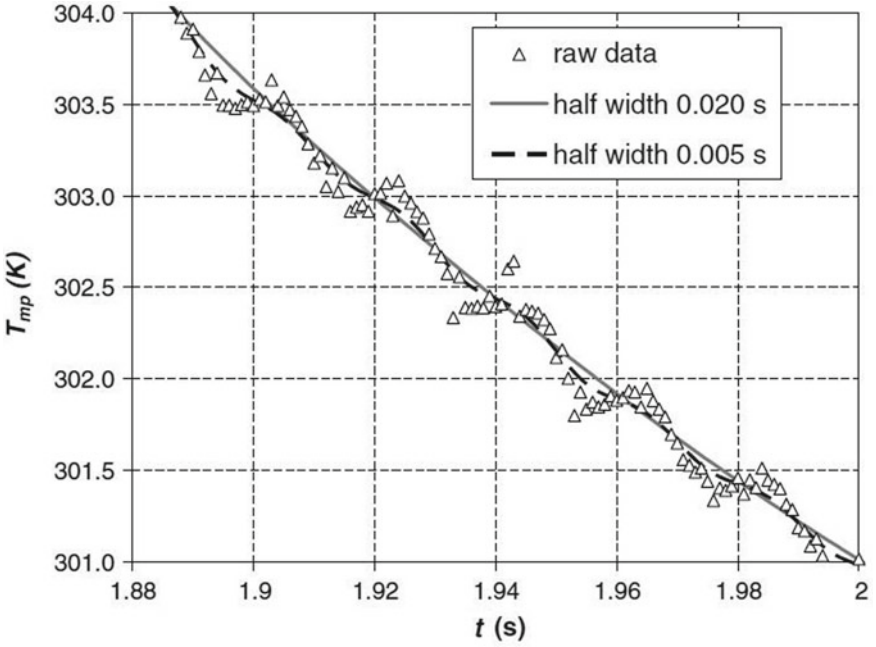

Fig. 9.4 Unfiltered (symbols) and filtered (lines) signal

4; a special treatment must be adopted for the initial region of the temperature–time history where $t < n\sigma$.

For example, Fig. 9.4 reports a short segment of a temperature–time history, corresponding to a data acquisition frequency of 1000 Hz. Interference from the grid ($f = 50$ Hz) is clearly visible. The effect of applying two Gaussian filters, of half-widths σ of 20 and 5 ms, respectively, is shown. Clearly, only the filter with $\sigma = 20$ ms ($=1/f$) is effective in eliminating the grid-related noise, which is still detectable in the signal filtered at $\sigma = 5$ ms.

Figure 9.5 reports two typical filtered midplane temperature (T_{mp}) histories, obtained for a given nozzle (SS3), an upstream pressure of 2 bar and a nozzle-target orthogonal distance L of 0.1 or 0.2 m.

The experiments reported by Ciofalo et al. (2007) gave for this configuration a drop mean volume diameter of 1.38 mm (mean volume $1.376 \cdot 10^{-9}$ m^3, i.e. 1.376 μL) and a drop velocity of 17.2 m/s. The numerical drop fluence varied roughly as L^{-2} and was $2.62 \cdot 10^6$ m^{-2} s^{-1} for $L = 0.1$ m and $7.99 \cdot 10^5$ m^{-2} s^{-1} for $L = 0.2$ m. The corresponding mass flow rates G impinging on the target were 3.6 kg m^{-2} s^{-1} for $L = 0.1$ m and 1.1 kg m^{-2} s^{-1} for $L = 0.2$ m. Therefore, the shorter the distance L, the faster the cooling transient; for $L = 0.1$ m peak cooling rates well above 1000 K/s were obtained at $t \approx 0.3$–0.4 s. In all cases, the cooling transient was very rapid and was practically completed after a few seconds.

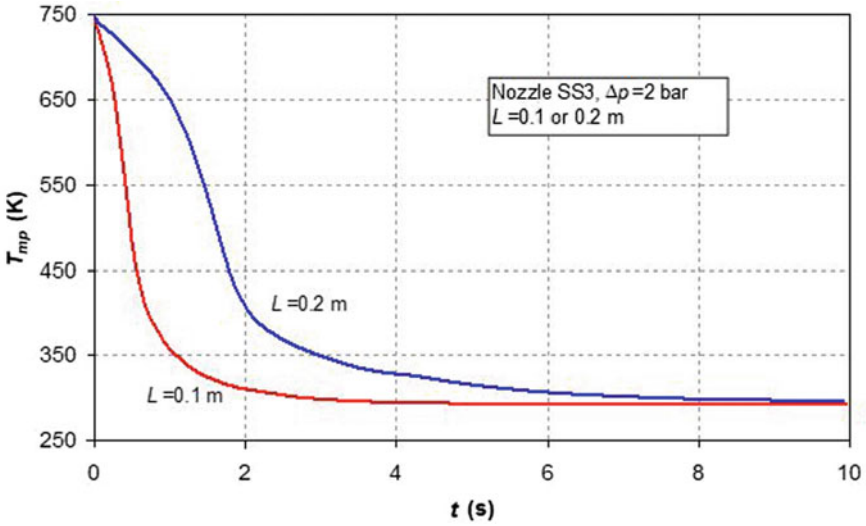

Fig. 9.5 Typical midplane temperature histories

Figure 9.6 reports corresponding time histories of the wall heat flux q''_w, as computed from the above time–temperature curves by applying Eq. (9.4). Despite filtering, the curves still exhibit a significant amount of noise, especially that corresponding to the larger nozzle-target distance of 0.2 m, yielding a lower heat flux and thus a lower signal-to-noise ratio. The peak heat flux (corresponding to the critical heat flux, i.e. to the condition known as Departure from Nucleate Boiling, or DNB) is ~3.64 MW m^{-2} for $L = 0.1$ m and ~1.52 MW m^{-2} for $L = 0.2$ m.

Corresponding boiling curves, in which the wall heat flux q''_w is reported against the wall temperature T_w as given by Eq. (9.3), are shown in Fig. 9.7. The fluid's temperature T_f (293.15 K, or 20 °C) and the saturation temperature T_{sat} (373.15 K, or 100 °C) are evidenced. As in Fig. 9.6, a certain residual amount of noise can be observed.

Figure 9.8 shows the main physical parameters that can be extracted from boiling curves like those in Fig. 9.7. In particular, they include the subcooled (single-phase) heat transfer coefficient h_1, which is the slope of the q''_w-T_w curve in its leftmost region $T_w \leq T_{sat}$, and the maximum, or critical, heat flux q''_c, attained at a wall temperature T_{wc} and corresponding to Departure from Nucleate Boiling (DNB) and transition to partial film boiling. A further feature of the curves, i.e., the Leidenfrost temperature, corresponding to transition from partial to complete film boiling, is not clearly visible in the experimental curves of Fig. 9.5 because it is close to the maximum temperature investigated (470 °C, or 743.15 K).

By applying the methodology sketched in Fig. 9.8 to the curves in Fig. 9.7, one obtains:

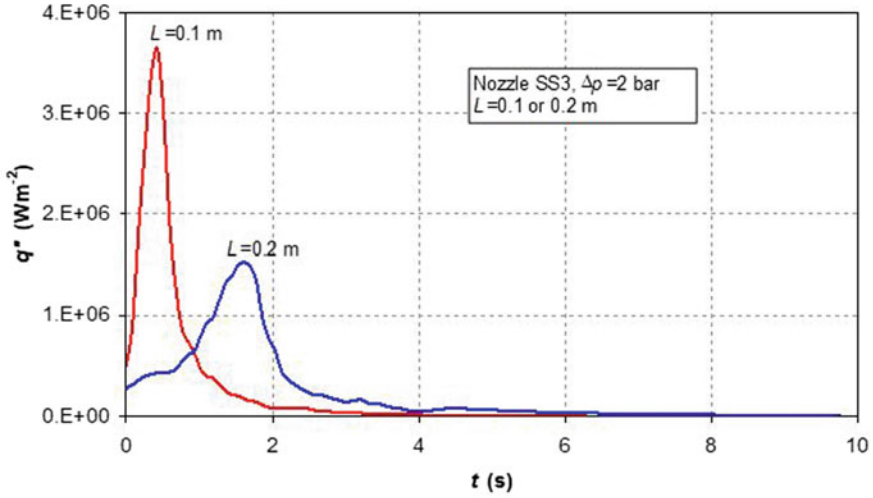

Fig. 9.6 Wall heat flux histories computed from the T_{mp}-t histories in Fig. 9.5

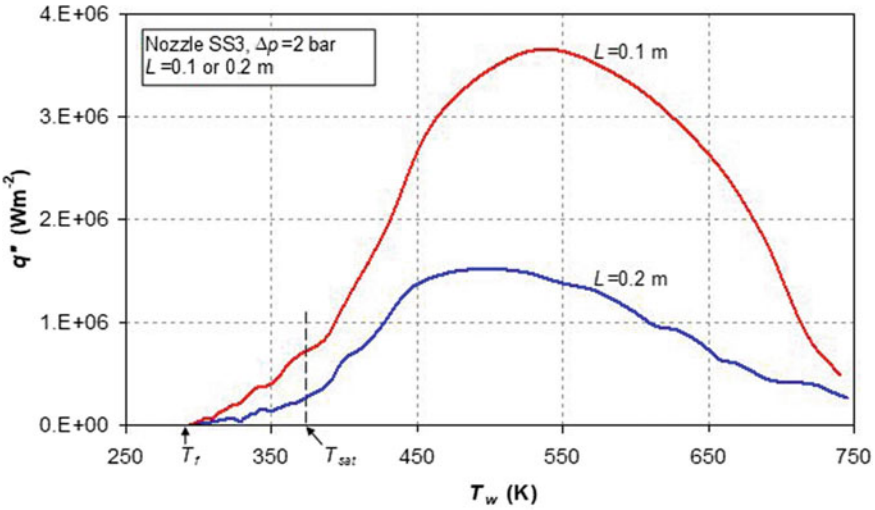

Fig. 9.7 Boiling curves corresponding to the q"-t time histories in Fig. 8.6

- For $L = 0.1$ m ($G = 3.6$ kg m^{-2} s^{-1}): $h_1 \approx 8000$ Wm^{-2} K^{-1}, $q''_c = 3.64 \cdot 10^6$ Wm^{-2}, $T_{wc} = 529$ K;
- For $L = 0.1$ m ($G = 1.1$ kg m^{-2} s^{-1}): $h_1 \approx 3100$ Wm^{-2} K^{-1}, $q''_c = 1.52 \cdot 10^6$ Wm^{-2}, $T_{wc} = 496$ K.

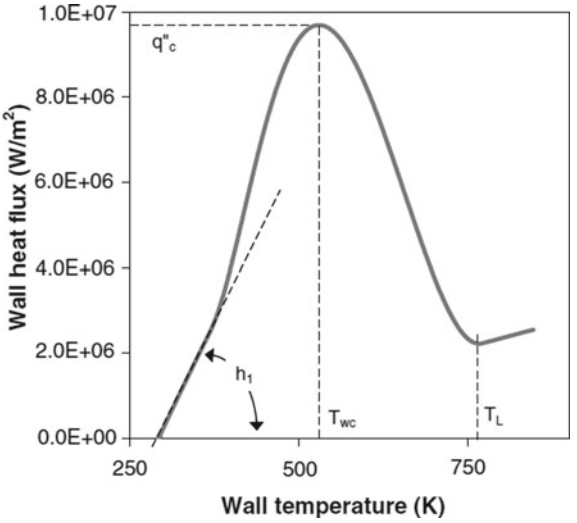

Fig. 9.8 Main features that can be extracted from boiling curves, including the single-phase heat transfer coefficient h_1 and the critical heat flux q''_c (arbitrary data)

Of course, the single-phase heat transfer coefficient h_1 can be obtained only approximately due to the "noisy" nature of the boiling curve, while the estimate of q''_c and T_{wc} can be more accurate since it concerns an extremal point.

The above results show that the DNB temperature increases with the mass flow rate. They also show that h_1 and q''_c remain roughly proportional, but they both increase less than linearly with the mass flow rate G (and thus with the numerical drop fluence), suggesting that the process of heat transfer to a single drop becomes less efficient when the numerical density of impinging drops increases.

This last concept can better be quantified by comparing the actual heat flux q''_w (as a function of the wall temperature T_w) with the corresponding maximum possible heat flux, associated with the complete transfer of both sensible heat and vaporization heat from the hot wall to the impinging drops. This latter quantity is

$$q''_{\max} = G\left[c_{p,f}\left(T_w - T_f\right)\right] \quad \text{if } T_w \le T_{sat} \tag{9.6}$$

$$q''_{\max} = G\left[c_{p,f}\left(T_{sat} - T_f\right) + J_{fg} + c_{p,g}(T_w - T_{sat})\right] \quad \text{if } T_w > T_{sat} \tag{9.7}$$

in which G, T_f and T_{sat} have been defined previously while $c_{p,f}$ and $c_{p,g}$ are the specific heats of the liquid and vapor phases (in J kg^{-1}K^{-1}) and J_{fg} is the latent heat of vaporization (in J kg^{-1}). Note that q''_{max} increases discontinuously in correspondence with $T_w = T_{sat}$.

Figure 9.9 shows the quantity $\eta = q''/q''_{max}$ (*cooling efficiency*) as a function of T_w for both cases $L = 0.1$ and $L = 0.2$ m.

Note that, being built as a ratio between noise-affected quantities, η is characterized by a highly irregular behaviour, especially in the single-phase region where it oscillates between ~0.3 and ~0.7. In the boiling region η becomes more regular but

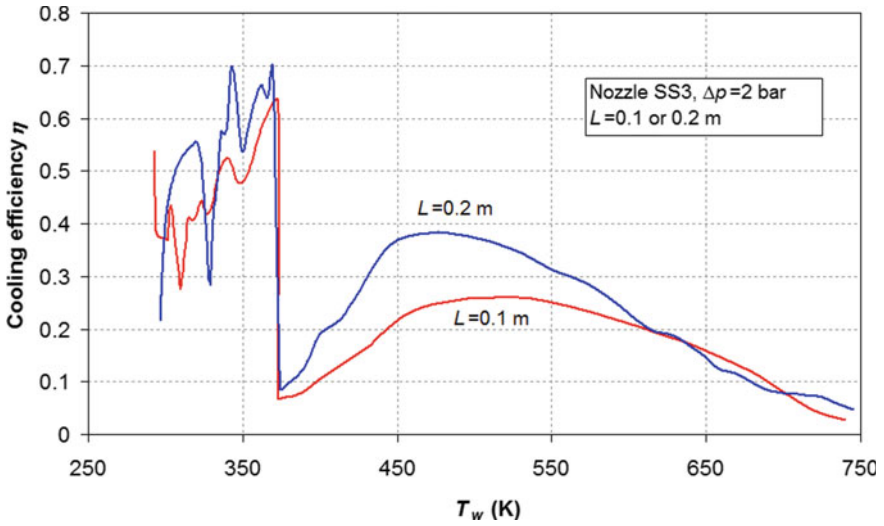

Fig. 9.9 Cooling efficiency as a function of the wall temperature

also significantly smaller, attaining maxima of ~0.25 for $L = 0.1$ m and ~0.38 for $L = 0.2$ m in correspondence with the critical heat flux. Over most of the temperature range investigated, η is larger for the larger nozzle-target distance, i.e. for the smaller numerical drop fluence.

In conclusion, an inverse heat transfer problem was dealt with on the basis of a classic analytic treatment by carefully designing the experimental setup so that it exhibited the required symmetries. In particular, two-side cooling was crucial for Stefan's analytic solution to be applicable.

Noise in the experimental data was still a major concern; the relatively crude filtering algorithm used here was sufficient to obtain acceptable results, but a more sophisticated approach would certainly improve their quality.

Chapter 10
Apparent Sherwood Number in Mass Transfer with Wall Transpiration

In questions of science, the authority of a thousand is not worth the humble reasoning of a single individual
(*Galileo Galilei*)

Abstract This problem regards the apparent Sherwood number in simultaneous diffusive and convective mass transfer from or into a transpiring wall. This is the Sherwood number that would explain the observed overall mass flux from or into the wall if there were no transpiration, i.e. no convective contribution to mass transport. Using only elementary definitions of diffusive and convective mass fluxes, a complete classification of the possible cases is presented and a synthetic map is built representing the apparent Sherwood number as a function of two dimensionless parameters, named "transpiration" and "flux" numbers.

A *transpiring* wall is a surface bounding a flow region through which fluid can pass either into the main stream (*injection*) or out of it (*suction*). As sketched in Fig. 10.1, transpiration may occur either through a porous wall (a) or through macroscopic orifices in an otherwise impermeable wall (b).

Here, we are mainly concerned with the influence of transpiration on mass transfer to or from a fluid flowing in a duct and bounded by a porous surface (e.g. a *membrane*). A typical example is the process of toxicant removal from the blood in hollow-fiber haemodiafiltration modules (Cancilla et al. 2022), which is driven partly by a concentration difference between the lumen-side fluid (blood) and the shell-side solution (dialysate), partly by ultrafiltration (caused in its turn by a pressure difference) through the membrane, either towards the dialysate (forward filtration) or towards the blood (back filtration).

Of course, transpiration is itself a mass transfer process; however, we will restrict this notion to the transport of a species ("solute", subscript "S") different from the carrying fluid ("solution", subscript "W"—often water). Note that the terms "solute" and "solution" are not used here in their rigorous physico-chemical sense, but may well denote a solid suspended in a liquid. Many of the equations governing the

M. Ciofalo, *Thermofluid Dynamics*, UNIPA Springer Series,
https://doi.org/10.1007/978-3-031-30470-5_10

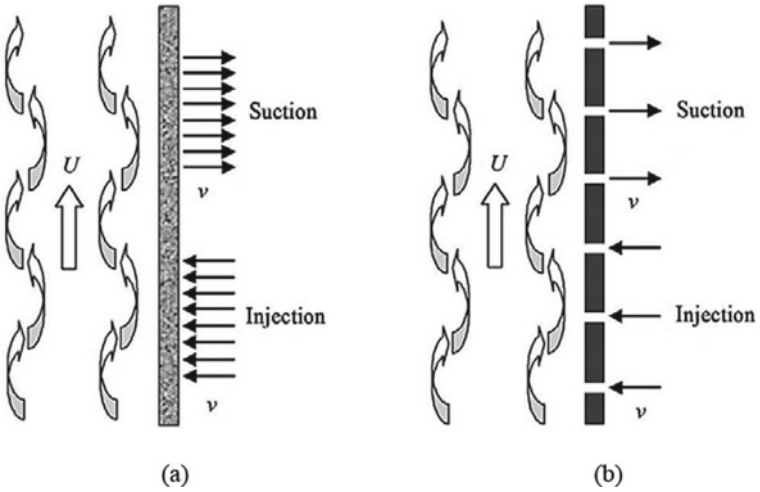

Fig. 10.1 Transpiring walls with injection or suction. **a** Porous. **b** Perforated

phenomenon and of the conclusions drawn can be applied, with small changes, to a process of *heat* (rather than *mass*) transfer.

With reference to Fig. 10.2, in the presence of transpiration the total solute mass flux into the solution, j_S (measured in kg m^{-2} s^{-1}) is the sum of a diffusive component j_{diff} and of a convective component j_{conv}:

$$j_S = j_{diff} + j_{conv} = -\rho D \left.\frac{\partial C}{\partial y}\right|_w + \rho v C_w \tag{10.1}$$

in which ρ is the fluid (solution) density in kg/m^3, D is the solute diffusivity in m^2/s, C is its concentration in kg/kg, w denotes the wall, y is the direction normal to it and towards the fluid, and v is the transpiration velocity in m/s. All mass fluxes are taken as positive if directed into the fluid. Note that the expression of the diffusive flux as proportional to the concentration gradient at the wall holds also in turbulent flow, because there will always exist a near-wall diffusive sublayer in which mass transfer occurs only by diffusion.

In the no transpiration case, graph (a), the mass flux at the wall is purely diffusive. For positive transpiration (injection, $v > 0$), graph (b), C_w, $C_w - C_b$ and the diffusive mass flux—$\rho D(\partial C/\partial y)_w$ decrease with respect to the no transpiration case (a), but this reduction is compensated by a positive (into the fluid) convective mass flux $\rho|v|C_w$, so that the overall mass transfer rate may increase. On the contrary, graph (c) is for a channel with negative transpiration (suction, $v < 0$) of the same intensity as in case (b). Here C_w, $C_w - C_b$ and the diffusive mass flux—$\rho D(\partial C/\partial y)_w$ increase with respect to the non-transpiring case (a), but this increment is compensated by a negative (out of the fluid) convective mass flux—$\rho|v|C_w$, so that the overall mass transfer coefficient rate may decrease with respect to the no transpiration case.

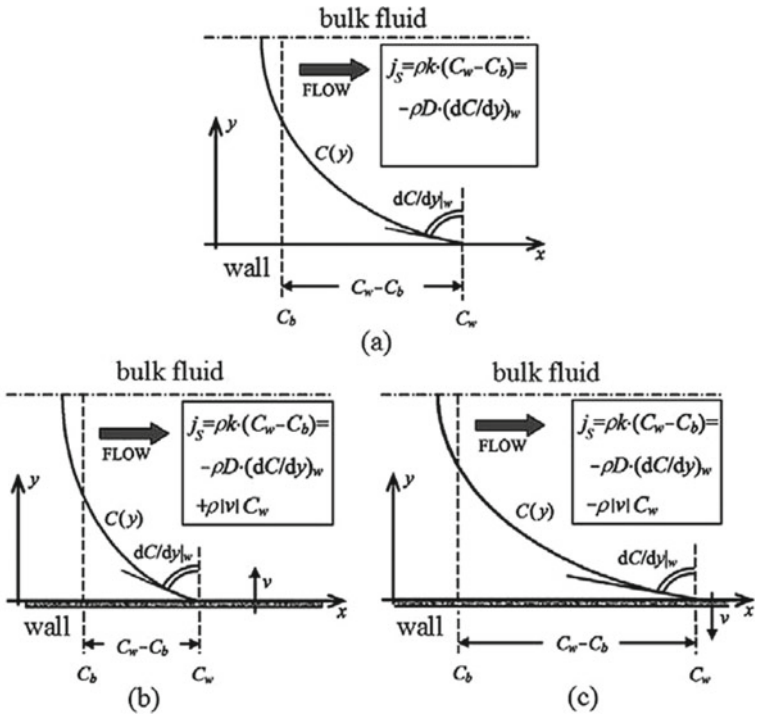

Fig. 10.2 Concentration profiles and mass fluxes with non-transpiring and transpiring walls for the same values of the bulk concentration C_b and total mass flux j_S. **a** No transpiration. **b** Injection. **c** Suction. Adapted from Ciofalo et al. (2019)

In all cases, the *diffusive* mass transfer coefficient is defined as

$$k_{diff} = \frac{j_{diff}}{\rho(C_w - C_b)} = -\frac{D}{C_w - C_b}\left.\frac{\partial C}{\partial y}\right|_w \tag{10.2}$$

It is a local quantity, is measured in m/s and is often made dimensionless as a (diffusive) Sherwood number

$$\mathrm{Sh}_{diff} = k_{diff}\frac{d_{eq}}{D} = -\frac{d_{eq}}{C_w - C_b}\left.\frac{\partial C}{\partial y}\right|_w \tag{10.3}$$

By analogy with k_{diff} and Sh_{diff}, also a convective mass transfer coefficient and a convective Sherwood number can be defined as

$$k_{conv} = \frac{j_{conv}}{\rho(C_w - C_b)} = \frac{vC_w}{C_w - C_b} \tag{10.4}$$

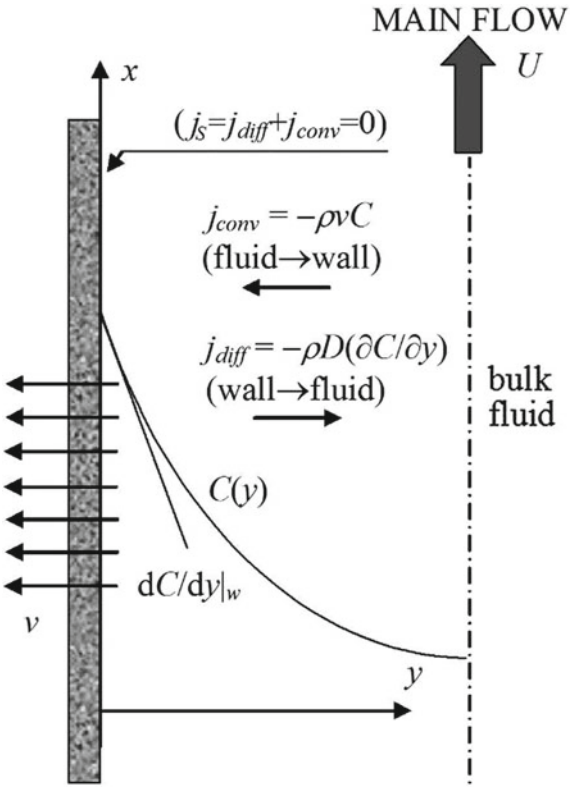

Fig. 10.3 Mass transfer in cross-flow filtration and reverse osmosis, with zero net solute flux. Adapted from Ciofalo et al. (2019)

$$\mathrm{Sh}_{conv} = k_{conv}\frac{d_{eq}}{D} = \frac{v d_{eq}}{D}\frac{C_w}{C_w - C_b} \tag{10.5}$$

Finally, an *apparent* (total) mass transfer coefficient k and an apparent Sherwood number Sh can be defined as

$$k = \frac{j_S}{\rho(C_w - C_b)} = k_{diff} + k_{conv} \tag{10.6}$$

$$\mathrm{Sh} = k\frac{d_{eq}}{D} = \mathrm{Sh}_{diff} + \mathrm{Sh}_{conv} \tag{10.7}$$

A special case of mass transfer with transpiration occurs in cross-flow filtration processes, including reverse osmosis (Fig. 10.3).

Here, the solute concentration builds up near the wall, causing a wall-to-fluid diffusive flux of solute $j_{diff} = -\rho D(\partial C/\partial y)$. At the same time, the (negative) y-component v of the solution velocity causes a convective flux $j_{conv} = \rho vC$ directed from the fluid to the wall. At the wall ($y = 0$), the two fluxes compensate each other (for a perfectly selective membrane), so that

$$j_S = -\rho D \left.\frac{\partial C}{\partial y}\right|_w + \rho v C_w = 0 \tag{10.8}$$

which is just a special case of Eq. (10.1).

In these cases, although the net solute flux j_S is nil, Eq. (10.8) is still required to establish a link between the transpiration velocity v and the wall concentration C_w. More precisely, if the diffusive mass transfer coefficient k_{diff} is known, one has $-D(\partial C/\partial y)_w = k_{diff}\,(C_w - C_b)$, which, together with Eq. (10.8), explicitly gives $C_w = C_b k_{diff}\,/(k_{diff} + v)$. If k_{diff} is not known (for example, because the channel has a complex geometry or is filled with a spacer/mixing promoter), then Eq. (10.8) plays the role of a Robin wall boundary condition for the concentration C, allowing—once v is imposed—the solution of a solute transport equation and thus the assessment of the C profile and, in particular, of C_w (Amokrane et al. 2015).

In the following, we will assume that concentration profiles across the channel are not excessively perturbed by transpiration, so that they remain self-similar at different transpiration intensities. Under this assumption, the diffusive Sherwood number Sh_{diff}, Eq. (10.3), coincides with that obtained under no-transpiration conditions, Sh_0, which depends on the duct's geometry and on the boundary conditions. In the fully developed region, it is exactly known from analytical solutions for parallel flow in simple ducts such as circular pipes or plane channels.

For physical reasons, the approximation $\mathrm{Sh}_{diff} = \mathrm{Sh}_0$ is the more accurate the smaller the transpiration intensity. Under this assumption, from the previous definitions one has:

$$j_S = j_{diff} + j_{conv} = \mathrm{Sh}_0 (C_w - C_b)\frac{\rho D}{d_{eq}} + j_W C_w \tag{10.9}$$

For any given C_b, if the transpiration flux j_W and the wall concentration C_w are known, then Eq. (10.9) directly provides the total solute mass flow rate j_S. Conversely, if both the solute and the solution mass flow rates j_S, j_W are known, then the wall concentration can be obtained by solving Eq. (10.9) for C_w:

$$C_w = \frac{j_S + \mathrm{Sh}_0 C_b \rho D/d_{eq}}{j_W + \mathrm{Sh}_0 \rho D/d_{eq}} \tag{10.10}$$

Equations (10.9) and (10.10) solve the problem of determining j_S for a given C_w or vice versa, once j_W, Sh_0 and the local bulk concentration C_b are known.

The above results can be cast into a more elegant and physically meaningful form by expressing the apparent Sherwood number Sh as a function of dimensionless parameters. To this purpose, let us define the following *local* dimensionless numbers:

$$\mathrm{Pe} = \frac{U d_{eq}}{D} \quad \text{(Péclet number)} \tag{10.11}$$

$$\tau = \frac{j_W}{\rho}\frac{d_{eq}}{D}\frac{1}{\mathrm{Sh}_0} \quad \text{(transpiration number)} \tag{10.12}$$

$$\phi = \frac{j_S}{\rho C_b}\frac{d_{eq}}{D}\frac{1}{\mathrm{Sh}_0} \quad \text{(flux number)} \tag{10.13}$$

in which ρ and D are the solution density and the solute diffusivity corresponding to the local bulk concentration C_b. Please note that these definitions are different from those used in Ciofalo et al. (2019).

The transpiration number τ expresses the importance of the transpiration flow. Consistent with the above assumptions, it is positive for injection and negative for suction. The flux number ϕ expresses the importance of the net solute mass flux crossing the walls; also this quantity is positive for a net solute flow into the channel, negative for a net solute flow out of it.

With some manipulations and taking account of the definitions in Eqs. (10.6), (10.7), (10.11)–(10.13), from Eq. (10.9) the following identity is obtained:

$$R = \frac{\mathrm{Sh}}{\mathrm{Sh}_0} = \frac{1+\tau}{1-\tau/\phi} \tag{10.14}$$

This shows that, under the assumption of self-similar concentration profiles, the ratio $R = \mathrm{Sh}/\mathrm{Sh}_0$ is a function of the dimensionless numbers τ and ϕ only, independent of the Péclet number and of Sh_0. Isolines of $\mathrm{Sh}/\mathrm{Sh}_0$ can be plotted in the (τ, ϕ) plane to build up the "universal" map shown in Fig. 10.4.

Note that the assumption of sufficiently small transpiration fluxes of solution and solvent, necessary for the approximation $\mathrm{Sh}_{diff} = \mathrm{Sh}_0$ to hold, translates into the fact that the identity (10.14), and thus its representative map in Fig. 10.4, must be restricted to absolute values of both τ and ϕ less than 1 (in this case, the map has been drawn for τ and ϕ ranging from -0.5 to $+0.5$).

The map can be divided into several regions differing in the sign and relative importance of τ and ϕ and in the values correspondingly attained by the normalized Sherwood number $\mathrm{Sh}/\mathrm{Sh}_0$. The various cases are discussed in detail in the following; the reported insets show the direction of solution and solute fluxes and the concentration profile associated to each value, or range of values, of the polar coordinate θ defined by $\phi/\tau = \tan(\theta)$.

- For $\theta = 0$, i.e. along the $\tau > 0$ half of the horizontal axis $\phi = 0$, the net solute flux is nil but a positive solution transpiration flux exists (except at the origin), creating a concentration profile and a (negative) concentration drop $\Delta C = C_w - C_b$. Therefore, one has $\mathrm{Sh} = 0$. The origin itself is a singular case in which neither solution nor solute fluxes exist and Sh is undefined.

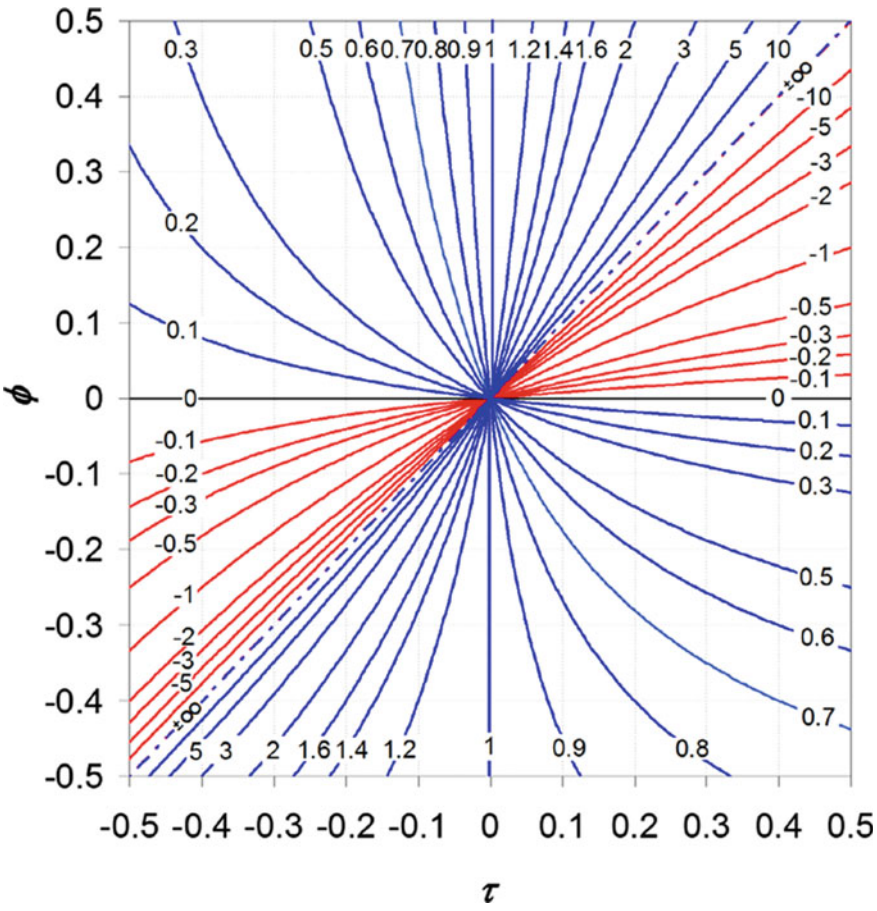

Fig. 10.4 Isolines $Sh/Sh_0 = \text{constant}$ in the (τ, ϕ) plane. Red lines: $Sh < 0$; blue lines: $Sh > 0$. Note the $\pm\infty$ asymptotes for $\phi = \tau$

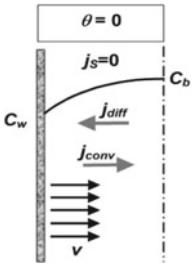

- For $0 < \theta < 45°$, both the solute and the solution fluxes are positive ($\tau > 0$, $\phi > 0$) but the convective solute flux is larger than the diffusive one ($\tau > \phi$) so that the

wall concentration is still lower than the bulk concentration, yielding $\Delta C < 0$ and thus $\mathrm{Sh} < 0$.

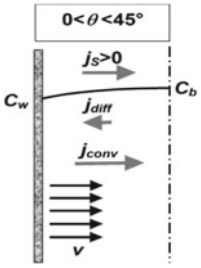

- For $\theta = 45°$, i.e. along the bisecting line $\phi = \tau$ (with $\phi > 0$, $\tau > 0$), the solute influx is purely convective, so that $\Delta C = 0$ and Sh diverges to $-\infty$ on the side $\theta < 45°$ and to $+\infty$ on the opposite side $\theta > 45°$.

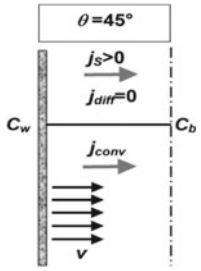

- For $45° < \theta < 90°$, both the solute and the solution fluxes are still positive ($\tau > 0$,$\phi > 0$), but the convective solute flux is less than the diffusive one ($\tau < \phi$); $\Delta C = C_w - C_b$ is now positive but less than it would be for the same j_S in the absence of transpiration, so that Sh exceeds Sh_0. This is the range in which blowing promotes mass or heat transfer from the wall to the fluid.

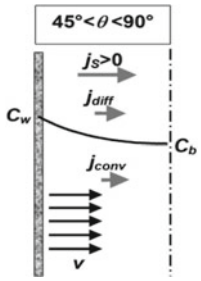

- For $\theta = 90°$, i.e. along the vertical axis ($\tau = 0$, $\phi > 0$), the classic condition of mass transfer from the wall to the fluid without transpiration is recovered, and Sh attains its reference value Sh_0.

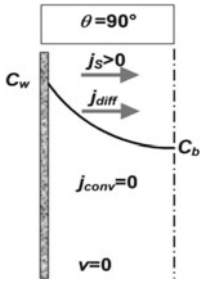

- For $90° < \theta < 180°$, one has $\tau < 0$, $\phi > 0$. The convective solute flux is negative but less, in absolute value, than the diffusive solute flux; for a given total solute flux, the diffusive component and $\Delta C = C_w - C_b$ (>0) are larger than for $\theta = 90°$, so that Sh becomes less than Sh_0. This is the range in which suction inhibits mass or heat transfer from the wall to the fluid.

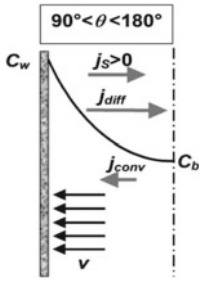

- The case $\theta = 180°$ (left part of the horizontal axis $\phi = 0$) is similar to the case $\theta = 0$: the solute flux is nil but a negative solution transpiration flux exists, creating a concentration profile and a (positive) concentration drop $C_w - C_b$. Therefore, $Sh = 0$. This case is, basically, that previously discussed for reverse osmosis or filtration (Fig. 10.3).

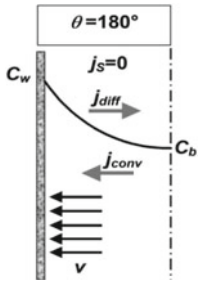

- For $180° < \theta < 225°$, both the solute and the solution fluxes are negative ($\tau < 0$, $\phi < 0$) but the convective solute flux dominates over the diffusive one ($|\tau| > |\phi|$), so that the wall concentration becomes higher than the bulk concentration and Sh < 0.

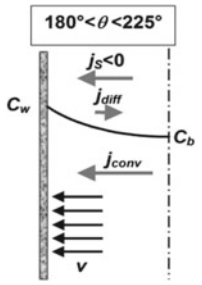

- For $\theta = 225°$, i.e. along the bisecting line $\phi = \tau$ (with $\phi < 0$, $\tau < 0$), the solute flux is purely convective, so that $C_w - C_b = 0$ and Sh diverges to $-\infty$ on the side $\theta < 225°$ and to $+\infty$ on the opposite side $\theta > 225°$.

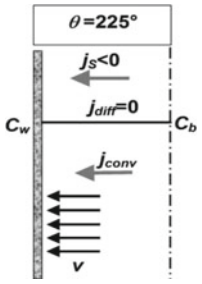

- For $225° < \theta < 270°$, both the solute and the solution fluxes are still negative ($\tau < 0$, $\phi < 0$), but the solution outflow is relatively small ($|\tau| < |\phi|$); the result is a reduction of $|C_w - C_b|$ (with $C_w - C_b$ negative) and an increment of Sh with respect to the non-transpiring case ($Sh > Sh_0$). In this range suction promotes mass or heat transfer from the fluid to the wall.

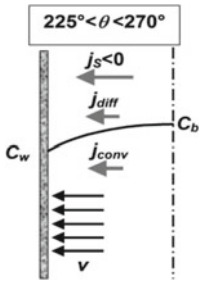

- For $\theta = 270°$, i.e. along the vertical axis ($\tau = 0$, $\phi < 0$), the classic condition of mass transfer (from fluid to wall) without transpiration is recovered, as in the case $\theta = 90°$, and $\mathrm{Sh} = \mathrm{Sh}_0$.

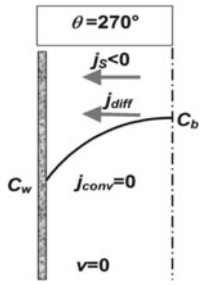

- Finally, for $270° < \theta < 360°$, one has $\tau > 0$, $\phi < 0$. The convective solute flux at the wall is positive but less, in absolute value, than the total (negative) solute flux; for a given total solute flux, the diffusive component and $|C_w - C_b|$ increase ($C_w - C_b$ is negative) with respect to the no-transpiration case, so that Sh becomes less than Sh_0. In this range blowing inhibits mass transfer from fluid to wall (mass transfer analogue of transpiration cooling).

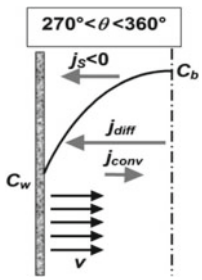

The singularities at $\theta = 45°$ and $225°$ correspond to $\phi = \tau$. Under this condition, the combined effect of solution and solute inflow or outflow is equivalent to the inflow

or outflow of a solution having a concentration equal to the bulk concentration in the channel: $j_S \neq 0$ but $C_w - C_b = 0$, hence $\mathrm{Sh} = \pm\infty$.

Figure 10.4 suggests that not only the qualitative behaviour of the solution, but also the ratio $\mathrm{Sh}/\mathrm{Sh}_0$ is mainly a function of the polar coordinate θ. In fact, an analysis of Eq. (10.14) shows that, for small values of τ, one has $\mathrm{Sh}/\mathrm{Sh}_0 \approx (1 - \tau/\phi)^{-1}$, i.e. $\mathrm{Sh}/\mathrm{Sh}_0$ is a function of the single dimensionless number $\phi/\tau = \tan(\theta)$ (ratio of flow and transpiration numbers). For larger values of τ, $\mathrm{Sh}/\mathrm{Sh}_0$ in Eq. (10.14) becomes a function of τ and ϕ separately, and not only of their ratio. This behaviour corresponds to the departure of the iso-lines in Fig. 10.4 from straight lines crossing the origin, a departure which is particularly visible in the second and fourth quadrants where ϕ and τ have opposite signs.

Chapter 11
One-Dimensional Mixed MHD Convection

He is the wisest philosopher, who holds his theory with some doubt
(*Michael Faraday*)

Abstract This problem concerns the magnetohydrodynamics (MHD) flow in a vertically indefinite rectangular channel. Internal heat generation and a nonuniform electric potential can optionally be present. If all present, magnetic field, gravity acceleration and electric potential gradient are mutually orthogonal, while the temperature gradient is parallel to the electric potential one. The governing equations include, besides the fluid's continuity, momentum and energy equations, also an equation for the electric potential and a phenomenological expression for the total current density. Exact solutions show that, according to the boundary conditions and the source terms, the system can operate in a variety of alternative regimes including direct and reverse EM pump, direct and reverse MHD generator, and a purely dissipative mode. In the presence of buoyancy, the system can also operate as a thermal engine converting thermal power into electrical and/or mechanical power.

Magnetohydrodynamics (MHD) deals with the motion of electrically conducting fluids under the influence of a magnetic field (Moreau 1990). MHD phenomena are widely exploited in different industrial processes ranging from metallurgy to the production of pure crystals and nuclear fusion engineering (Ciofalo et al. 2005).

Two- or three-dimensional MHD problems are rarely amenable to exact (analytical) solutions, and a combination of asymptotic analysis and numerical methods usually has to be employed (Bühler 1998; Di Piazza and Bühler 2000) which often obscures the meaning of the results since closed form expressions for various quantities of physical relevance cannot be written.

However, exact solutions exist for *one-dimensional* MHD problems (Sposito and Ciofalo 2006). Consider, in particular, the configuration in Fig. 11.1: a plane channel, indefinite along y and z and delimited along x by two plane parallel walls placed at a distance D, in which a conducting fluid flows vertically with velocity $\mathbf{w}$ in the presence of a horizontal magnetic induction field $\mathbf{B}$.

M. Ciofalo, *Thermofluid Dynamics*, UNIPA Springer Series,
https://doi.org/10.1007/978-3-031-30470-5_11

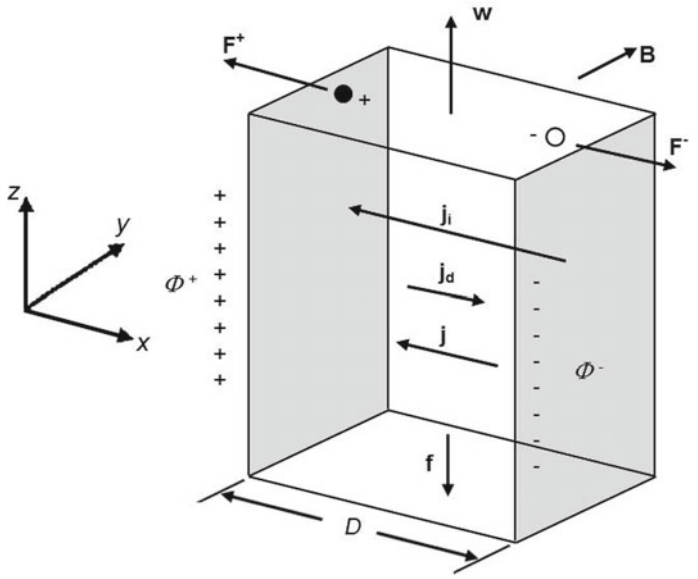

Fig. 11.1 Lorentz forces and electric currents as an electrically conducting fluid flows upwards in a straight duct with velocity **w** in the presence of a horizontal magnetic induction field **B**

The Lorentz forces $\mathbf{F} = q\mathbf{w} \times \mathbf{B}$ acting on the (positive and negative) electric charges q convected by the fluid yield an induced current density $\mathbf{j}_i = \sigma\mathbf{w} \times \mathbf{B}$, σ being the fluid's electric conductivity. At the same time, charge separation creates through the duct a gradient of electric potential which, in addition to any possibly present imposed potential difference between the two walls, results in a total potential φ and in a potential-driven electric current of density $\mathbf{j}_d = -\sigma\nabla\varphi$. The overall current density $\mathbf{j} = \sigma(\mathbf{w} \times \mathbf{B} - \nabla\varphi)$ is shown in Fig. 11.1 as possessing the same direction of $\mathbf{j}_i$, but, depending on the boundary conditions, this is not necessarily true. The interaction between the current density **j** and the magnetic induction field **B** causes, in its turn, a magnetohydrodynamic force of volume density $\mathbf{f} = \mathbf{j} \times \mathbf{B}$, which may locally oppose or aid the fluid's motion according to whether the induced or the diffusive current (i.e., $\mathbf{j}_i$ or $\mathbf{j}_d$) prevails.

The only nonzero velocity component is w, and the only nonzero electric current density component is j_x. These quantities, as well as electric potential and temperature, depend only on x, while pressure depends only on z. Assuming, for greater generality, buoyancy forces to be present (which can be described by the usual Boussinesq approximation), the z-momentum equation for steady parallel flow can be written as

$$0 = -\frac{\mathrm{d}p}{\mathrm{d}z} + \mu\frac{\mathrm{d}^2 w}{\mathrm{d}x^2} + g\beta\rho\vartheta + j_x B \tag{11.1}$$

in which g is the gravity acceleration, ϑ is the temperature relative to some arbitrary reference value and β is the fluid's thermal expansion coefficient. Note that, for

sufficiently large B, MHD flows tend to remain steady even at large Reynolds numbers due to turbulence damping by MHD forces.

As mentioned above, the total current density can be written as

$$j_x = -\sigma\left(wB + \frac{\mathrm{d}\varphi}{\mathrm{d}x}\right) \tag{11.2}$$

By substituting Eq. (11.2) for j_x into Eq. (11.1), one obtains the following inhomogeneous modified Helmholtz equation governing the velocity w:

$$\mu\frac{\mathrm{d}^2 w}{\mathrm{d}x^2} - \sigma B^2 w = \frac{\mathrm{d}p}{\mathrm{d}z} - g\beta\rho\vartheta + \sigma B\frac{\mathrm{d}\varphi}{\mathrm{d}x} \tag{11.3}$$

The electric potential φ follows the Poisson equation

$$\frac{\mathrm{d}^2\varphi}{\mathrm{d}x^2} = -B\frac{\mathrm{d}w}{\mathrm{d}x} \tag{11.4}$$

while the energy transport equation reduces, for a fully developed thermal field, to

$$\frac{\mathrm{d}^2\vartheta}{\mathrm{d}x^2} = -\frac{q'''}{\lambda} \tag{11.5}$$

in which q''' is the volumetric thermal power density (if any) and λ is the fluid's thermal conductivity.

Equations (11.3) through (11.5) are the complete set of governing equations for the problem under consideration. They can be set in a dimensionless form by choosing, for example, the following reference scales (here, $\nu = \mu/\rho$ is the kinematic viscosity of the fluid):

- Length: D;
- Velocity: ν/D;
- Temperature: $q'''D^2/(8\lambda)$;
- Electric potential: νB;
- Electric current density: $\nu B\sigma/D$.

Equations (11.3)–(11.5) then become

$$\frac{\mathrm{d}^2 W}{\mathrm{d}X^2} - \mathrm{M}^2 W = -\frac{\mathrm{Gr}}{8}\Theta + \mathrm{M}^2\frac{\mathrm{d}\Phi}{\mathrm{d}X} - \mathrm{P} \tag{11.6}$$

$$\frac{\mathrm{d}^2\Phi}{\mathrm{d}X^2} = -\frac{\mathrm{d}W}{\mathrm{d}X} \tag{11.7}$$

$$\frac{\mathrm{d}^2\Theta}{\mathrm{d}X^2} = -8 \tag{11.8}$$

in which $X = x/D$, $W = wD/\nu$, $\Theta = \vartheta \cdot (8\lambda)/(q''' D^2)$, $\Phi = \varphi/(\nu B)$, and M, Gr, P are dimensionless numbers defined as

$$\mathrm{M} = B D \sqrt{\frac{\sigma}{\mu}} \quad \text{(Hartmann number)} \tag{11.9}$$

$$\mathrm{Gr} = \frac{g\beta q''' D^5}{\lambda \nu^2} \quad \text{(Grashof number)} \tag{11.10}$$

$$\mathrm{P} = -\frac{\mathrm{d}p}{\mathrm{d}z} \frac{\rho D^3}{\mu^2} \quad \text{(pressure head number)} \tag{11.11}$$

The case $\mathrm{M} = 0$ corresponds to no MHD effects, the case $\mathrm{Gr} = 0$ to no buoyancy and the case $\mathrm{P} = 0$ to no forced flow.

Similarly, the electric current in Eq. (11.2) is replaced by its dimensionless counterpart:

$$J_x = -\left(W + \frac{\mathrm{d}\Phi}{\mathrm{d}X} \right) \tag{11.12}$$

Boundary conditions must now be imposed to the above system. In regard to velocity and temperature, the following ones will be considered here:

- No slip conditions at the walls (located, say, at $x = \pm D/2$):

$$W\left(\pm \frac{1}{2} \right) = 0 \tag{11.13}$$

- Uniform and equal temperature at both walls; choosing this as the reference temperature for buoyancy, one has:

$$\Theta\left(\pm \frac{1}{2} \right) = 0 \tag{11.14}$$

The heat Eq. (11.8) with B.C.s (11.14) immediately yields the parabolic temperature distribution:

$$\Theta(X) = 1 - 4X^2 \tag{11.15}$$

whose mean value is $\overline{\Theta} = 2/3$.

In regard to the electric potential, two alternatives will be considered.

(a) **Equipotential walls**

In this case, the boundary conditions for Φ are simply

$$\Phi\left(\pm\frac{1}{2}\right) = 0 \tag{11.16}$$

The potential Eq. (11.7) can be formally integrated once to give:

$$\frac{\mathrm{d}\Phi}{\mathrm{d}X} = -W + c_1 \tag{11.17}$$

in which c_1 is an integration constant. Taking Eqs. (11.15) and (11.17) into account, the momentum Eq. (11.6) becomes:

$$\frac{\mathrm{d}^2 W}{\mathrm{d}X^2} = -\frac{\mathrm{Gr}}{8}\left(\frac{1}{3} - 4X^2\right) + \mathrm{M}^2 c_1 - \mathrm{P} \tag{11.18}$$

By integrating twice with respect to X and imposing the boundary conditions (11.13), one has:

$$W(X) = \frac{\mathrm{Gr}}{384} + \frac{\mathrm{P}}{8} - \frac{c_1 \mathrm{M}^2}{8} + \frac{1}{2}\left(-\frac{\mathrm{Gr}}{24} + c_1 \mathrm{M}^2 - \mathrm{P}\right)X^2 + \frac{\mathrm{Gr}}{24}X^4 \tag{11.19}$$

This last expression, which still depends upon the integration constant c_1, can be substituted for W in Eq. (11.17), which, once integrated again, gives:

$$\Phi(X) = \left[c_1\left(1 + \frac{\mathrm{M}^2}{8}\right) - \frac{\mathrm{Gr}}{384} - \frac{\mathrm{P}}{8}\right]X - \frac{1}{6}\left(c_1 \mathrm{M}^2 - \mathrm{P} - \frac{\mathrm{Gr}}{24}\right)X^3 - \frac{\mathrm{Gr}}{120}X^5 + c_2 \tag{11.20}$$

Finally, by imposing the boundary conditions (11.16) one obtains the two constants c_1 and c_2 which, once substituted in Eqs. (11.19) and (11.20), explicitly yield the profiles of W and Φ as functions of X:

$$\begin{aligned} W(X) = {} & \frac{1}{8}\left(\frac{\mathrm{Gr}}{48} + \mathrm{P} - \frac{\mathrm{M}^2}{\mathrm{M}^2 + 12}\frac{60\mathrm{P} + \mathrm{Gr}}{60}\right) + \\ & + \frac{1}{2}\left(\frac{\mathrm{M}^2}{\mathrm{M}^2 + 12}\frac{60\mathrm{P} + \mathrm{Gr}}{60} - \frac{\mathrm{Gr}}{24} - \mathrm{P}\right)X^2 + \frac{\mathrm{Gr}}{24}X^4 \end{aligned} \tag{11.21}$$

$$\begin{aligned} \Phi(X) = {} & \frac{1}{96}\left(\frac{60\mathrm{P} + \mathrm{Gr}}{5}\frac{\mathrm{M}^2 + 8}{\mathrm{M}^2 + 12} - \frac{48\mathrm{P} + \mathrm{Gr}}{4}\right)X + \\ & + \frac{1}{72}\left(-\frac{60\mathrm{P} + \mathrm{Gr}}{5}\frac{\mathrm{M}^2}{\mathrm{M}^2 + 12} + \frac{24\mathrm{P} + \mathrm{Gr}}{2}\right)X^3 - \frac{\mathrm{Gr}}{120}X^5 \end{aligned} \tag{11.22}$$

These profiles are reported in Figs. 11.2 and 11.3 for an arbitrary choice of the Grashof and pressure head numbers ($\mathrm{Gr} = 10^{10}$, $\mathrm{P} = 10^9$) and different values of the Hartmann number M.

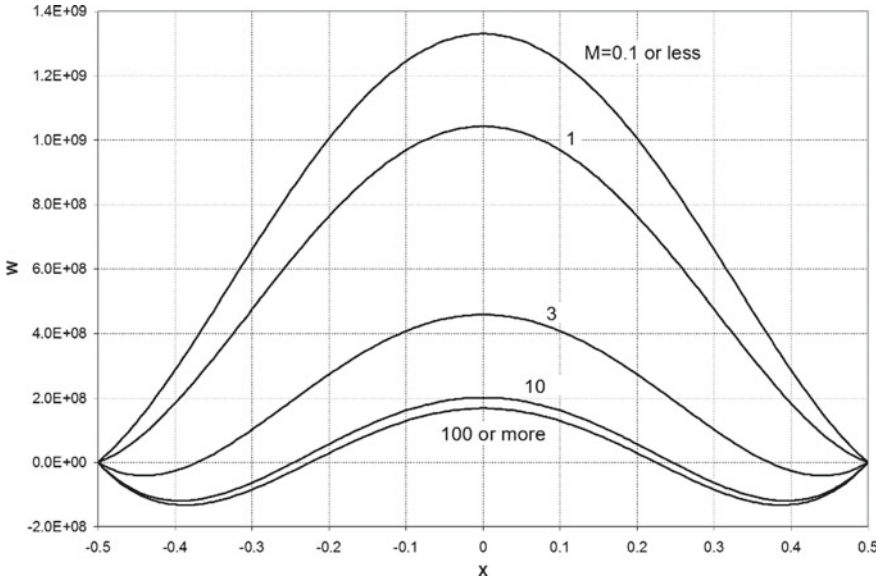

Fig. 11.2 Dimensionless velocity for $Gr = 10^{10}$, $P = 10^9$ and various M (equipotential walls)

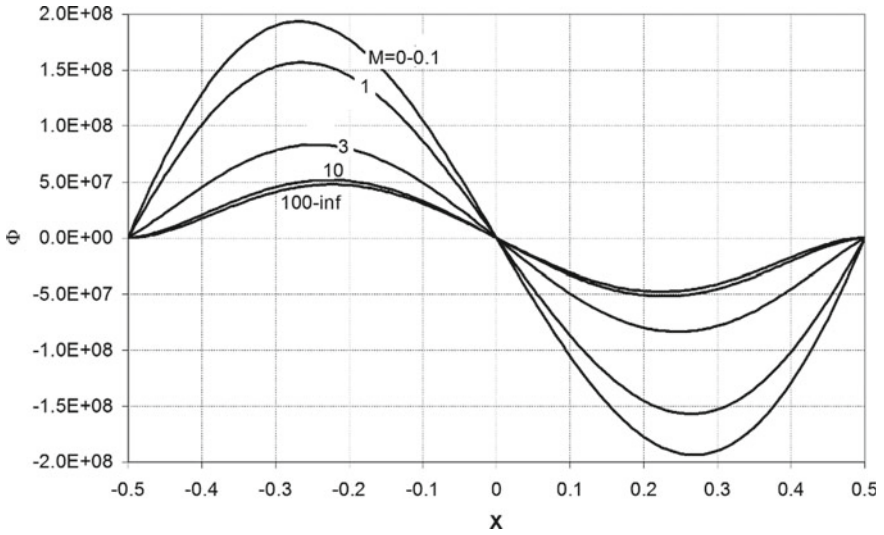

Fig. 11.3 Dimensionless potential for $Gr = 10^{10}$, $P = 10^9$ and various M (equipotential walls)

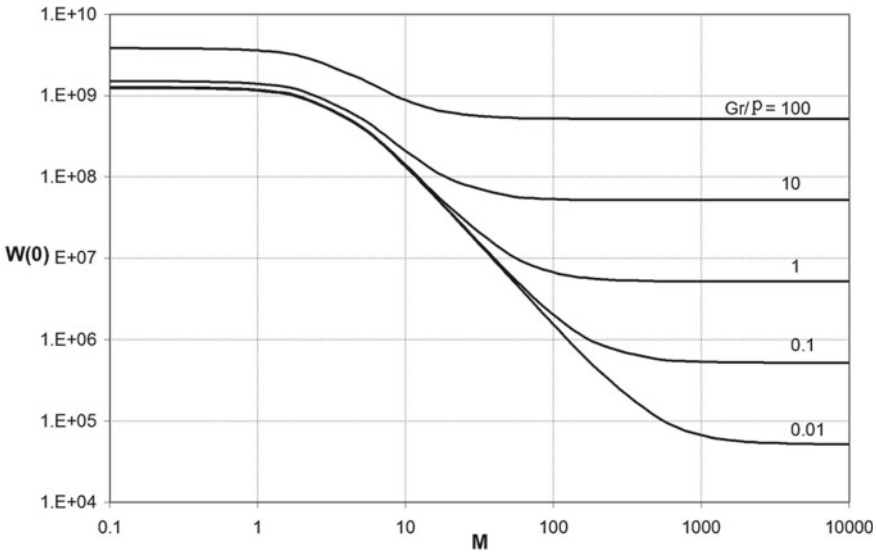

Fig. 11.4 Dimensionless centreline velocity as a function of the Hartmann number M for $P = 10^{10}$ and various Gr/P ratios

Note that, for sufficiently large M, the velocity profile $W(X)$ exhibits two descending near-wall layers and an ascending core, whereas, for small M, W is directed upward everywhere. The centerline velocity $W_{CL} = W(0)$ tends to the following limiting values for $M \to 0$ and $M \to \infty$, respectively:

$$W_{CL}(M \to 0) = \frac{Gr}{384} + \frac{P}{8} \tag{11.23}$$

$$W_{CL}(M \to \infty) = \frac{Gr}{1920} \tag{11.24}$$

Therefore, as the magnetic induction increases, the forced-flow velocity component, proportional to P, is completely suppressed, but the velocity component associated with natural convection, independent of P, can only be reduced by a factor of 5 at most.

This is also illustrated in Fig. 11.4, which reports the dimensionless centerline velocity W_{CL} as a function of the Hartmann number M for $P = 10^{10}$ and different values of the Gr/P ratio.

The Figure also shows that MHD effects become significant as the Hartmann number M exceeds the value of ~1. This behaviour is different from that observed in *two-dimensional* channel flow, where MHD effects become significant only for M greater than ~100 and where also the natural convection component of the velocity is drastically suppressed by large values of the magnetic induction (Ciofalo and Cricchio 2002).

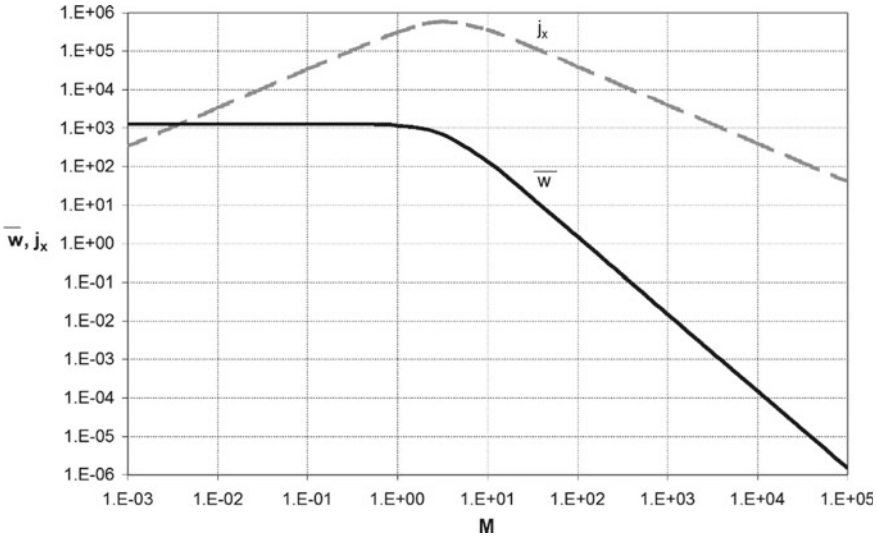

Fig. 11.5 Dimensioned mean velocity and electric current as functions of the Hartmann number M for Pb-17Li, $D = 0.15$ m, $B_y = 5$ T and $q''' = 1$ MW/m^3 yielding P $\approx 10^{10}$, Gr $\approx 10^{11}$

The average W velocity is:

$$\overline{W} = \frac{1}{\mathrm{M}^2 + 12} \frac{60\mathrm{P} + \mathrm{Gr}}{60} \tag{11.25}$$

By substituting Eq. (11.17) for $\mathrm{d}\Phi/\mathrm{d}X$ into Eq. (11.12), one obtains for the current density J_x the constant value:

$$J_x = -\frac{1}{\mathrm{M}^2 + 12} \frac{60\mathrm{P} + \mathrm{Gr}}{60} = -\overline{W} \tag{11.26}$$

The behaviour of mean velocity and electric current as functions of the Hartmann number is best appreciated by considering these quantities in dimensioned, rather than dimensionless, form. For example, Fig. 11.5 reports $\overline{w}$ and j_x for a particular choice of the geometrical dimension D of the channel and of the physical properties of the fluid (corresponding to the eutectic 83%Pb-17%Li alloy proposed for the breeder blanket of fusion nuclear reactors).

The electric current attains its maximum values for M ≈ 3, which corresponds to the "knee" in the curve describing $\overline{w}$ as a function of M. The difference with respect to *two-dimensional* channel flow (Ciofalo and Cricchio 2002), in which current maxima are attained at M ≈ 100, is again clear.

This difference is due to the fact that in two-dimensional flows the electric currents induced by MHD effects close themselves through the solid walls and the adjacent fluid layers orthogonal to **B** (Hartmann layers), whose electric resistance limits the

current intensity and makes high values of the Hartmann number necessary for significant damping effects to occur. On the contrary, in the present 1-D configuration no return resistance is encountered by the electric current, so that lower values of the Hartmann number are sufficient to cause significant MHD braking effects.

Equations (11.25) and (11.26) show that both the average velocity and the current density vanish for:

$$\mathrm{Gr} = -60\,\mathrm{P} \tag{11.27}$$

If the above condition is satisfied, there are no MHD effects on the flow, no matter how large the Hartmann number M. Equation (11.21) then gives for $W(X)$ the following profile, which is independent from M and thus from the applied magnetic induction B_x:

$$W = \frac{\mathrm{Gr}}{1920}\left(1 - 24X^2 + 80X^4\right) \tag{11.28}$$

This coincides with the W profile obtained for internal heating in the absence of MHD effects by Geršuni and Žukovitskij (1958) [as reported e.g. by Kulacki and Richards (1985)], and later by Di Piazza and Ciofalo (2000).

(b) **Imposed potential difference between the opposite walls**

The solution obtained for equipotential walls can easily be generalized to the case in which an electric potential difference V (made dimensionless by the same scale vB used for φ) is imposed between the opposite walls of the channel. The boundary conditions (11.16) are replaced by:

$$\Phi\left(-\frac{1}{2}\right) = \frac{V}{2}, \quad \Phi\left(\frac{1}{2}\right) = -\frac{V}{2} \tag{11.29}$$

Note that the potential difference V, like the pressure head number P, is taken to be positive if it drives the fluid towards positive z and the electric current towards positive x.

Accordingly, the solutions (11.21), (11.22), (11.12) obtained above for W, Φ and J_x are replaced by:

$$\begin{aligned} W(X) = {} & \frac{1}{8}\left(\frac{\mathrm{Gr}}{48} + \mathrm{P} - \frac{\mathrm{M}^2}{\mathrm{M}^2+12}\,\frac{60\mathrm{P} + \mathrm{Gr} - 720V}{60}\right) + \\ & + \frac{1}{2}\left(\frac{\mathrm{M}^2}{\mathrm{M}^2+12}\,\frac{60\mathrm{P} + \mathrm{Gr} - 720V}{60} - \frac{\mathrm{Gr}}{24} - \mathrm{P}\right)X^2 + \frac{\mathrm{Gr}}{24}X^4 \end{aligned} \tag{11.30}$$

$$\Phi(X) = \frac{1}{96}\left(\frac{60\mathrm{P} + \mathrm{Gr} - 720V}{5} \cdot \frac{\mathrm{M}^2+8}{\mathrm{M}^2+12} - \frac{48\mathrm{P} + \mathrm{Gr}}{4}\right)X +$$

$$+\frac{1}{72}\left(-\frac{60\mathrm{P}+\mathrm{Gr}-720V}{5}\frac{\mathrm{M}^2}{\mathrm{M}^2+12}+\frac{24\mathrm{P}+\mathrm{Gr}}{2}\right)X^3-\frac{\mathrm{Gr}}{120}X^5 \tag{11.31}$$

$$J_x=-\frac{1}{\mathrm{M}^2+12}\frac{60\mathrm{P}+\mathrm{Gr}-720V}{60} \tag{11.32}$$

while the average velocity becomes now:

$$\overline{W}=\frac{1}{\mathrm{M}^2+12}\frac{60\mathrm{P}+\mathrm{Gr}+60\mathrm{M}^2V}{60} \tag{11.33}$$

Note that $J_x=V-\overline{W}$, which generalizes the previous result $J_x=-\overline{W}$ obtained for equipotential walls ($V=0$).

When a difference of electric potential is imposed between the opposite walls, it is possible to compute the electrical and mechanical powers P_E, P_M provided *by* the system. Let us consider the two cases in which buoyancy is present or not separately.

(a) **No buoyancy**

If no buoyancy forces act on the fluid (isothermal flow, negligible thermal expansion coefficient, or negligible gravity), by letting $\mathrm{Gr}=0$ in Eqs. (11.32) and (11.33) one has:

$$J_x=-\frac{\mathrm{P}-12V}{\mathrm{M}^2+12} \tag{11.34}$$

$$\overline{W}=\frac{\mathrm{P}+\mathrm{M}^2V}{\mathrm{M}^2+12} \tag{11.35}$$

By analogy with the working diagram of a hydraulic pump, working diagrams for the present generalized MHD engine can be drawn in a plane having abscissa $\overline{W}$ (directly proportional to the volumetric flow rate Q) and ordinate P (pressure head number, corresponding to the prevalence of a pump).

The mechanical power provided *by* the system (positive if the mean velocity is opposite to the external applied force) can be expressed in dimensionless form as:

$$P_M=-\mathrm{P}\overline{W} \tag{11.36}$$

The electric power provided *by* the system is $-VJ_x$ and is positive if the electric current flows in the direction of the imposed electric potential gradient. By using Eq. (11.34) for J_x and eliminating V through Eq. (11.35) one has:

$$P_E=-VJ_x=-\frac{1}{\mathrm{M}^4}\left[\mathrm{P}^2-\left(\mathrm{M}^2+24\right)\mathrm{P}\overline{W}+12\left(\mathrm{M}^2+12\right)\overline{W}^2\right] \tag{11.37}$$

Therefore, one has $P_M = 0$ if $\overline{W} = 0$ (P axis) or P = 0 ($\overline{W}$ axis), while $P_E = 0$ if P $= 12\,\overline{W}$ or P $= (M^2 + 12)\overline{W}$ (i.e., along two straight lines crossing the first and third quadrants). It is thus possible to build 8-region working diagrams like those shown in Fig. 11.6 for two values of the Hartmann number M.

The regions in which $P_E > 0$, $P_M < 0$ correspond to the *MHD generator* mode, in which the system converts the mechanical energy of the forced flow to electrical energy. The regions in which $P_E < 0$, $P_M > 0$ correspond to the *MHD pump* mode, in which the system converts electrical energy to mechanical energy. In the four remaining regions the system works as a *pure dissipator* since it absorbs both electric and mechanical energy ($P_E < 0$, $P_M < 0$).

The comparison of the two plots shows that the amplitude of the two sectors representing the MHD generator mode increases as M (i.e., the imposed magnetic induction field B) increases, while the two sectors representing the MHD pump mode have a fixed amplitude of 90°, independent of M.

Alternative working diagrams could be drawn in the plane (V, P) or in the plane ($\overline{W}$, V).

(b) **Buoyancy**

In the presence of buoyancy forces, using again $\overline{W}$ and P as independent variables, the mechanical power is still $P_M = -\mathrm{P}\overline{W}$, as in Eq. (11.36), but the electric power $P_E = -VJ_x$ must be expressed using for J_x and V the more general Eqs. (11.32) and (11.33) instead of the simpler (11.34) and (11.35). This amounts to substituting P+Gr/60 for P in Eq. (11.37), which thus becomes

$$P_E = -\frac{1}{M^4}\left[\left(\mathrm{P} + \frac{\mathrm{Gr}}{60}\right)^2 - \left(\mathrm{M}^2 + 24\right)\left(\mathrm{P} + \frac{\mathrm{Gr}}{60}\right)\overline{W} + 12\left(\mathrm{M}^2 + 12\right)\overline{W}^2\right] \tag{11.38}$$

The electric power P_E now vanishes for

$$\mathrm{P} = 12\,\overline{W} - \frac{\mathrm{Gr}}{60} \tag{11.39}$$

$$\mathrm{P} = (\mathrm{M}^2 + 12)\,\overline{W} - \frac{\mathrm{Gr}}{60} \tag{11.40}$$

Both these last two equations represent straight lines of the ($\overline{W}$, P) plane which do *not* intersect the origin of the axes. Therefore, the ($\overline{W}$, P) plane is divided into 10 regions rather than 8, as shown in Fig. 11.7 for an intermediate value of the Hartmann number (M = 20) and two different values of Gr.

It is possible to observe, for small positive values of $\overline{W}$ and negative values of P, a region in which the system provides *both* electric and mechanical power by converting the thermal power received, and thus operates as a (low efficiency) thermal engine (Mahmud et al. 2003).

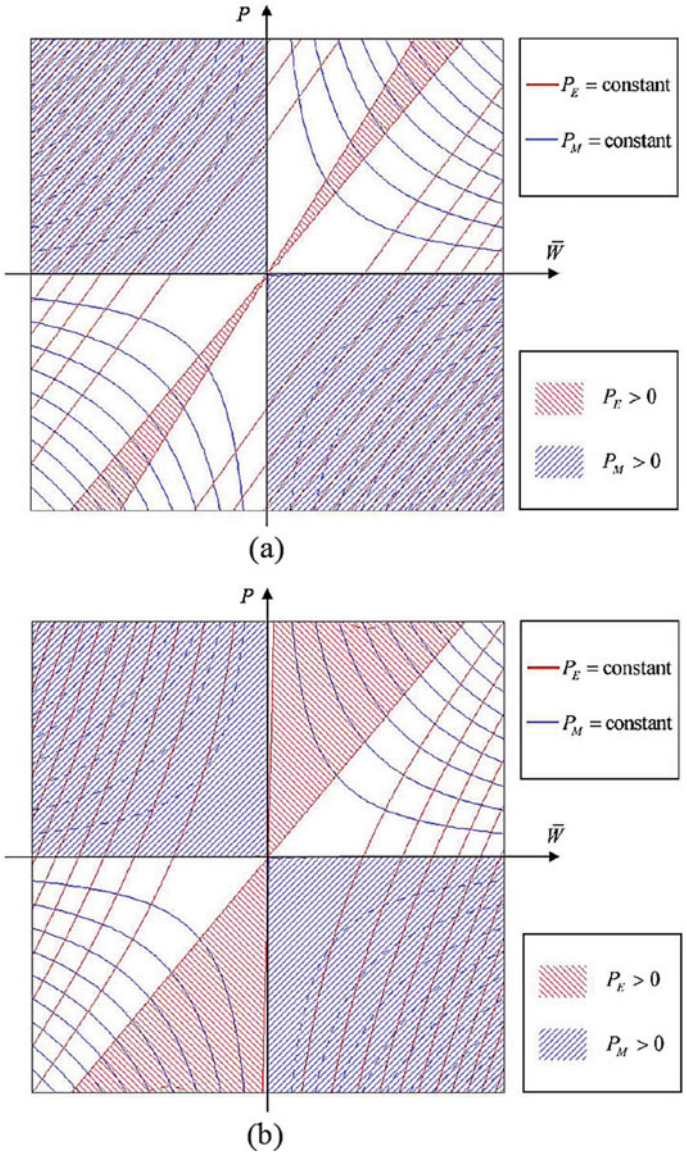

Fig. 11.6 Working diagrams in the ($\overline{W}$, P) plane for a generalized MHD engine in the absence of buoyancy forces (Gr = 0) and for two different values of the Hartmann number M. **a** Low Hartmann number (M = 2). **b** high Hartmann number (M = 1000)

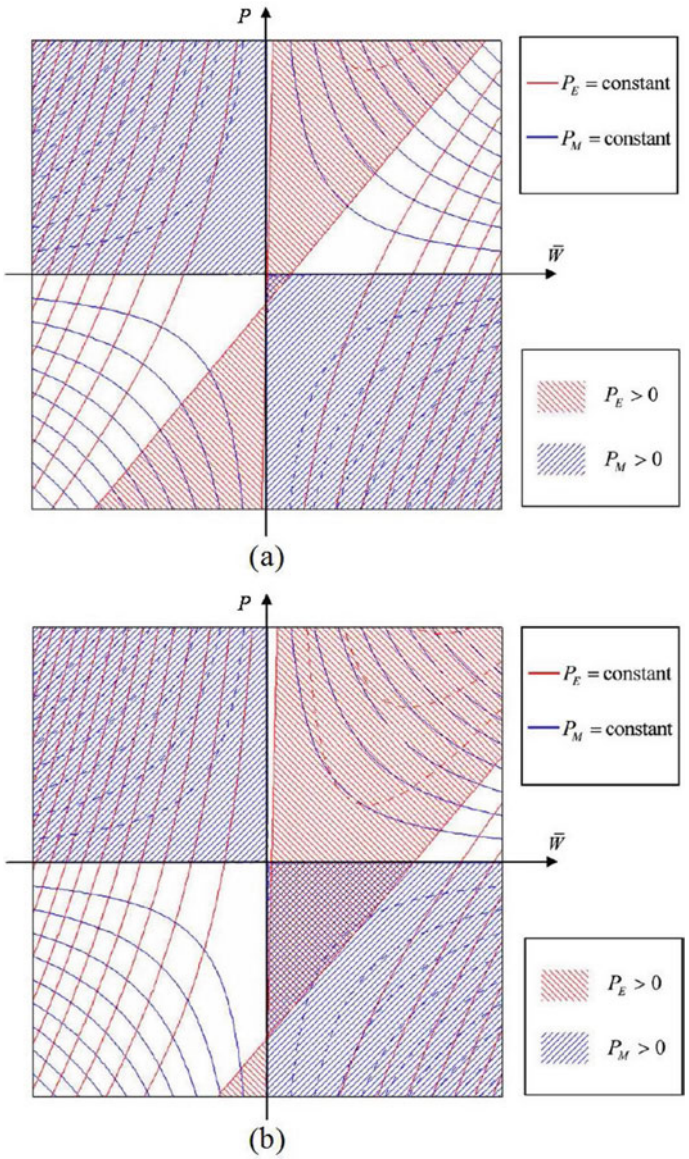

Fig. 11.7 Working diagrams in the ($\overline{W}$, P) plane for a generalized MHD engine in the presence of buoyancy forces for M = 20 and two different values of the Grashof number Gr. **a** Low Grashof number (Gr = 7200). **b** High Grashof number (Gr = 45,000)

As in the previous non-buoyant case, alternative working diagrams can be drawn in the (V, P) or ($\overline{W}$, V) planes.

In summary, when a difference of electric potential is imposed between the opposite walls, it is possible to define the electrical and mechanical powers P_E, P_M provided *by* the system; in a suitable state space (e.g. the plane whose axes are the dimensionless mean velocity $\overline{W}$ and pressure head P), according to the signs of P_E an P_M one can distinguish alternative working regimes which, in the absence of buoyancy, include direct and reverse EM pumps, direct and reverse MHD generators, and purely dissipating modes. In the presence of buoyancy, a further regime is observed in which the system operates as a thermal engine by converting thermal power into both electrical and mechanical power.

As a final *caveat*, it should be observed that the solutions derived here apply only to one-dimensional, fully developed flow, thermal and electric fields in a plane channel which is indefinite in the streamwise and spanwise directions. Some aspects of the solutions obtained, e.g. the fact that MHD effects cause the buoyancy component of the flow to decrease at most by a factor of 5, are peculiar to the present 1-D configuration and would not be observed in two-dimensional channels having a finite extent along the direction of the magnetic field, exhibiting closed current loops.

The problem can be generalized by assuming the side walls to be of finite thickness and electric conductivity, and thus imposing to the electric potential Robin (third type) conditions *in lieu* of the Dirichlet conditions considered so far. For example, in the symmetric case:

$$\left[\Phi + L\frac{\mathrm{d}\Phi}{\mathrm{d}X}\right]_{X=\pm 1/2} = 0 \tag{11.41}$$

in which L is an extrapolation distance.

A further generalization can be obtained by assuming the side walls to be differentially heated and/or to possess a relative velocity as in Couette flow. The corresponding boundary conditions on W and T would change accordingly, but it can be shown that the solutions obtained for $\overline{W}$ and J_x, and therefore the working diagrams in Figs. 11.6 and 11.7, would still be valid.

References[1]

Abramowitz, M., & Stegun, I. A., (Eds.) (1972). *Handbook of mathematical functions with formulas, graphs, and mathematical tables* (9th printing). Dover, New York.

Amokrane, M., Sadaoui, D., Koutsou, C. P., Karabelas, A. J., & Dudeck, M. (2015). A study of flow field and concentration polarization evolution in membrane channels with two-dimensional spacers during water desalination. *Journal of Membrane Science, 477*, 139–150.

Ardourel, V., & Jebeile, J. (2017). On the presumed superiority of analytical solutions over numerical methods. *European Journal for Philosophy of Science, 7*(2), 201–220.

Arnold, V. I. (1992). *Catastrophe theory* (3rd ed.). Springer-Verlag, Berlin.

Beck, J. V. (1970). Nonlinear estimation applied to the nonlinear inverse heat conduction problem. *International Journal of Heat and Mass Transfer, 13*, 703–716.

Belendez, A., Pascual, C., Mendez, D. I., Belendez, T., & Neipp, C. (2007). Exact solution for the nonlinear pendulum. *Revista Brasileira De Ensiño De Fisica, 29*(4), 645–648.

Blasius, H. (1908). Grenzschichten in Flüssigkeiten mit kleiner Reibung. *Zeitschrift Fur Angewandte Mathematik Und Physik, 56*, 1–37.

Boussinesq, M. J. (1868). Mémoire sur l'influence des frottements dans les mouvements régulier des fluids. *Journal de Mathématiques Pures et Appliquées, 2me Série*, *13*, 377–424.

Boussinesq, M. J. (1897). *Théorie de l'écoulement tourbillonnant et tumultueux des liquides dans les lits rectilignes a grande section* (Vol. 1). Gauthier-Villars, Paris.

Brenn, G. (2018). *Analytical solutions for transport processes—fluid mechanics.* Springer.

Butterworth, D., & Hewitt, G. F. (Eds.). (1977). *Two-phase flow and heat transfer.* Oxford University Press, Harwell Series, Oxford, UK.

Bühler, L. (1998). Laminar Buoyant magnetohydrodynamic flow in vertical rectangular ducts. *Physics of Fluids, 10*(1), 223–236.

Cancilla, N., Gurreri, L., Marotta, G., Ciofalo, M., Cipollina, A., Tamburini, A., & Micale, G. (2022). A porous media CFD model for the simulation of hemodialysis in hollow fiber membrane modules. *Journal of Membrane Science*, *646*, article #120219.

Carslaw, H. S., & Jaeger, J. C. (1959). *Conduction of heat in solids* (2nd ed.). Oxford University Press, Oxford, UK.

Chisholm, D. (1983). *Two-phase flow in pipelines and heat exchangers.* Longman Higher Education, New York.

Ciofalo, M. (2022). *Lezioni di Termoidraulica.* Società Editrice Esculapio, Bologna (in Italian).

[1] *When we can't think for ourselves, we can always quote*
(*Ludwig Wittgenstein*)

M. Ciofalo, *Thermofluid Dynamics*, UNIPA Springer Series,
https://doi.org/10.1007/978-3-031-30470-5

Ciofalo, M., & Cricchio, F. (2002). Influence of a magnetic field on liquid metal free convection in an internally heated cubic enclosure. *International Journal of Numerical Methods for Heat and Fluid Flow, 12*(6), 687–715.

Ciofalo, M., Di Maio, P. A., Sposito, G., & Vella, G. (2005). Mixed MHD convection and tritium transport in fusion-relevant configurations. *Fusion Engineering and Design, 75–79*, 697–702.

Ciofalo, M., Caronia, A., Di Liberto, M., & Puleo, S. (2007). The Nukiyama curve in water spray cooling: its derivation from temperature-time histories and its dependence on the quantities that characterize drop impact. *International Journal of Heat and Mass Transfer, 50*, 4948–4966.

Ciofalo, M., La Cerva, M., Di Liberto, M., & Tamburini, A. (2017). Influence of the boundary conditions on heat or mass transfer in complex channels. *Journal of Physics—Conference Series*, *923*(1), article #012053.

Ciofalo, M., Di Liberto, M., Gurreri, L., La Cerva, M., Scelsi, L., & Micale, G. (2019). Mass transfer in ducts with transpiring walls. *International Journal of Heat and Mass Transfer, 132*, 1074–1086.

Clift, R., Grace, J. R., & Weber, M. E. (1978). *Bubbles, drops, and particles*. Academic Press, New York.

Di Piazza, I., & Bühler, L. (2000). A general computational approach for magnetohydrodynamic flows using the CFX code: buoyant flow through a vertical square channel. *Fusion Technology, 28*(2), 180–189.

Di Piazza, I., & Ciofalo, M. (2000). Low-Prandtl number natural convection in volumetrically heated rectangular enclosures—I. Slender Cavity. *AR*=4, *International Journal of Heat and Mass Transfer*, *43*(17), 3027–3051.

Emanuel, G. (2015). *Analytical fluid dynamics* (3rd ed). CRC Press.

Geršuni, G. Z., & Žukovitskij, E. M. (1958). Stationary convective motions of an electrically conducting fluid between parallel planes in a magnetic field. *ZETF* (*Zhurnal eksperimental'noi i Theoreticheskoi Fiziki*), *34*(3), 670–674 (in Russian).

Kerr, P. G., & Huang, L. (2010). Review: membranes for haemodialysis. *Nephrology, 15*(4), 381–385.

Kulacki, F. A., & Richards, D. E. (1985). Natural convection in plane layers and cavities with volumetric energy sources. In S. Kakaç, W. Aung & R. Viskanta (Eds.) *Natural convection: Fundamentals and applications.* Hemisphere, New York.

Lahey, R. T., & Moody, E. J. (1996). *The thermal hydraulics of a boiling water nuclear reactor* (2nd edn). ANS monograph, the American Nuclear Society, New York.

Landau, L. D., & Lifshitz, E. M. (1959). *Fluid mechanics.* Pergamon Press, Reading, MA.

Lockhart, R. W., & Martinelli, R. C. (1949). Proposed correlation of data for isothermal two-phase, two-component flow in pipes. *Chemical Engineering Progress, 45*(1), 39–48.

Loudon, C., & Tordesillas, A. (1998). The use of the dimensionless Womersley number to characterize the unsteady nature of internal flow. *Journal of Theoretical Biology, 191*, 63–78.

Mackley, M. R., & Stonestreet, P. (1995). Heat transfer enhancement and energy dissipation for oscillatory flow in baffled tubes. *Chemical Engineering Science, 50*, 2211–2224.

Mahmud, S., Tasnim, S. H., & Mamun, M. A. H. (2003). Thermodynamic analysis of mixed convection in a channel with transverse hydromagnetic effect. *International Journal of Thermal Sciences, 42*, 731–740.

McAdams, W. H. (1933). *Heat transmission.* McGraw-Hill, New York.

Moreau, R. (1990). *Magnetohydrodynamics.* Kluwer Academic Publishers, Amsterdam.

Nakatsuka, S., Nakate, I., & Miyano, T. (1996). Drinking water treatment by using ultrafiltration hollow fiber membranes. *Desalination, 106*(1), 55–61.

Perry, R. H., Green, & D. W., (Eds.) (1984). *Perry's chemical engineering handbook* (6th Edn, pp. 5.63–5.67). McGraw-Hill, New York.

Sposito, G., & Ciofalo, M. (2006). One-dimensional mixed MHD convection. *International Journal of Heat and Mass Transfer, 49*(17–18), 2939–2949.

Stefan, J. (1889). Über die Theorie der Eisbildung; insbesondere über die Eisbildung im Polarmeere. *Sitzungsberichte der Kaiserlichen Akademie Wiss., Wien Math. Natur., 98*, 965–983.

Stokes, G. G. (1850). On the effect of the internal friction of fluids on the motion of a pendulum. In *Transactions of the Cambridge philosophical society* (vol. IX, pp. 8–106).

Tikhonov, A. N., & Arsenin, V. Y. (1977). *Solutions of Ill-posed problems.* V. H. Winston, Washington, DC.

United Kingdom Committee on the Properties of Steam. (1970). *UK steam tables in SI units.* E. Arnold, London, UK.

Womersley, J. R. (1955). Method for the calculation of velocity, rate of flow and viscous drag in arteries when the pressure gradient is known. *Journal of Physiology, 127*, 553–563.

Yang, X., Yu, Y., Wang, R., & Fane, A. G. (2012). Optimization of microstructured hollow fiber design for membrane distillation applications using CFD modeling. *Journal of Member Science, 421–422*, 258–270.